

To appear in *Advances in Physics*  
Vol. 00, No. 00, Month 20XX, 1–78

## REVIEW

### Universal High-Frequency Behavior of Periodically Driven Systems: from Dynamical Stabilization to Floquet Engineering

Marin Bukov<sup>a\*</sup>, Luca D'Alessio<sup>a,b</sup>, and Anatoli Polkovnikov<sup>a</sup>

<sup>a</sup>*Department of Physics, Boston University, 590 Commonwealth Ave., Boston, MA 02215, USA,*

<sup>b</sup>*Department of Physics, The Pennsylvania State University, University Park, PA 16802, USA;*

(Received 00 Month 20XX; final version received 00 Month 20XX)

We give a general overview of the high-frequency regime in periodically driven systems and identify three distinct classes of driving protocols in which the infinite-frequency Floquet Hamiltonian is not equal to the time-averaged Hamiltonian. These classes cover systems, such as the Kapitza pendulum, the Harper-Hofstadter model of neutral atoms in a magnetic field, the Haldane Floquet Chern insulator and others. In all setups considered, we discuss both the infinite-frequency limit and the leading finite-frequency corrections to the Floquet Hamiltonian, using the Magnus expansion. We also provide a short overview of Floquet theory focusing on the gauge structure associated with the choice of stroboscopic frame and the differences between stroboscopic and non-stroboscopic dynamics. In the latter case, the evolution is still governed solely by the Floquet Hamiltonian, but one has to work with a properly dressed initial density matrix and dressed observables. We derive perturbative expressions in the driving period for the dressed operators using the Magnus expansion. We also comment on the application of the Magnus expansion to systems described by static Hamiltonians with well-separated energy scales and, in particular, discuss parallels between the Magnus expansion and the Schrieffer-Wolff transformation also extending the latter to driven systems.

**PACS:** 05.45.-a Nonlinear dynamics and chaos, 67.85.-d Ultracold gases, trapped gases, 67.85.Hj Bose-Einstein condensates in optical potentials, 71.10.-w Theories and models of many-electron systems

**Keywords:** Floquet theory, effective Hamiltonian, Magnus expansion, high-frequency limit, quantum simulation, dynamical stabilisation and localisation, artificial gauge fields, topological insulators, spin systems.

#### Index to information contained in this review

---

\*Corresponding author. Email: mbukov@bu.edu

1. Introduction.
2. Floquet Theory. Stroboscopic and Non-Stroboscopic Time Evolution.
  - 2.1. Floquet Hamiltonian and Kick Operators.
  - 2.2. A Two-Level System in a Circularly Driven Magnetic Field
  - 2.3. Stroboscopic vs Non-Stroboscopic Dynamics.
3. The Magnus Expansion.
  - 3.1. Deriving Floquet Hamiltonians with the Magnus Expansion.
  - 3.2. The Magnus Expansion in the Rotating Frame.
  - 3.3. Convergence of the Magnus Expansion.
4. The Rotating Wave Approximation and the Schrieffer-Wolff transformation.
  - 4.1. A Two-level System.
  - 4.2. The Magnus Expansion vs. the Schrieffer-Wolff Transformation for the Anderson Model.
  - 4.3. The Rabi Model.
5. The Kapitza Class
  - 5.1. The Kapitza Pendulum.
  - 5.2. The Kapitza Hamiltonian in the Rotating Frame. Floquet Gauge Freedom.
  - 5.3. Finite-Frequency Corrections.
  - 5.4. Dressed observables and Dressed Density Matrix.
  - 5.5. Multi-dimensional and Multi-particle Generalization of the Kapitza Pendulum.
6. The Dirac Class.
  - 6.1. Periodically Driven Magnetic Fields.
  - 6.2. Periodically Driven External Potentials.
7. The Dunlap-Kenkre (DK) Class.
  - 7.1. Noninteracting Particles in a Periodically Driven Potential: Floquet theory and experimental realization.
  - 7.2. Cold Atoms Realization of the Harper-Hofstadter Hamiltonian.
  - 7.3. The Periodically Driven Fermi-Hubbard Model. Floquet Topological Insulators.
  - 7.4. Spin Systems.
8. Conclusion.
  - A. Lattice vs. Continuum Models.
  - B. First-order Coefficients for the 1D Driven Boson Model.
  - C. First-order Coefficients for the Harper-Hofstadter Model.

## 1. Introduction

Periodically driven systems have a long history, one paradigmatic example being the Kicked-Rotor model of a particle moving on a ring subject to time-periodic ‘kicks’ [1], which realizes the famous Chirikov standard map [2] and the Kapitza pendulum [3]. The behavior of such systems is very rich - they can display interesting integrability-to-chaos transitions, as well as counter-intuitive effects, such as dynamical localization [4–13] and dynamical stabilization [3, 14, 15]. The latter manifests itself in reduced ionisation rates in atomic systems irradiated by electromagnetic fields in the regime of high frequencies and high intensities [16–21], or as diminished spreading of wave packets in systems subject to periodic driving [22, 23]. The consequences of an AC-drive for quantum phase transitions have been investigated in a variety of models [24–27], such as the Dicke model [24] and the Ising model [25]. The modification of transport properties in periodically driven systems has been the subject of multiple studies, too [28–33].

In the recent years, it has been shown that periodic perturbations can be used as a flexible experimental knob to realize new phases not accessible in equilibrium systems [34–37], synthetic (engineered) matter [38–53], and quantum motors, which are similar to a quantum ratchet [54, 55]. This new line of research, which can be termed ‘Floquet engineering’, has motivated a renaissance of interest in periodically driven systems. Floquet systems also naturally appear in digital quantum computation schemes, where one implements a continuous unitary evolution by effectively ‘trotterizing’ it [56, 57].

Periodic perturbations arise naturally in many experimental setups. Examples include irradiating materials with electromagnetic waves, testing the response of a system to periodic currents or to mechanical shaking and deformations. Periodic driving protocols also appear in non-driven systems, after a transformation into a rotating frame, which typically results in the emergence of fast oscillating terms in the Hamiltonian.

In the simplest case, one considers a single monochromatic driving protocol, characterized by a coupling strength (driving amplitude), and a single frequency  $\Omega = 2\pi/T$ .

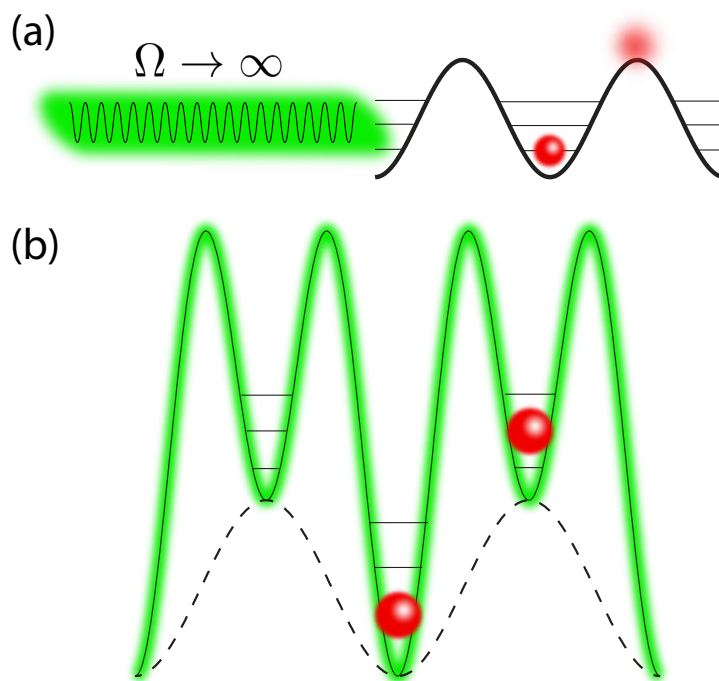


Figure 1. (Color online) The application of a high-frequency periodic perturbation to a static Hamiltonian, (a), may lead to the emergence of an effective high-frequency Hamiltonian with renormalized parameters (b). The purpose of this review is to discuss under which conditions this is possible, and what types of effective Hamiltonians can be engineered in this way.

The dynamics of the periodically driven systems can be highly complex even in few-body systems. Usually, it can be analyzed in the two extreme regimes of slow and fast driving. In the former regime, the system almost adiabatically follows the instantaneous Hamiltonian. In the latter regime, where the driving frequency is fast compared to the natural frequencies of the non-driven model, the system typically feels an effective static potential, which can depend on the driving amplitude, c.f. Fig. 1. If one deviates from either of these limits, one expects that sufficiently complex systems would heat up, and eventually reach infinite temperature in the absence of a coupling to a heat bath. This has been confirmed numerically and analytically in different setups [58–64].

Away from the adiabatic limit, the analysis of periodically driven systems often relies on the Floquet theorem, which is very similar to the Bloch theorem in quantum mechanics. In its most general form, it states that one can write the evolution operator as

$$U(t_2, t_1) = P(t_2)e^{-iH_F(t_1-t_2)}P^\dagger(t_1), \quad (1)$$

where  $P(t) = P(t + T)$  is a unitary periodic operator, and  $H_F$  is the time-independent Floquet Hamiltonian. It is clear that the choices of the periodic operator and the Floquet Hamiltonian are not unique, and there is some freedom in defining them. As we will discuss in the next section, in addition to the standard gauge freedom related to the choice of basis, there is an additional freedom associated with the choice of the beginning of the period. This choice affects the Floquet Hamiltonian and we refer to it as ‘Floquet gauge’. The particular choice of the Floquet gauge is dictated by convenience: e.g. often one works in the gauge where the Floquet Hamiltonian assumes its simplest form. The periodic operator  $P(t)$  has a direct physical interpretation in terms of the initial and the final ‘kicks’ introduced in Ref. [65].

The formulation of the Floquet’s theorem simplifies if one observes the system strobo-

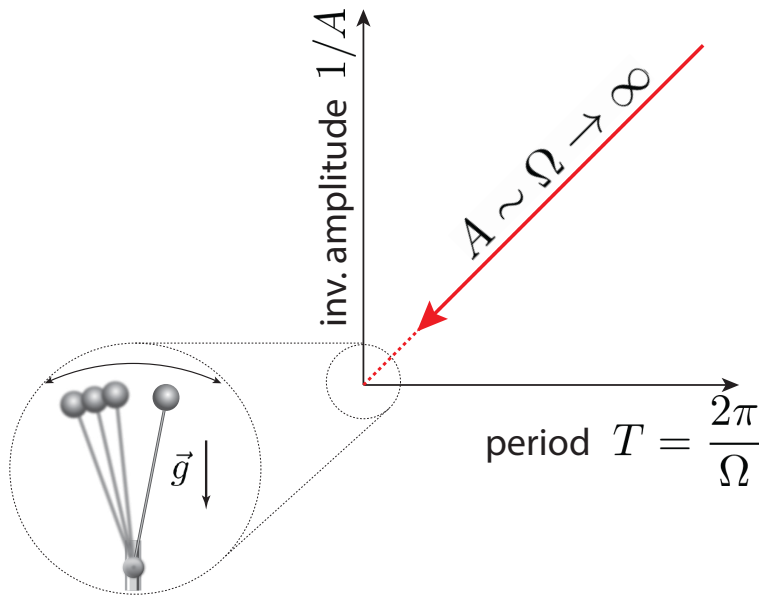


Figure 2. (Color online). Schematic representation of the parameter space of periodically driven systems. In this work we consider a setup in which the amplitude of the driving scales with the frequency, i.e.  $A \sim \Omega$ . In the infinite-frequency limit we obtain a well-defined local Floquet Hamiltonian which is qualitatively different from the time-averaged Hamiltonian. For example, in the case of the Kapitza pendulum, the Floquet Hamiltonian allows for oscillations around the upright position, a phenomenon known as dynamical stabilization (see Sec. 5).

scopically, i.e. at times  $t_2 = t_1 + nT$ , where  $nT$  is the stroboscopic time measured in units of the driving period. In this case the operators  $P(t_2)$  and  $P^\dagger(t_1)$  are independent of the stroboscopic interval  $nT$ , and the full evolution operator is equivalent (up to two unitary transformations) to the evolution of the system generated by the time-independent Hamiltonian  $H_F$ .

In general, it is not possible to evaluate  $H_F$ , nor  $P(t)$ , explicitly and one has to rely on approximations [66–70]. Moreover, in macroscopic systems there is no guarantee that  $H_F$  is a local physical Hamiltonian. In fact, in the case of generic interacting systems, a local  $H_F$  might not exist [62]. In such situations, the dynamics of the system can be completely chaotic and the Floquet theorem is not particularly useful.

An important limit, where the Floquet Hamiltonian can be defined at least perturbatively, corresponds to the fast driving regime, in which the driving frequency is higher than any natural frequency in the problem. Then the driving does not couple resonantly to the slow degrees of freedom, but rather results in renormalization and dressing of the slow Hamiltonian. In many instances the Floquet Hamiltonian in the high-frequency limit is simply the time-averaged Hamiltonian,  $\frac{1}{T} \int_0^T H(t) dt$ . But there are important exceptions, in which the Floquet Hamiltonian is *not* given by  $\frac{1}{T} \int_0^T H(t) dt$ , even in the infinite-frequency limit. These situations are of particular interest since the system can display interesting and counterintuitive behavior, such as dynamical stabilization, as it happens in the Kapitza pendulum [15]. Such situations naturally occur, for instance, when the amplitude of the driving is proportional to a power of the driving frequency, c.f. Fig. 2. This was the case in recent experimental realisation of the Harper-Hofstadter Hamiltonian [47, 48, 71], and the Haldane Chern insulator [41]<sup>1</sup> using cold atoms. A general understanding of such nontrivial limits is the main purpose of the present work.

<sup>1</sup>We note that the key equilibrium property of topological states, namely robustness against various small perturbations, is not guaranteed to hold due to generic heating in ergodic driven systems [61–63]

Of course, in real systems the infinite-frequency limit is a mathematical abstraction. Typically, as one increases the driving frequency, new degrees of freedom can enter the game. Examples include internal molecular or atomic resonances in solid state systems or intra-band transitions in cold atom systems confined to optical lattices. Thus, one always deals with finite driving frequencies, which could still be larger than any natural frequency of the non-driven system. In such situations, the infinite-frequency limit of the Floquet Hamiltonian can be a good reference point, but finite frequency corrections can still be significant. For this reason, in this work we discuss both the infinite-frequency limit of various model Hamiltonians, and the leading  $\Omega^{-1}$ -corrections [72].

The main purpose of this review is to discuss different generic scenarios, where one can engineer non-trivial Floquet Hamiltonians in the high-frequency limit. While these scenarios are not exhaustive, they cover a large class of driving protocols, and identify possible roots for finding new interesting Floquet systems. We shall refer to the different classes of driving protocols corresponding to these scenarios as (i) *Kapitza class*: the Hamiltonian is quadratic in momentum, and the driving potential couples only to the coordinates of the particles (either as an external potential or through the interaction term). (ii) *Dirac class*: same as the Kapitza class but for the system with relativistic linear dispersion such as Graphene. (iii) *Dunlap-Kenkre (DK) class*: the periodic drive couples to a single particle potential such as a periodically driven external electric or magnetic field. In the DK class the dispersion relation between particles is not restricted. These classes are not mutually exclusive, e.g. there is a clear overlap between the *Kapitza* class and the *DK* class if one drives a system of non-relativistic particles by an external field, and a similar overlap exists between the *Dirac* class and the *DK* class for particles with a relativistic dispersion.

We will argue that, in models belonging to these three classes, the Floquet Hamiltonian has a nontrivial high-frequency limit, which is qualitatively different from the time-averaged Hamiltonian allowing the systems to display new, qualitatively different features. These non-trivial limits can be used as a tool to realize synthetic matter, i.e. matter with specific engineered properties. On the theoretical side, we justify the existence of stable high-frequency fixed points in  $\Omega$ -space, whose physics is governed by a well-defined effective Hamiltonian. Although such fixed-point Hamiltonians may never be accessible experimentally, they provide a good reference point in many realistic situations. Moreover, the corrections to the effective Hamiltonian, which we also discuss in detail, allow one to estimate the finite frequency effects for particular setups, and find the regimes where these corrections are negligible. We stress that these non-trivial limits exist even for driven ergodic interacting many-particle systems, though interactions often lead to additional finite-frequency corrections to the effective Hamiltonian, which may ultimately result in faster heating rates.

*This review is organized as follows.*

- In Section 2 we review some general properties of the Floquet's theory and define the concept of the Floquet gauge. Then we explicitly analyze an exactly solvable model of a two-level system in a circularly polarized periodic drive. Finally we introduce the concept of the Floquet non-stroboscopic (FNS) and Floquet stroboscopic (FS) dynamics, and compare them. In particular, we explain how the Floquet theory extends to systems where the initial phase of the drive and/or the measurement time fluctuate within the driving period.
- In Section 3 we briefly review the Magnus expansion used for finding the Floquet Hamiltonians in the high frequency limit. We discuss the Magnus expansion both in the lab and in the rotating frames. In the end of this section we briefly comment on the convergence properties of the Magnus expansion.

- Section 4 discusses applications of the Floquet theory to static and driven Hamiltonians with large energy separation between levels. We show how one can derive the rotating wave approximation (RWA) as the leading term in the Magnus expansion and how one can find systematic corrections to RWA. After discussing the toy model of a static two-level system, we show that one can apply the Magnus expansion to derive the Kondo model from the Anderson impurity model, and discuss its relation to the well-established Schrieffer-Wolff transformation extending it to driven systems. We conclude this section with the discussion of the RWA and leading finite frequency corrections applied to the Rabi model effectively deriving corrections to the Jaynes-Cummings Hamiltonian.
- In Section 5 we define the Kapitza high-frequency driving class. We study thoroughly the prototypical example of dynamical stabilization: the Kapitza pendulum. We derive the leading corrections, and analyze dressed observables and the dressed density matrix appearing in FNS dynamics. At the end of this section we discuss higher-dimensional and many-body generalizations of the Kapitza model.
- In Section 6 we define and study the Dirac class, which describes relativistic systems with linear dispersion. We derive the infinite-frequency Hamiltonian and describe some interesting effects, such as a dynamically generated spin-orbit coupling. We show that in this class the leading  $1/\Omega$  corrections to the infinite frequency Hamiltonian vanish and the first non-zero corrections are of order  $1/\Omega^2$  suggesting that systems in this class should be more robust against heating.
- In Section 7, we define the Dunlap-Kenkre (DK) driving class, which includes periodically driven tight-binding models. We begin by studying the shaken bosonic chain, and demonstrate the consequences of FS and FNS dynamics for different observables. Afterwards, we derive the leading corrections to the Harper-Hofstadter Hamiltonian, and the driven Fermi-Hubbard model relevant for Floquet topological insulators. Finally, we briefly discuss some spin Hamiltonians which can be implemented in existing NMR setups.
- In Section 8 we give the summary of this review and an outlook to some open problems.

## 2. Floquet Theory. Stroboscopic and Non-Stroboscopic Time Evolution.

In this section we review Floquet's Theorem. We shall use the language of quantum mechanics but, as will become apparent later on in the next section, all results have a well-defined classical limit. Except in Sec. 3 we will work in the units with  $\hbar = 1$ .

### 2.1. Floquet Hamiltonian and Kick Operators.

Let us consider a dynamical process in which the Hamiltonian depends periodically on time, e.g. through a periodically modulated coupling constant. This means that the evolution operator defined as

$$U(t_2, t_1) = T_t \exp \left[ -i \int_{t_1}^{t_2} H(t) dt \right] \quad (2)$$

is invariant under discrete translations in time  $t_1 \rightarrow t_1 + nT$ ,  $t_2 \rightarrow t_2 + nT$ , where  $n$  is an integer. The factorization (group) property of the evolution operator,  $U(t_2, t_1) = U(t_2, t')U(t', t_1)$  for arbitrary  $t'$ , implies that  $U(t_0 + 2T, t_0) = U(t_0 + 2T, t_0 + T)U(t_0 +$

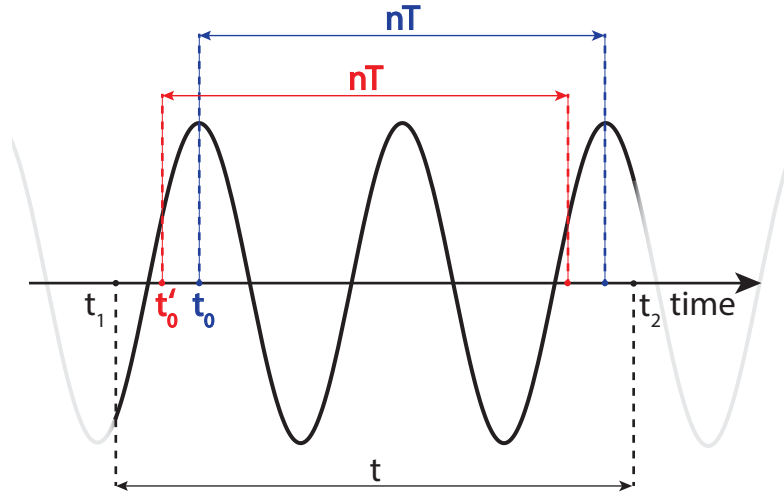


Figure 3. (Color online) Floquet gauge: the system evolves from time  $t_1$  to time  $t_2$ . The stroboscopic evolution starts at time  $t_0$  which can be chosen to be anywhere within the first period  $[t_1, t_1 + T)$ . The choice of the Floquet gauge, i.e. the choice of  $t_0$ , in general affects the form of the Floquet Hamiltonian.

$T, t_0) = U(t_0 + T, t_0)^2$ , which generalizes to

$$U(t_0 + nT, t_0) = U(t_0 + T, t_0)^n. \quad (3)$$

It is convenient to formally define the evolution within one period as an evolution with the time-independent (effective) Floquet Hamiltonian

$$U(t_0 + T, t_0) = \exp[-iH_F[t_0]T]. \quad (4)$$

This representation is always possible because  $U(t_0 + T, t_0)$  is a unitary operator. The Floquet Hamiltonian  $H_F[t_0]$  defined in this way depends on the choice of the initial time  $t_0$ , which can change within a driving period. This is a gauge choice, and it is completely arbitrary. To avoid confusion with conventional gauge transformations, related to the arbitrary choice of basis, we shall term the gauge associated with the choice of  $t_0$  the *Floquet gauge*. For example, the Floquet gauge invariance of an observable implies invariance w.r.t. the choice of  $t_0$ , and so on. Usually, one chooses a particular Floquet gauge, in which the effective Hamiltonian assumes its simplest form. This often happens when  $t_0$  is a symmetric point of the driving protocol. For example, if the driving field is  $\cos \Omega t$ , it is often convenient to choose  $t_0 = 0$ .

It becomes clear from Fig. 3 that for arbitrary times  $t_1$  and  $t_2$  the evolution operator can always be written as

$$U(t_2, t_1) = U(t_2, t_0 + nT) \exp[-iH_F[t_0]nT] U(t_0, t_1). \quad (5)$$

The initial and final evolution operators  $U(t_0, t_1)$  and  $U(t_2, t_0 + nT)$  effectively occur during small intervals of time  $\delta t_1 = (t_1 - t_0)$  and  $\delta t_2 = (t_2 - nT - t_0)$  which can always be chosen such that  $\delta t_1 \in [-T, 0]$  and  $\delta t_2 \in [0, T]$ . The operators  $U(t_0, t_1)$  and  $U(t_2, t_0 + nT)$  are necessary to bring the time from the initial point of the evolution  $t_1$  to  $t_0$ , and from the last full period  $t_0 + nT$  to the final point of evolution  $t_2$ . These are precisely the times associates with the initial and final kicks, discussed in Ref. [65]. By construction  $U(t_0, t_0) = \mathbf{1}$  and  $U(t_0 + T, t_0) = \exp[-iH_F[t_0]T]$ . Now we can easily rewrite Eq. (5) in

the form of Eq. (1) by doing a simple trick

$$U(t_2, t_1) = U(t_2, t_0 + nT) e^{iH_F[t_0](t_2 - t_0 - nT)} e^{-iH_F[t_0](t_2 - t_0 - nT)} e^{-iH_F[t_0]nT} \\ e^{-iH_F[t_0](t_0 - t_1)} e^{iH_F[t_0](t_0 - t_1)} U(t_0, t_1) = P(\delta t_2) e^{-iH_F[t_0](t_2 - t_1)} P^\dagger(\delta t_1), \quad (6)$$

where

$$P(t) \equiv U(t_0 + t, t_0) e^{iH_F[t_0]t}. \quad (7)$$

Note that, with the above definition, the operator  $P$  is periodic and, by construction, it satisfies the property  $P(nT) = 1$  for an arbitrary integer  $n$ .

Let us mention that the Floquet's theorem can also be formulated in two other ways. In one formulation, it states that the evolution operator can be written as the product of two unitary operators:

$$U(t_2, t_1) = P(t_2) e^{-iH_F[t_1](t_1 - t_2)}, \quad (8)$$

where  $H_F[t_1]$  is a particular Floquet Hamiltonian. Alternatively, one can formulate Floquet's theorem as

$$U(t_2, t_1) = e^{-iH_F[t_2](t_1 - t_2)} P^\dagger(-t_1), \quad (9)$$

where  $H_F[t_2]$  is another Floquet Hamiltonian. These versions of Floquet's theorem given by Eqs. (8) and (9) can be derived from the most general case, Eq. (1), if we choose  $t_0 = t_1 \bmod T$  or  $t_0 = t_2 \bmod T$ . In this way, the expression for the evolution operator simplifies, since only one periodic operator appears. However, this simplification can be somewhat deceptive, because in these cases, the Floquet Hamiltonian is tied to the initial (final) times of the evolution, and its definition continuously changes with one of those times. Since in experiments, especially in the high-frequency limit, both the initial time and the final (measurement) time often fluctuate within a period, it is more convenient to tie the Floquet Hamiltonian to some fixed Floquet gauge, independent of both  $t_1$  and  $t_2$ .

From Eq. (5) and the factorization property of the evolution operator it becomes clear that the choice of  $t_0$ , defining the Floquet Hamiltonian, is indeed a gauge choice. To see this, we write the evolution operator  $U(t_0 + nT, t_0)$  in two different (but equivalent) ways:

$$U(t_0 + nT, t_0) = e^{-iH_F[t_0]nT} = U^\dagger(t_0 + \delta t_0, t_0) e^{-iH_F[t_0 + \delta t_0]nT} U(t_0 + \delta t_0, t_0). \quad (10)$$

This is equivalent to the gauge transformation of the Floquet Hamiltonian

$$H_F[t_0 + \delta t_0] = U(t_0 + \delta t_0, t_0) H_F[t_0] U^\dagger(t_0 + \delta t_0, t_0). \quad (11)$$

As expected, this Floquet gauge is periodic and continuous, such that  $H_F[t_0 + T] = H_F[t_0]$ . We emphasise that the Floquet gauge transformation is a direct consequence of Eqs. (4) and (5). Therefore, we conclude that changing the Floquet gauge  $t_0 \rightarrow t_0 + \delta t_0$  leads to  $H_F[t] \rightarrow H_F[t_0 + \delta t_0]$  and to the redefinition  $\delta t_1 \rightarrow \delta t_1 - \delta t_0$  and  $\delta t_2 \rightarrow \delta t_2 - \delta t_0$  of the time intervals appearing in the kick operator  $P$ , see Eqs. (6) and (7).

Let us also point out that one can rewrite Floquet's theorem in a differential form [6, 69, 73]. Indeed, on the one hand, for any Hamiltonian evolution one can write

$$i\partial_{t_2} U(t_2, t_1) = H(t_2) U(t_2, t_1). \quad (12)$$



On the other hand, using Eq. (6) we arrive at

$$i\partial_{t_2}U(t_2, t_1) = (i\partial_{t_2}P(t_2))e^{-iH_F[t_0](t_2-t_1)}P^\dagger(t_1) + P(t_2)H_F[t_0]e^{-iH_F[t_0](t_2-t_1)}P^\dagger(t_1).$$

Equating these two expressions, we find

$$H_F[t_0] = P^\dagger(t_2)H(t_2)P(t_2) - iP^\dagger(t_2)\partial_{t_2}P(t_2) \quad (13)$$

or, equivalently,

$$H(t_2) = P(t_2)H_F[t_0]P^\dagger(t_2) + i(\partial_{t_2}P(t_2))P^\dagger(t_2). \quad (14)$$

Equation (13) can be viewed as a statement of the existence of a periodic operator  $P(t)$  such that the RHS of this equation is time-independent. Very often, in the literature this equation is used as a starting point to find the Floquet Hamiltonian iteratively [6, 66, 69, 73]. Due the gauge freedom associated with the choice of  $t_0$ , the solution of this equation is not unique, but all solutions are gauge-equivalent. Another possible application of Eq. (14) is that it allows one to do ‘reverse-engineering’. Once the Floquet Hamiltonian  $H_F$  and the periodic operator  $P(t)$  with interesting properties are chosen, one can use Eq. (14) to determine which time-dependent driving protocol  $H(t)$  needs to be experimentally implemented to realize those properties.

## 2.2. A Two-Level System in a Circularly Driven Magnetic Field

Let us illustrate the construction above using a simple example of a two-level system in a rotating magnetic field:

$$H(t) = B_z\sigma_z + B_\parallel (\cos\Omega t \sigma_x + \sin\Omega t \sigma_y). \quad (15)$$

This Hamiltonian becomes time independent in the rotating frame:

$$H^{\text{rot}} = V^\dagger(t)H(t)V(t) - iV^\dagger(t)\dot{V}(t) = B_z\sigma_z + B_\parallel\sigma_x - \frac{\Omega}{2}\sigma_z \quad (16)$$

where  $V(t) = \exp[-i\frac{\sigma_z}{2}\Omega(t-t_0)]$  is the operator which transforms from the rotating frame into the lab frame. The evolution operator in the original (lab frame) can be evaluated by first going into the rotating reference frame where the Hamiltonian is time-independent (and therefore the evolution is simple), and then transforming back to the lab reference frame:

$$U(t_2, t_1) = V(t_2) e^{-iH^{\text{rot}}[t_0](t_2-t_1)} V^\dagger(t_1). \quad (17)$$

This structure of the evolution operator resembles the Floquet ansatz (6) with the only caveat that the function  $V(t)$  is periodic with twice the period of the driving. This would imply that  $U(t_0 + T, t_0) \neq \exp(-iH^{\text{rot}}[t_0]T)$ , which is inconsistent with Eq. (4). However, if we double the period  $T \rightarrow 2T$  then we will restore the correct form of the evolution:  $U(t_0 + 2T, t_0) = \exp(-iH^{\text{rot}}[t_0]2T)$ . It is easy to see that this period doubling is related to the fact that we are dealing here with a half integer spin. It is, however, easy to find the correct Floquet Hamiltonian without period doubling by adding a simple

spin-independent phase shift to the rotation operator  $V$ :

$$V(t) \rightarrow \tilde{V}(t) = \exp \left[ -i \frac{\sigma_z - \mathbf{1}}{2} \Omega(t - t_0) \right]. \quad (18)$$

It is clear that  $\tilde{V}$  does the same transformation to the rotating frame as  $V$  apart from a constant energy shift. So we can now write the full evolution operator in the form given by Eq. (6) where

$$P(t) = \tilde{V}(t), \quad H_F = H^{\text{rot}} + \frac{\Omega}{2} \mathbf{1}. \quad (19)$$

The discussion here is not limited to two-level systems and the transformation to the rotating frame can be performed for any system using the operator  $V(t) = \exp[-i \mathbf{L} \cdot \boldsymbol{\Omega} t]$  where  $\mathbf{L}$  is the total angular momentum. Obviously doing a transformation to the rotating frame only helps, if the stationary part of the Hamiltonian is rotationally invariant. Otherwise, Floquet's theory tells us that Eq. (6) still applies but the Floquet Hamiltonian  $H_F$  is not directly related to the Hamiltonian in the rotating reference frame.

In certain situations one can completely eliminate the time dependence of the lab-frame Hamiltonian, and find  $H_F$  by performing two consecutive transformations in two rotating frames [74]. In general, however,  $H_F$  can only be written through an infinite series of transformations. In Refs. [6, 66, 73] it was realized that the operator  $P(t)$  can be interpreted as a quantum analogue of the generating function of a canonical transformation, and  $H_F$  - as the Hamiltonian in the new reference frame (see Eq. (13)). Therefore the Floquet theorem could be stated as follows. For *any* time-periodic Hamiltonian, there exist infinitely many reference frames in which the time evolution is generated by a time-independent Hamiltonian, i.e. the Floquet Hamiltonian. Unfortunately, in general, it is not possible to find the transformation from the lab to these new reference frames explicitly.

The Floquet Hamiltonian we just obtained by going to the rotating frame (c.f. Eq. (19)) is not well-defined in the infinite frequency limit. Indeed, it has two eigenvalues

$$\epsilon_{\pm} = \frac{\Omega}{2} \pm \sqrt{(B_z - \Omega/2)^2 + B_{\parallel}^2},$$

one of which diverges as  $\Omega \rightarrow \infty$ . On the other hand, from Eq. (15), one would naively expect that in this limit the Floquet Hamiltonian reduces to the time-averaged Hamiltonian  $\frac{1}{T} \int_0^T H(t) dt = B_z \sigma_z$ . There is no fundamental issue here since the Floquet energies are defined modulo  $\Omega$ . To identify the proper infinite-frequency  $H_F$  in this simple case one has to find the spectrum  $\epsilon \bmod \Omega$  first (if necessary by Taylor-expanding the Floquet energies), and only then take the limit  $\Omega \rightarrow \infty$ .

It is possible to obtain the Floquet Hamiltonian, which does not suffer from the infinite-frequency divergence, but the transformation to the rotating frame becomes much more complicated. Choosing the Floquet gauge  $t_0 = 0$ , from the identity

$$\exp(-i H_F 2T) = U(2T, 0) = \exp(-i H^{\text{rot}} 2T). \quad (20)$$

it is clear that  $H_F$  and  $H^{\text{rot}}$  share the same eigenstates while their eigenvalues can only differ by a shift  $\pm \Omega/2$ . Thus, if the Hamiltonian  $H^{\text{rot}}$  (see Eq. (16)) has energies  $\pm \epsilon_{\text{rot}}$ , where

$$\epsilon_{\text{rot}} = \sqrt{(B_z - \Omega/2)^2 + B_{\parallel}^2}$$

diverges as  $\Omega \rightarrow \infty$ , the Floquet Hamiltonian should have energies  $\pm\epsilon_F$  where

$$\epsilon_F = \left( \epsilon_{\text{rot}} - \frac{\Omega}{2} \right) = \epsilon_{\text{rot}} \left( 1 - \frac{\Omega}{2\epsilon_{\text{rot}}} \right).$$

If  $S$  is a unitary matrix diagonalizing  $H^{\text{rot}}$ , such that  $SH^{\text{rot}}S^\dagger = \epsilon_{\text{rot}}\sigma_z$  then it is clear that the Floquet Hamiltonian, which does not suffer from the infinite frequency divergence is

$$H_F = S^\dagger \epsilon_F \sigma_z S = \left( 1 - \frac{\Omega}{2\epsilon_{\text{rot}}} \right) H^{\text{rot}}.$$

From Eq. (17), the Floquet ansatz in Eq. (8), and the relation between  $H_F$  and  $H^{\text{rot}}$  in Eq. (20) it immediately follows that the operator  $P(t)$  corresponding to this Floquet Hamiltonian is the composition of two rotations in spin space:

$$P(t) = \exp\left(-i\frac{\sigma_z}{2}\Omega t\right) \exp\left(-i\frac{H^{\text{rot}}}{2\epsilon_{\text{rot}}}\Omega t\right).$$

Note that, as required,  $P(t)$  is periodic with period  $T = 2\pi/\Omega$ .

The analysis above can be extended to more complex rotating setups. However, finding the properly folded Floquet Hamiltonian in general can be a formidable task, since it requires the knowledge of the spectrum of  $H^{\text{rot}}$ , which may be quite complicated if the system is interacting. In the next section, we shall discuss how one can perturbatively construct Floquet Hamiltonians, which have well-behaved infinite-frequency limits.

### 2.3. *Stroboscopic vs. Non-stroboscopic Dynamics*

As we discussed in the beginning of the section, the evolution operator for Floquet systems can be written as the exponential of the Floquet Hamiltonian sandwiched between two periodic unitary operators, c.f. Eq. (6). We now use this observation to find the expectation values of observables. To simplify the discussion, we shall focus only on equal-time expectation values. The generalization to nonequal-time correlation functions is straightforward.

Consider an observable  $\mathcal{O}(t_2)$  in the Heisenberg picture, where it explicitly depends on time. Also, let us assume that initially (at time  $t_1$ ) the system is prepared in some state described by the density matrix  $\rho$ , which in the Heisenberg picture remains time-independent. Then

$$\begin{aligned} \langle \mathcal{O}(t_2) \rangle &= \text{Tr} \left( \rho U^\dagger(t_2, t_1) \mathcal{O} U(t_2, t_1) \right) \\ &= \text{Tr} \left( \rho P(\delta t_1) e^{iH_F(t_2-t_1)} P^\dagger(\delta t_2) \mathcal{O} P(\delta t_2) e^{-iH_F(t_2-t_1)} P^\dagger(\delta t_1) \right) \\ &= \text{Tr} \left( P^\dagger(\delta t_1) \rho P(\delta t_1) e^{iH_F(t_2-t_1)} P^\dagger(\delta t_2) \mathcal{O} P(\delta t_2) e^{-iH_F(t_2-t_1)} \right), \end{aligned} \quad (21)$$

where as before  $\delta t_1 = t_1 - t_0 \in [-T, 0]$  and  $\delta t_2 = t_2 - nT - t_0 \in [0, T]$  (c.f. Fig. 4), and we remind that  $t_0$  is the Floquet gauge choice. We see that the dynamics of the system is solely generated by the Floquet Hamiltonian if we properly identify a new density matrix and a new observable as

$$\rho \rightarrow P^\dagger(\delta t_1) \rho P(\delta t_1), \quad \mathcal{O} \rightarrow P^\dagger(\delta t_2) \mathcal{O} P(\delta t_2).$$

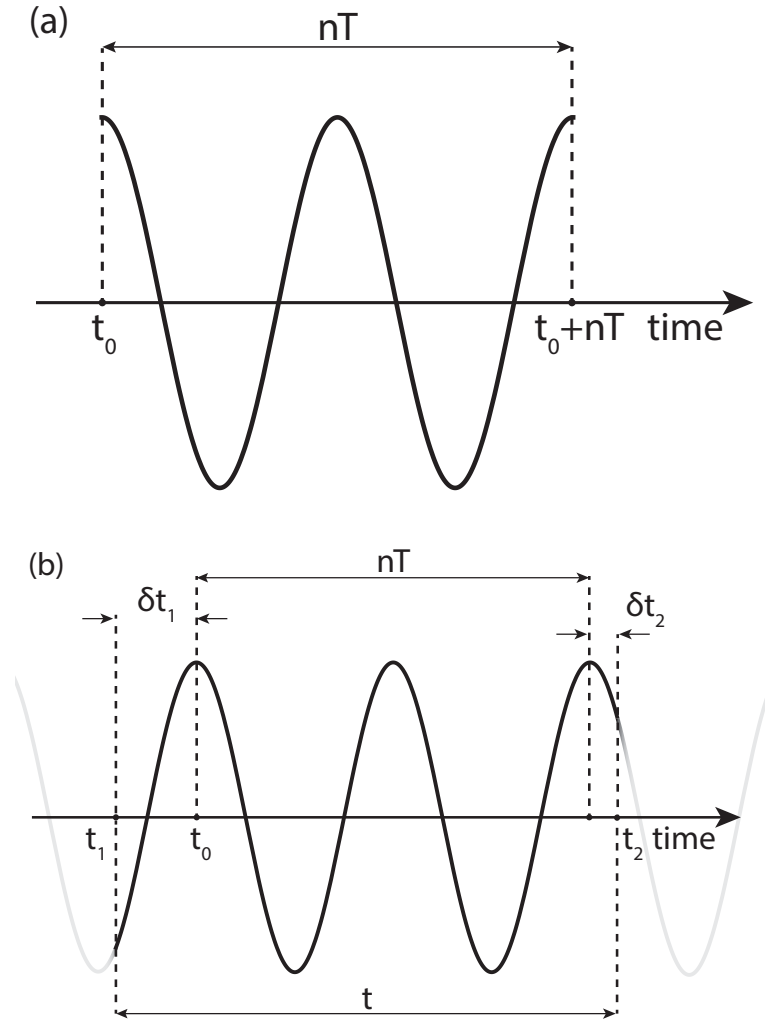


Figure 4. Floquet stroboscopic (FS) vs Floquet non-stroboscopic (FNS) schemes. (a) In the FS scheme the driving is initialized at time  $t_0 = 0$  when the stroboscopic frame starts and the measurement is performed after exactly  $n$  periods at time  $nT$ . (b) In the FNS scheme the driving is initiated at time  $t_1$ , the stroboscopic evolution begins at  $t_0$  and the measurement is carried out at time  $t_2$  within the  $(n + 1)$ -st driving period. We chose the convention  $\delta t_1 = t_1 - t_0 \in [-T, 0]$  and  $\delta t_2 = t_2 - nT - t_0 \in [0, T]$ . In the FNS scheme, the expectation values of the observables are obtained by averaging over  $\delta t_1$  and  $\delta t_2$ .

The operators  $P(\delta t_1)$  and  $P(\delta t_2)$  can be viewed as time-dependent gauge transformations applied to the initial density matrix (wave function) and the observable. In Ref. [65] they were termed the initial and the final ‘kicks’. These operators are periodic and depend only on the times  $\delta t_1$  and  $\delta t_2$ , bringing the system to the beginning of the first period and to the measurement point after the last period, respectively (see Fig. 4).

The simplest case, which is often discussed in the literature, is when the initial time  $t_i$  coincides with  $t_0$  and the final time is  $t_f = t_0 + nT$  (see Fig. 4, Panel (a)). Then  $P(\delta t_1) = P(\delta t_2) = \mathbf{1}$  are identity operators, and the operators  $\rho$  and  $\mathcal{O}$  are not modified. This setup defines the so called *Floquet stroboscopic (FS)* dynamics. Very often, analyzing such FS dynamics is sufficient for describing the whole time evolution. This happens when the observable and the initial density matrix are almost Floquet-gauge invariant, i.e. almost do not change within a period. However, often one deals with more complex setups where this is not the case. Then the kick operators  $P^\dagger(\delta t_1)$  and  $P(\delta t_2)$  are essential for understanding the full dynamics [65].

Another common setup, which naturally occurs in experiments, emerges if the initial

phase of the driving and the measurement time, defining the intervals  $\delta t_1$  and  $\delta t_2$ , are essentially random variables (c.f. Fig. 4, Panel (b)). Then one has to average the expectation value of  $\mathcal{O}(t)$  over these times. From Eq. (21) it becomes clear that this averaging procedure affects both the density matrix and the observable while it does not affect the time-evolution which is always generated by the same Floquet Hamiltonian. This scenario, in which both the initial phase and the measurement time are random within the period, but independent from each other, we term *Floquet non-stroboscopic (FNS)* dynamics. One can also consider other schemes, where e.g. the initial phase is deterministic but the measurement time is random, or conversely the initial phase is random but the measurement is locked to the phase of the drive. We shall not consider such situations but from our discussion it will become clear how one can find the appropriate density matrix and the observable. With our definitions, the Floquet Hamiltonian will always stay the same, no matter which evolution scheme is assumed.

In order to obtain an accurate description of the FNS evolution, one needs to average the density matrix and the operator in Eq. (21) with respect to  $\delta t_1$  and  $\delta t_2$ :

$$\bar{\rho} = \overline{P^\dagger(\delta t_1)\rho P(\delta t_1)}, \quad \bar{\mathcal{O}} = \overline{P^\dagger(\delta t_2)\mathcal{O}P(\delta t_2)}, \quad (22)$$

where the bar implies averaging over some, say Gaussian, distribution for  $\delta t_{1/2}$ . Note that because  $P(t)$  is a periodic operator, the averaging over  $\delta t_1$  and  $\delta t_2$  becomes equivalent to averaging over the period if the width of the distribution becomes larger than the driving period. In the following, we shall focus on this situation. We note that averaging over the period in  $\delta t_1$  is also equivalent to the averaging over the initial phase of the driving protocol. Then the whole time evolution is effectively described by the quench to the Floquet Hamiltonian starting from the dressed density matrix  $\bar{\rho}$  instead of  $\rho$  and measuring the dressed operator  $\bar{\mathcal{O}}$  instead of  $\mathcal{O}$ . There is a certain care needed in precisely understanding this statement. We assumed that  $\delta t_1$ ,  $\delta t_2$  and  $t = t_2 - t_1$  are statistically independent variables, while in reality they are related by  $\delta t_2 - \delta t_1 + nT = t$ . However, they become effectively independent if the number of periods  $n$  is large, so that either  $n$  itself is a fluctuating number, or the period  $T$  has small fluctuations from experiment to experiment. Then the equivalence between the FNS evolution and the exact dynamics should be understood in a sense that if we do yet a third average of both expectation values over a small time window  $2\Delta t$  (longer than the period  $T$  but much shorter than the total time  $t$ ), we obtain identical results:

$$\int_{\tilde{t}-\Delta t}^{\tilde{t}+\Delta t} dt \langle \mathcal{O}(t) \rangle = \int_{\tilde{t}-\Delta t}^{\tilde{t}+\Delta t} dt \text{Tr} [\bar{\rho} e^{iH_F t} \bar{\mathcal{O}} e^{-iH_F t}]. \quad (23)$$

Practically, this averaging only implies that we get rid of the spurious high-frequency oscillations. Clearly  $\bar{\rho}$  and  $\bar{\mathcal{O}}$  are Floquet-gauge invariant, i.e. independent of the stroboscopic time  $t_0$ , because they involve averaging over the full driving period. Note that, even if one starts from a pure state described by a wave function, in the FNS scheme, averaging over  $\delta t_1$  generates a mixed state. In this sense, the initial uncertainty in the phase of the driving plays a similar role to temperature since both broaden the distribution. Intuitively, the difference between  $\rho$  and  $\bar{\rho}$  is determined by how much the density matrix changes within one period. Similarly, the difference between  $\mathcal{O}$  and  $\bar{\mathcal{O}}$  can be large or small, depending on how much the observable changes within one period. For instance, in the rotating spin example  $\sigma_z$  is gauge invariant, and hence  $\sigma_z$  and  $\bar{\sigma}_z$  coincide, while for  $\sigma_x$  the difference with  $\bar{\sigma}_x = 0$  is very significant.

The dressed operators have some unusual properties. In particular, from the definition

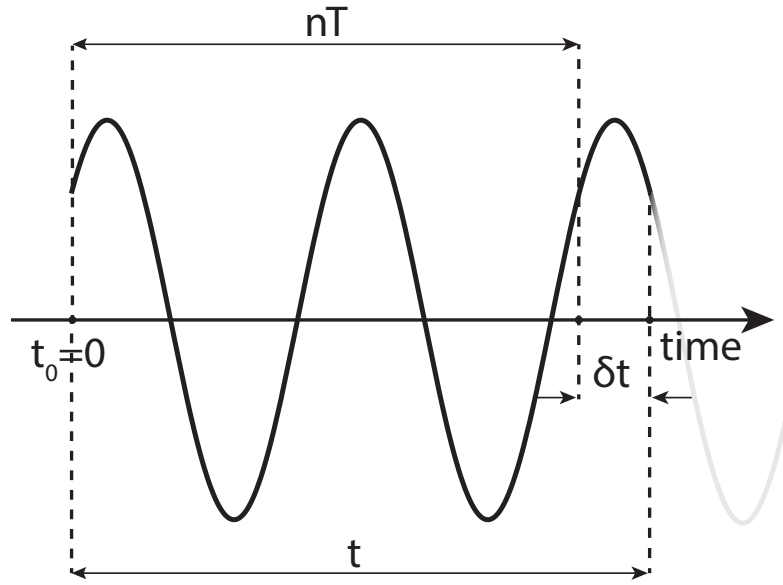


Figure 5. (Color online). Floquet gauge used for deriving Heisenberg's equation of motion for the dressed operator, c.f. Eq. (25).

it becomes clear that  $\overline{\mathcal{O}^2} \neq (\overline{\mathcal{O}})^2$ , e.g. in the rotating spin example  $\overline{\sigma_x^2} = 1 \neq (\overline{\sigma_x})^2 = 0$ . Another example illustrating this property of dressed operators is discussed in detail in Sec. 5.4, Eq. (87). We also observe that, in the high-frequency limit, the dressed operators satisfy the Heisenberg equations of motion with the Floquet Hamiltonian. Indeed, let us consider the Heisenberg equation of motion for some operator  $\mathcal{O}(t)$ . To simplify notations, let us fix the Floquet gauge so that the initial time coincides with the beginning of the stroboscopic reference frame, i.e.  $t_1 = t_0 = 0$ , from which it also follows that  $t = t_2$  and  $\delta t_2 = t - nT = \delta t$  (see Fig. 5). Using the Floquet ansatz (8), we obtain:

$$\begin{aligned} i\partial_t \mathcal{O}(t) &= i\partial_t \left( e^{iH_F t} P^\dagger(\delta t) \mathcal{O} P(\delta t) e^{-iH_F t} \right) \\ &= e^{iH_F t} [P^\dagger(\delta t) \mathcal{O} P(\delta t), H_F] e^{-iH_F t} + i e^{iH_F t} \partial_t \left( P^\dagger(\delta t) \mathcal{O} P(\delta t) \right) e^{-iH_F t}. \end{aligned} \quad (24)$$

We can average both sides of this equation over a period w.r.t. the variable  $\delta t$  assuming, as before, that  $t$  and  $\delta t$  are independent variables. The latter has to be understood in the sense of Eq. (23). Notice that the last term vanishes, since the average of a derivative of a periodic function is zero. As a result we find

$$i\partial_t \overline{\mathcal{O}(t)} = i\partial_t \overline{\mathcal{O}(t)} = [\overline{\mathcal{O}(t)}, H_F], \quad (25)$$

This equation is the Heisenberg equation of motion for the dressed operator. The left equality in Eq. (25) is similar to the Hellmann-Feynman theorem, in which the average over the quantum state plays a role analogous to the average over the periodic operators  $P(\delta t)$ . If  $\mathcal{O}$  represents a conserved quantity, then we can define an associated current  $\mathbf{J}_{\mathcal{O}}$  through

$$\partial_t \mathcal{O}(t) + \nabla \cdot \mathbf{J}_{\mathcal{O}}(t) = 0. \quad (26)$$

Averaging both sides of this equation over time and using Eq. (25), we see that the time average of the current operator must represent the dressed current  $\overline{\mathbf{J}_{\mathcal{O}}}$  governing the

slow evolution of  $\mathcal{O}$ :

$$\overline{\mathbf{J}}_{\mathcal{O}} = \overline{P^\dagger(\delta t) \mathbf{J}_{\mathcal{O}} P(\delta t)}. \quad (27)$$

Thus, both in numerical simulations and in experiments, in order to measure the current associated with the Floquet Hamiltonian one has to average the current operator in the lab frame over the period. In contrast, the current evaluated at some fixed stroboscopic time  $t = nT$  will be a different object, involving both information about the Floquet evolution governed by  $H_F$ , and an additional contribution related to the derivative of the kick operator. We shall return to this issue as well as to general differences between FS and FNS dynamics later on, when we discuss specific examples. We will show that, using stroboscopic measurements, one can *not* obtain the current corresponding to the Floquet Hamiltonian at any driving frequency. On the other hand, implementing the FNS scheme and averaging the expectation values over the driving period, the Floquet current can be obtained in the high-frequency limit 7.1. Recently, it was proposed to detect the topological character of the ground state in fermionic systems by measuring the magnetisation of a finite-size sample due to the chiral currents flowing at the edges [75]. This proposal explicitly made use of the FNS measurement.

### 3. The Magnus Expansion

With very few exceptions, like uniform rotations or driven harmonic systems where the evolution operator can be found exactly, it is impossible to obtain the Floquet Hamiltonian in a closed form. Moreover, in situations where the periodic driving leads to chaotic dynamics at a single particle level [1, 2] or to heating to infinite temperatures for many-particle systems [61–64] local Floquet Hamiltonians do not exist. An important limit where one can define the Floquet Hamiltonian at least perturbatively corresponds to the situations of fast driving, where the driving frequency is much faster than all natural frequencies of the system. For example, for a pendulum the driving should be fast compared to the oscillation period, for particles in a periodic potential the driving should be faster than the band width or a typical interaction scale. In such situations, the system has a hard time absorbing energy from the drive, which results in virtual processes dressing the Hamiltonian.

#### 3.1. Deriving Floquet Hamiltonians with the Magnus Expansion

A very efficient tool to compute the Floquet Hamiltonian in the high-frequency limit is the Magnus expansion, which is a perturbative scheme in the driving period  $T$  to compute  $H_F$ . See Ref. [76] for a summary of other perturbative methods to find effective Hamiltonians in the high-frequency limit. In general, it is not known whether the Magnus expansion is asymptotic or has a finite radius of convergence, especially in the thermodynamic limit. The issue of the convergence of the Magnus expansion is important for understanding the behavior of the system in the limit  $t \rightarrow \infty$ . However, if one is interested in describing a finite-time evolution, then the short period expansion is well behaved and the Magnus expansion can be safely used. The evolution operator over a full driving cycle is, in general, given by the time-ordered exponential of  $H(t)$ :

$$U(T + t_0, t_0) = \mathcal{T}_t \exp \left( -\frac{i}{\hbar} \int_{t_0}^{T+t_0} dt H(t) \right) = \exp \left( -\frac{i}{\hbar} H_F[t_0]T \right)$$

where we have used the Floquet Theorem (4) setting  $t_0 = 0$  to simplify the notation. In this section we explicitly insert the factors of  $\hbar$  to highlight that the limit  $\hbar \rightarrow 0$  is well-defined, and the expansion applies both to quantum and classical systems. Taking the logarithm of both sides of the equation above and expanding the exponents in a Taylor series, which is justified if the period is sufficiently short, one can represent  $H_F$  as [72]:

$$H_F = \sum_{n=0}^{\infty} H_F^{(n)}.$$

The first few terms are given by

$$\begin{aligned} H_F^{(0)} &= \frac{1}{T} \int_0^T dt H(t), \\ H_F^{(1)}[t_0] &= \frac{1}{2!T i \hbar} \int_{t_0}^{T+t_0} dt_1 \int_{t_0}^{t_1} dt_2 [H(t_1), H(t_2)], \\ H_F^{(2)}[t_0] &= \frac{1}{3!T (i \hbar)^2} \int_{t_0}^{T+t_0} dt_1 \int_{t_0}^{t_1} dt_2 \int_{t_0}^{t_2} dt_3 \left( [H(t_1), [H(t_2), H(t_3)]] + (1 \leftrightarrow 3) \right). \end{aligned} \quad (28)$$

Note that the corrections to the Magnus Hamiltonian, in general depend on the Floquet gauge  $t_0$ .

The zeroth-order term  $H_F^{(0)}$  is simply the time-averaged Hamiltonian. Higher-order terms contain nested casual commutators of  $H(t)$  and multiple time-ordered integrals. For classical systems, the equivalent expansion can be obtained by substituting the commutators between the operators with the Poisson brackets of the corresponding classical functions:  $[\cdot, \cdot]/i\hbar \rightarrow \{\cdot, \cdot\}$ . For a numerical algorithm to implement the Magnus series, see Ref. [77].

One can obtain a useful formula [49, 65] for  $H_F^{(1)}[t_0]$  by Fourier-decomposing the time-periodic Hamiltonian in its harmonics as:

$$\begin{aligned} H(t) &= \sum_{l \in \mathbb{Z}} H_l e^{il\Omega t} \\ H_F^{(1)}[t_0] &= \frac{1}{\Omega} \sum_{l=1}^{\infty} \frac{1}{l} \left( [H_l, H_{-l}] - e^{il\Omega t_0} [H_l, H_0] + e^{-il\Omega t_0} [H_{-l}, H_0] \right), \end{aligned} \quad (29)$$

where  $H_l$  is an operator-valued expansion coefficient. It can be tempting to average the Floquet Hamiltonian over different Floquet gauges, i.e. over  $t_0$ , and truncate the sum above retaining only the first term, i.e.  $l = 1$ . However, as it was shown in details in Ref. [49], especially in the case of strong driving terms with  $l > 1$  need to be included to correctly describe the experimental results. Moreover, while the averaging over  $t_0$  is effectively implemented using the dressed observables measured in FNS dynamics (see Sec. 2.3), one cannot do this for the Hamiltonian governing the evolution. This is because the average (over gauges) of the evolution operator is not the same as the evolution operator with the averaged Hamiltonian. Instead, one should *fix the Floquet gauge* at any convenient value once and for all, and use this value consistently throughout the calculation. This is in complete analogy with, for example, what it is routinely done in the case of electromagnetic gauges. In that case the Hamiltonian is written in a specific



gauge and the only requirement is that the outcome of a gauge-invariant observables is independent on the gauge chosen.

Whenever the parameters in the Hamiltonian do not scale with the driving frequency, the  $n$ -th order term in the Magnus expansion is proportional to  $T^n$ . Thus, the higher-order terms get more and more suppressed as the period  $T \rightarrow 0$ . It then follows that in the infinite-frequency limit  $H_F$  reduces to the time-averaged Hamiltonian, as one would intuitively expect. As we shall discuss later in greater detail, very interesting nontrivial limits can occur when some couplings in the Hamiltonian scale with frequency. In this case, higher-order terms in the Magnus expansion can be of the same order in the period  $T$ . Then in the infinite-frequency limit, one can obtain nontrivial Floquet Hamiltonians, very different from  $H_F^{(0)}$ , as it is the case for the Kapitza pendulum. The Magnus expansion helps one to identify both the leading and subleading terms in the driving period  $T$  for different models. It also allows one to understand the required scaling behavior of the driving amplitude with the frequency to obtain interesting infinite-frequency limits. And finally, it can be used to design protocols suitable for engineering synthetic Floquet Hamiltonians with prescribed properties.

### 3.2. The Magnus Expansion in the Rotating Frame

In many instances, in particular when the driving amplitude scales with frequency, one needs to re-sum an infinite sub-series in the Magnus expansion to obtain the proper infinite-frequency Floquet Hamiltonian. For example, let us imagine the simplest protocol

$$H(t) = H_0 + \lambda(t)H_1, \quad (30)$$

where  $\lambda(t)$  is a periodic function with zero mean, whose period is  $T$ , and whose amplitude is proportional to the driving frequency  $\Omega$ . Then from Eq. (28) it is clear that the terms in the  $n$ -th order of the Magnus expansion containing once  $H_0$  and  $(n-1)$  times  $H_1$  are all independent of the period, while the other terms which contain  $H_0$  more than once are subleading and vanish in the limit  $T \rightarrow 0$ . This may look like a special case, but it is precisely the setup necessary to obtain interesting Floquet Hamiltonians with nontrivial properties.

One can significantly simplify the analysis of the Magnus series if the Hamiltonian can be written in the form (30) or more generally as

$$H(t) = H_0 + \sum_{j=1}^n \lambda_j(t)H_j,$$

where  $\lambda_j(t)$  are periodic functions with the same common period and  $H_j$   $j = 1, \dots, n$ , are mutually commuting terms (but not commuting with  $H_0$ ). Notice that since the driving amplitude scales with the driving frequency, it is not immediately clear what the infinite-frequency limit is. In such situations, it is convenient to first make a transformation into a rotating frame (rot frame). Focusing on the Hamiltonian (30) we define the rotation operator as

$$V(t) = \exp \left[ -\frac{i}{\hbar} \left( \int_{t_0}^t \lambda(t') dt' \right) H_1 \right], \quad (31)$$

where as before the choice of  $t_0$  is the gauge choice. We adopt the convention that  $V(t)$  transforms from the rot frame into the lab frame. In the rotating frame the density matrix

and the operators transform as

$$\begin{aligned} |\psi^{\text{rot}}(t_1)\rangle &= V^\dagger(t_1)|\psi(t_1)\rangle, \quad \rho^{\text{rot}}(t_1) = V^\dagger(t_1)\rho(t_1)V(t_1), \\ \mathcal{O}^{\text{rot}}(t_2) &= V^\dagger(t_2)\mathcal{O}(t_2)V(t_2). \end{aligned} \quad (32)$$

The Hamiltonian in the rotating frame acquires an extra time-dependent term due to the fact that the transformation is time-dependent:

$$\begin{aligned} H^{\text{rot}}(t) &= V^\dagger(t)[H_0 + \lambda(t)H_1]V(t) - i\hbar V^\dagger(t)\partial_t V(t) \\ &= V^\dagger(t)H_0V(t). \end{aligned} \quad (33)$$

Thus, the transformation to the rotating frame removes the oscillating term with a divergent amplitude  $H_1$ , effectively replacing it by a Hamiltonian with a fast oscillating phase. Note that  $H^{\text{rot}}(t)$  is a periodic function of time, if  $\lambda(t)$  has a zero mean (if the mean is nonzero the rot frame Hamiltonian can be still periodic in special cases, e.g. when the spectrum of  $H_1$  is quantized in integers, as will be the case for the realisation of the Harper-Hofstadter Hamiltonian discussed in Sec. 7.2, or when we discuss the static and the dynamic Schrieffer-Wolff transformation in Sec. 4.2). If  $V^\dagger(t)H_0V(t)$  is a local operator, one can find the Floquet evolution in the rotating frame by applying the Magnus expansion. But unlike in the original lab frame, there are no more divergent terms in the transformed Hamiltonian. Hence, the infinite-frequency limit is simply determined by the time average of  $H^{\text{rot}}(t)$ , and the  $n$ -th order corrections in inverse frequency are precisely given by the  $n$ -th order of Magnus expansion in the rotating frame. Evaluating  $H^{\text{rot}}(t)$  explicitly is only possible when  $V(t)$  is simple. This is the case, for example, when  $H_1$  is a single-particle operator. These are precisely the situations, in which one can do a partial resummation of the Magnus expansion in the lab frame. We note in passing that for  $V(-t) = V(t)$  the driving protocol in the rot frame is an even function of time, and hence all odd-order corrections in the Magnus expansion vanish identically [72].

It is straightforward to find the relation between the Floquet Hamiltonians as well as kick operators in both frames. Recall from the general Floquet theory (6) that in the lab and the rot frames the evolution operator reads as:

$$\begin{aligned} U(t_2, t_1) &= P(t_2)e^{-(i/\hbar)H_F(t_2-t_1)}P^\dagger(t_1) \\ U^{\text{rot}}(t_2, t_1) &= P^{\text{rot}}(t_2)e^{-(i/\hbar)H_F^{\text{rot}}(t_2-t_1)}P^{\dagger, \text{rot}}(t_1). \end{aligned} \quad (34)$$

On the other hand, the evolution operators in the two frames are related as

$$U(t_2, t_1) = V(t_2)U^{\text{rot}}(t_2, t_1)V^\dagger(t_1). \quad (35)$$

Comparing these three expressions and noting that  $V(t)$  is a periodic function by construction, we see that in the Floquet gauge where  $P(nT) = \mathbf{1} = P^{\text{rot}}(nT)$  one can always identify

$$P(t) = V(t)P^{\text{rot}}(t)V^\dagger(0), \quad H_F = V(0)H_F^{\text{rot}}V^\dagger(0). \quad (36)$$

Moreover, if  $V(nT) = \mathbf{1}$ , the transformation to the rotating frame is stroboscopic and the above formulas simplify further. Up to a gauge transformation, the Floquet Hamiltonian is the same in the lab and the rot frame. But it is important to notice that the kick operators in the lab frame and the rot frames are generally different. Since the operator

transforming to the rot frame  $V(t)$  is not unique, there is an additional gauge freedom in defining the Floquet Hamiltonian in the rotating frame.

Using specific examples, we shall illustrate that a successful strategy for finding the Floquet Hamiltonian and the kick operators is: i) first to perform the transformation to the rotating frame w.r.t. the driving Hamiltonian in order to remove the terms which diverge with the driving frequency, and ii) then use the Magnus expansion to find the Floquet Hamiltonian as well as the kick operators. Finally, iii), (if needed) we return back to the lab frame.

In the most general case, the transformation to the rotating frame  $V(t)$  need not be stroboscopic. Then the dressed operators in the two frames are related by

$$\overline{\rho^{\text{rot}}} = V^\dagger(0)\overline{\rho}V(0), \quad \overline{\mathcal{O}^{\text{rot}}} = V^\dagger(0)\overline{\mathcal{O}}V(0). \quad (37)$$

For the special case that  $V(nT) = \mathbf{1}$ , in the FNS expectation value there is no difference between the dressed density matrix  $\overline{\rho}$  and the dressed observable  $\overline{\mathcal{O}}$  evaluated in the lab and in the rotating frame. Physically, this is because we are averaging both of them over a period. Mathematically, this follows from combining Eqs. (22, 32, 36). Thus, one can find these operators in any frame, keeping in mind that a static operator in the lab frame becomes time-dependent in the rotating frame. The leading terms in the Magnus series in the rotating frame are given by

$$\overline{\mathcal{O}^{\text{rot}}} = \frac{1}{T} \int_0^T dt \mathcal{O}^{\text{rot}}(t) + \frac{i}{T} \int_0^T dt \int_0^t dt' [H^{\text{rot}}(t') - H_F^{\text{rot}}, \mathcal{O}^{\text{rot}}(t)] + \dots \quad (38)$$

$$\overline{\rho^{\text{rot}}} = \frac{1}{T} \int_0^T dt \rho^{\text{rot}}(t) + \frac{i}{T} \int_0^T dt \int_0^t dt' [H^{\text{rot}}(t') - H_F^{\text{rot}}, \rho^{\text{rot}}(t)] + \dots \quad (39)$$

Going to the rotating frame can offer the same benefits for calculating dressed operators (including the density matrix) as for calculating Floquet Hamiltonians. Namely, if the amplitude of the driving diverges with the frequency, going to the rot frame and evaluating a simple time-average of the corresponding operator (or density matrix) is equivalent to a re-summation of an infinite sub-series for  $\overline{\mathcal{O}}$  in the lab frame. We note that the Magnus expansion in the rotating frame (where the driving amplitude does not scale with frequency) is effectively a  $1/\Omega$  expansion.

### 3.3. Convergence of the Magnus Expansion

As we have seen, the Magnus expansion (ME) is a very powerful tool to compute the Floquet Hamiltonian in the high-frequency limit, and find the leading corrections. However, as it often happens in physics, perturbative expansions can be asymptotic, i.e. can have a zero radius of convergence. This does not mean that these expansions are useless because they still can give very accurate predictions for the behavior of the system, but eventually such asymptotic expansions break down.

In the context of the Magnus expansion, the question of true vs. asymptotic convergence is ultimately related to the question of heating in the driven system. A convergent ME implies that the Floquet Hamiltonian is local and, thus, the evolution of the system (up to the periodic kick operators) is governed by a local static Hamiltonian so the total energy of the system is conserved [61]. This leads to a dynamical localization transition where the system does not absorb energy from the external drive even in the infinite-time limit. On the other hand, a divergent Magnus series indicates that there exists no local Floquet Hamiltonian, and the system is gradually heated up.

From a mathematical point of view, this issue has been extensively investigated in the

literature, and a few different theorems are known (see Ref. [72] and references therein). In particular, the Magnus expansion is guaranteed to converge to the Floquet Hamiltonian if:

$$\int_0^T dt |\epsilon_{\max}(t) - \epsilon_{\min}(t)| < \hbar \xi$$

where  $\epsilon_{\max}(t)$ ,  $\epsilon_{\min}(t)$  are the largest and smallest eigenvalues of the Hamiltonian  $H(t)$ , and  $\xi$  is a number of order one.

While this result is exact, it is not particularly useful for many-particle systems. It only guarantees the convergence if the driving frequency scales with the system size, while the relevant time scales, separating the fast and slow driving regimes, are never extensive. This condition for the convergence of the Magnus expansion is only sufficient. It does not give much insight about what happens at longer periods. To the best of our knowledge, there are no rigorous results about the convergence of the ME for interacting systems in the thermodynamic limit, and it is unknown whether in this case the radius of convergence of the ME is zero or finite. The Magnus expansion can be definitely convergent even in the thermodynamic limit, if the time-dependent Hamiltonian can be mapped to a static one, by going to some rotating frame. For instance, this is the case for an arbitrary interacting lattice gas in a magnetic field such that the vector potential varies linearly in time (which results in hopping amplitudes which are periodic in time). By doing a gauge transformation the linearly varying vector potential is equivalent to a constant electric field  $\mathbf{E} \sim \partial_t \mathbf{A}$ . We discuss additional examples of such effectively static systems in Sec. 4.

In more generic situations, where local transformation to the constant Hamiltonian does not exist the situation is not well understood. In Refs. [58, 59, 61], a numerical evidence indicated that for particular driving protocols in one-dimensional fermionic or spin chains, the radius of convergence of the Magnus expansion is finite even in the thermodynamic limit. In other words, there exists a critical period  $T_c$  separating regimes of finite and infinite heating. At the critical period there is a dynamical transition between these two regimes, which can be interpreted as a many-body localization transition [78–83] in energy space. This finding is also consistent with previous numerical results obtained by T. Prosen for periodically kicked spinless fermions in one dimension [58, 59, 84] equivalent to a periodically kicked  $XXZ$  spin chain. In these works T. Prosen also found two qualitatively different regimes. In the first one the evolution is well described by random matrices from the circular ensemble (see also Ref. [62]) strongly suggesting that the ME is divergent while in the other regime the system displays properties which are consistent with the ME being convergent to a local Hamiltonian.

However, a numerical study of a different driving protocol in a spin chain indicated a zero radius of convergence [62], i.e.  $T_c = 0$ . In Ref. [63], using the Eigenstate Thermalization Hypothesis, it was argued that an ergodic system with a local driving term always heats up to infinite temperature in the thermodynamic limit, while the energy can stay localized (and thus the Magnus expansion converges) if the system is in the many-body localized phase. In Ref. [85] it was shown that the Magnus expansion has zero radius of convergence for a Kondo model if the driving frequency is smaller than the bandwidth of the conduction electrons, though for faster driving the numerical results seem to indicate convergence of the Magnus expansion [86]. There is no contradiction with Ref. [63] because in the Kondo model the conduction band electrons were considered non-interacting (i.e. non-ergodic).

The Magnus expansion can be rigorously shown to have a finite radius of convergence for integrable systems, which can be factorized into uncoupled sectors, e.g. in momentum space. Then the extensivity of the system is not important and the criterion 3.3 can be

applied to each sector independently. Such systems do not heat up indefinitely and, in the long-time limit, effectively reach a steady state with respect to the Floquet Hamiltonian (dressed by the kick operators) [87, 88].

From a physical point of view, the divergence of the ME, and the corresponding heating of the system can be traced back to the existence of resonances [89]. When the frequency of the drive  $\Omega$  matches a single particle energy scale  $J$ , i.e.  $\hbar\Omega \approx J$ , the system can efficiently absorb energy from the periodic drive leading to fast heating. Here  $J$  can represent, for example, the energy associated with a single spin flip in a spin system, and then the process described above corresponds to the absorption of a photon of the driving field and a subsequent spin flip in the system. When the driving frequency is increased,  $\hbar\Omega \gg J$ , the photon energy can be absorbed, only if many spins are flipped simultaneously. These *many-body* processes are described by higher-order perturbation theory and, therefore, occur with small probabilities. Hence, they can become important only at very long times. The same large-energy absorption processes determine whether in the *off-resonance* regime, i.e.  $\hbar\Omega \gg J$ , the heating is slow and finite, or completely absent. It is unclear at the moment whether the heating can be understood through including more and more terms in the Magnus expansion or if it is non-perturbative in the period.

Even in the situations, where the ME formally diverges, the heating remains slow at fast driving frequencies [66]. Then the Magnus expansion truncated to the first few orders can accurately describe the transient dynamics of the system for many periods of oscillations. In particular, in Ref. [66] it was shown that, for a dipolar-coupled periodically driven spin systems, the magnetization quickly approaches a quasi-stationary value predicted by the Magnus expansion truncated at second order. Then, at much longer times, the magnetization decays to zero due to slow heating processes which are not captured by the ME. Therefore, in this context, an important question is not whether the Magnus expansion has a finite radius of convergence or only asymptotic, but rather whether there is a time scale separation between interesting transient dynamics described by the local truncated Floquet Hamiltonian and eventual heating. While this issue is also not very well understood in general, there is sufficient evidence that such time scale separation always exists at high driving frequencies [90]. For this reason, in Secs. 7.2, 7.3 and 7.4, the approximate Floquet Hamiltonians obtained by truncating the Magnus expansion to order  $1/\Omega$  are at the very least expected to describe the transient dynamics and the relaxation to a quasi-steady state.

A natural way to prevent infinite heating is to couple the driven system to a thermal bath. In this case it is natural to expect that the system will eventually approach a non-equilibrium steady state in which the energy absorbed from the driving is balanced by the energy dissipated into the environment [91–94]. The value of measurable quantities (such as transport coefficients and correlation functions) will depend crucially on the nature of the (putative) non-equilibrium steady state [40, 41, 95] which, for this reason, has been the focus of intense research [96, 97]. Despite this intense effort, a general understanding of the non-equilibrium steady state is still missing but it seems clear that the steady state will, in general, be non-thermal. Therefore the thermodynamic behavior of periodically driven systems is expected to be qualitatively different from those of non-driven systems [98, 99].

#### 4. The Rotating Wave Approximation and the Schrieffer-Wolff transformation.

In this section we show that the Magnus expansion can be used even in static, i.e. non-driven systems, by first going into the interaction picture (see for example Refs. [100] and

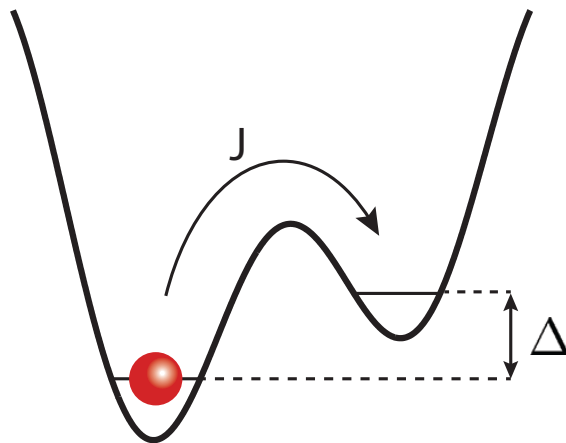


Figure 6. (Color online) A single particle in a tilted double well: the two wells have an energy difference  $\Delta$  and are connected by the matrix element  $J$ .

[101]). In particular, it can be used to eliminate highly excited states, which are never populated but nevertheless lead to renormalization and modification of the low-energy Hamiltonian. These ideas are also behind the widely used Schrieffer-Wolff transformation [102] which, as we shall show, is closely related to the Magnus expansion<sup>2</sup>. The formalism introduced in Sec. 3 can be applied to find the leading behavior and the first subleading correction to the effective Hamiltonian, the dressed operators and the density matrix. As we illustrate below, this framework has an additional advantage allowing one to extend the Schrieffer-Wolff transformation to periodically driven systems.

#### 4.1. A Two-level System

*Non-driven two-level system.* To understand the relation between the Magnus expansion and time-independent perturbation theory, consider first a time-independent problem of a single particle hopping in a tilted double well potential, c.f. Fig. 6. This model is exactly solvable and, with the correct identification of the lab and rotating frames, it is equivalent to the two-level system in a circularly driven magnetic field described in Sec. 2.2. Here we revisit this model paying special attention to the convergence properties of the Magnus expansion. The system is described by the Hamiltonian

$$H = -J \left( d_2^\dagger d_1 + d_1^\dagger d_2 \right) + \Delta n_2, \quad (40)$$

where the operator  $d_m^\dagger$  creates a particle on site  $m$  and  $n_m = d_m^\dagger d_m$  is the particle number operator. The tilt is given by the parameter  $\Delta$ , while the hopping matrix element is denoted by  $J$ . We are interested in the limit  $\Delta \gg J$ . The exact eigenenergies of this Hamiltonian are  $E_{\pm} = 1/2 \left( \Delta \pm \sqrt{\Delta^2 + 4J^2} \right)$ .

The Hamiltonian in Eq. (40) does not have any explicit time dependence, let alone a periodic one. In order to make use of the Magnus expansion, we apply a unitary transformation into the interaction picture w.r.t. the diagonal part  $H_1 = \Delta n_2$ , given by  $V(t) = \text{diag}(1, \exp(-i\Delta t))$  in the Fock basis. We thus obtain a time-dependent Hamil-

---

<sup>2</sup>We are grateful to A. Rosch for pointing this out.

tonian in the interaction picture:

$$H^{\text{int}}(t) = -J \left( e^{i\Delta t} d_2^\dagger d_1 + e^{-i\Delta t} d_1^\dagger d_2 \right) \quad (41)$$

which is similar to Eq. (15) with the identification  $B_z \rightarrow 0$ ,  $B_\parallel \rightarrow -J$ , and  $\Delta \rightarrow \Omega$ , whenever the system is populated by a single particle. Observe that by doing the transformation to the interaction picture we eliminate the high-energy level from the problem at the expense of introducing an explicit time dependence. This transformation is identical to the gauge transformation in electromagnetism, where a static scalar potential can be traded for a linear in time vector potential. Now we can apply Floquet theory to the Hamiltonian (41). Using Eqs. (16) and (19) we find that the full time-independent Floquet Hamiltonian coincides with the original Hamiltonian, i.e.  $H_F = H$ , as expected. Moreover, from Eqs. (18) and (19) we also see that the kick operator is  $P(t) = V^\dagger(t)$ . This implies that, if we are interested in the time evolution at scales slower than  $1/\Delta$ , we can compute the dressed density matrix for the initial state and the dressed operator for the observable of interest and evolve them in time with the Floquet Hamiltonian. If we are interested in the high-frequency (i.e. large  $\Delta$ ) structure of the dynamics, we can fully recover it from the operator  $P(t)$ .

For the Hamiltonian (41) the leading few orders in the Magnus expansion result in

$$\begin{aligned} H_F^{(0)} &= 0, \\ H_F^{(1)} &= \frac{J^2}{\Delta} (n_2 - n_1), \\ H_F^{(2)} &= 2 \frac{J^3}{\Delta^2} (d_2^\dagger d_1 + d_1^\dagger d_2). \end{aligned} \quad (42)$$

It is easy to see that the Floquet Hamiltonian in the first two orders of the Magnus expansion,  $H_F^{(1)} + H_F^{(2)}$ , is equivalent to the original static Hamiltonian when one rescales the original couplings  $\Delta$  and  $J$  by a factor of  $2J^2/\Delta^2$ . In fact, for this simple problem one can re-sum the entire series to obtain the Hamiltonian (40), i.e.  $H = \sum_{n=0}^{\infty} H_F^{(n)}$ . However, for more complicated Hamiltonians, the Magnus series is not guaranteed to converge (c.f. Sec. 3.3).

Let us now briefly comment on the physical meaning of the different terms in the Hamiltonian. In the leading approximation, the Floquet Hamiltonian is zero, which indicates that, in the infinite-frequency limit, the system remains frozen, when the energy offset of the two wells is larger than the hopping ( $\Delta \gg J$ ), since the two levels are effectively uncoupled. The first correction is responsible for the (opposite) energy shifts of the ground and the excited states and introduces a level repulsion. The second correction, in turn, leads to renormalisation of the eigenstates, since it represents a hopping (mixing) between the two levels.

*Periodically Driven Two-Level System.* The application of the Magnus expansion in the previous example might not be the easiest way to study this simple system, but it paves the way towards studying the behavior of a more complicated system containing both a high-energy level and periodic driving. Suppose that we now shake the higher-energy level with an amplitude  $A$  and a frequency  $\Omega$ , c.f. Fig. 7. The Hamiltonian becomes

$$H = -J (d_2^\dagger d_1 + d_1^\dagger d_2) + (\Delta - A \cos \Omega t) n_2. \quad (43)$$

We will be interested in the limit  $\Delta, \Omega \gg J$ . Our first goal is to understand how the drive

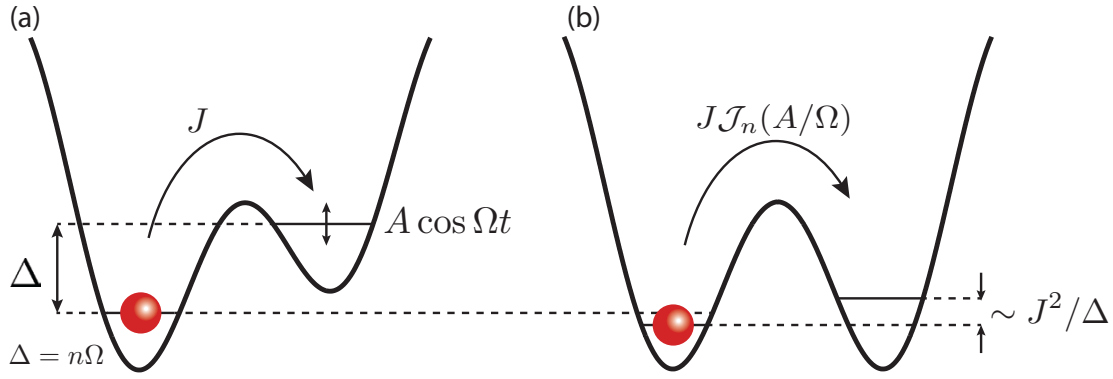


Figure 7. (Color online) The periodically driven two-level system. (a) The higher energy level is modulated periodically w.r.t. the lower level in the lab frame. (b) As a result, the effective Floquet Hamiltonian governing the slow dynamics features a mixing term between the two levels to leading order (absent in the non-driven system), while the first Magnus correction has the physical meaning of a small level repulsion.

changes the physics compared to the non-driven case. Extending the procedure from the static example to the driven case above, we eliminate both the higher-energy level and the driving term altogether by a transformation to a rotating frame:

$$V(t) = \exp \left[ -i \left( \Delta t - \frac{A}{\Omega} \sin \Omega t \right) n_2 \right],$$

$$d_2 \rightarrow e^{i\Delta t - i\zeta \sin \Omega t} d_2, \quad d_1 \rightarrow d_1, \quad (44)$$

where we defined  $\zeta = A/\Omega$ . The Hamiltonian in the rotating frame is given by

$$H^{\text{rot}}(t) = -J \left( e^{i\Delta t - i\zeta \sin \Omega t} d_2^\dagger d_1 + e^{-i\Delta t + i\zeta \sin \Omega t} d_1^\dagger d_2 \right). \quad (45)$$

Note that, as before, in the rotating frame there is no energy offset between the two levels, but the hopping term has a more complex time dependence encoding both static and dynamic information.

In general, the new Hamiltonian (45) is not strictly periodic in time, since  $\Delta$  and  $\Omega$  are arbitrary real numbers. One can deal with this in several ways. One possibility is to find co-prime integers  $n$  and  $m$  and a frequency  $\Omega_0$  such that  $n\Omega_0 \approx \Delta$  and  $m\Omega_0 \approx \Omega$ . As long as  $\Omega_0 \gg J$  the Floquet analysis should hold. If the frequencies are not exactly commensurate then one can define commensurate  $\tilde{\Delta} = n\Omega_0$  and make the transformation to the rotating frame using  $\tilde{\Delta}$  instead of  $\Delta$  in Eq. (44). It is easy to see that this will result in a small extra static term  $(\Delta - \tilde{\Delta})d_2^\dagger d_2$  in the Hamiltonian (45). And finally one can take the commensurate limit, e.g.  $\Delta = n\Omega$  and make an analytic continuation in the final result to non-integer  $n$ . This should work if the result, e.g. the effective Floquet Hamiltonian is a simple analytic function of  $n$ . We will show below that this trick works indeed in the case of the Schrieffer-Wolff transformation. It is intuitively clear that especially in many-particle systems with continuous spectra the exact commensurability of the driving should not play a crucial role.

We now leave all these subtleties aside and assume that  $\Delta$  and  $\Omega$  are commensurate such that  $\Delta = n\Omega_0$  and  $\Omega = m\Omega_0$ , where  $n$  and  $m$  are positive co-prime integers. We shall also assume that  $\Omega_0 \gg J$ . First, let us understand the leading time averaged Hamiltonian



$H_F^{(0)}$ , which was strictly zero in the non-driven case. We note the mathematical identity:

$$\frac{1}{T_0} \int_0^{T_0} dt e^{i\Delta t - i\zeta \sin \Omega t} = \sum_{l \in \mathbb{Z}} \mathcal{J}_l(\zeta) \frac{1}{T_0} \int_0^{T_0} dt e^{i(-lm+n)\Omega_0 t}, \quad (46)$$

where  $\mathcal{J}_l(\zeta)$  is the  $l$ -th Bessel function of the first kind and  $T_0 = 2\pi/\Omega_0$  is the common period. The integral above is nonzero if and only if there is a solution to the equation  $lm = n$ , or in other words  $n$  is a multiple integer of  $m$ . Because by assumption  $m$  and  $n$  are co-prime this equality can only be satisfied when  $m = 1$  (and hence  $\Omega_0 = \Omega$  and  $\Delta = n\Omega$ ). This means that the leading Floquet Hamiltonian  $H_F^{(0)}$  simply corresponds to the  $n$ -photon resonance. Let us focus on this resonant scenario. Clearly in this case

$$H_F^{(0)} = -J \mathcal{J}_n(\zeta) \left( d_2^\dagger d_1 + d_1^\dagger d_2 \right). \quad (47)$$

In the infinite-frequency limit (at fixed  $n$ )  $H_F^{(0)}$  determines the Floquet Hamiltonian. It splits the two levels into the symmetric and antisymmetric combinations. This is very different from the non-driven or non-resonantly driven case, where  $H_F^{(0)} = 0$  and the leading order contribution in the Magnus expansion, i.e.  $H_F^{(1)}$ , gives the energy splitting between the levels (c.f.  $H_F^{(1)}$  in Eq. 42) and hence keeps the eigenstates essentially unmixed (up to a small correction of the order  $J/\Delta$ ). This observation already hints toward possible heating mechanisms in the Floquet picture. For example, if one prepares the two-level system in the lower-energy state then in the resonant case this state is equally projected on the symmetric and antisymmetric Floquet eigenstates, resulting in an equal population of the two levels. This is equivalent to heating to an infinite-temperature state. In the non-resonant case, conversely, the Floquet eigenstates are still predominantly the eigenstates of the non-driven Hamiltonian, and thus the initial state is only weakly perturbed while excited state is only weakly populated. Admittedly, this example is too simple to understand real heating mechanisms in more complex interacting systems, but it shows how resonant periodic driving can fundamentally change the nature of the Floquet eigenstates [90].

If the amplitude of the driving is small, then  $\zeta \ll 1$  and we find  $\mathcal{J}_m(\zeta) \sim \zeta^m$  such that the effective hopping is proportional to the  $n$ -th power of the driving amplitude. This is not surprising, since it means that the  $n$ -photon absorption processes are exponentially suppressed. This result can also be obtained using time-dependent perturbation theory. However, for  $\zeta \sim 1$ , i.e. in the strong-coupling regime, this term becomes non-perturbative and the multi-photon absorption processes are not suppressed.

For completeness, we give the leading correction term in the Magnus expansion for this resonant case:

$$H_F^{(1)} = \frac{J^2}{\Delta} g_n(\zeta) (n_2 - n_1),$$

$$g_n(\zeta) = -n \operatorname{Im} \left\{ \int_0^{2\pi} \frac{d\tau_1}{2\pi} \int_0^{\tau_1} d\tau_2 e^{-in(\tau_1 - \tau_2) + i\zeta(\sin \tau_1 - \sin \tau_2)} \right\}. \quad (48)$$

Similarly to the non-driven case this correction gives the level repulsion term, but with a renormalized coefficient. If the driving is not very strong,  $\zeta \lesssim 1$ , then except when  $n = 1$  the presence of the driving results in a small modification to the non-driven result, i.e.  $g_n(\zeta) \approx 1$ . However, we want to emphasize again that this term is now only a sub-dominant correction provided that  $\mathcal{J}_n(\zeta) \gg J/\Delta = J/(n\Omega)$ .

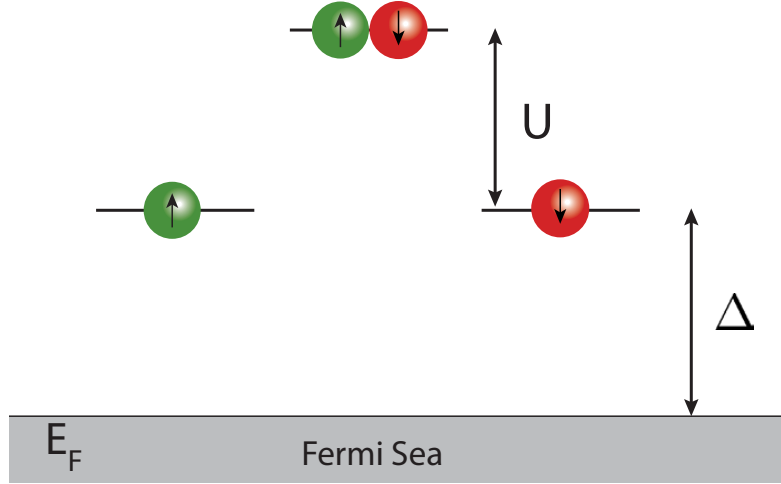


Figure 8. (Color online) The Anderson Model: spinful fermions can occupy an impurity level, separated by the Fermi sea by the energy  $\Delta$ . The coupling between the impurity atom and the conducting electrons is  $V_d$ . Moreover, in the presence of interactions, an additional energy cost  $U$  has to be paid for the double occupancy of the impurity atom.

#### 4.2. The Magnus Expansion vs. Schrieffer-Wolff Transformation

A standard way to eliminate high energy states in static systems is the Schrieffer-Wolff (SW) transformation. It represents a perturbative unitary rotation of the Hamiltonian, which eliminates the coupling to the high-energy states at the expense of creating effective low-energy terms. A famous example of the SW transformation, where it was first applied, is the reduction of the Anderson impurity model to the Kondo model [102]. In this section we show that the SW transformation is essentially equivalent to the Magnus expansion. Moreover, similarly to the simple case of a two-level system, we shall show how one can extend SW transformation to the driven systems. To make the discussion more transparent we shall analyze three specific examples of increasing complexity. First, we describe the non-driven non-interacting system, then a driven non-interacting one, and finally an interacting, non-driven one. The driven interacting system is very similar to the driven non-interacting one, and we only comment on the result.

*A non-interacting impurity coupled to a conducting band.* We begin by generalizing the simple two-level setup. Consider the non-interacting Anderson model describing a single impurity coupled to free electrons:

$$\begin{aligned}
 H &= H_0 + H_1, \\
 H_0 &= \sum_{k,s} \epsilon_k n_{ks} + \Delta \sum_s n_{ds}, \\
 H_1 &= \frac{1}{\sqrt{L^D}} \sum_{ks} \left( V_d c_{ks}^\dagger d_s + \text{h.c.} \right).
 \end{aligned} \tag{49}$$

Here  $d$  refers to the impurity atom with an energy  $\Delta$ ,  $s = \uparrow, \downarrow$  is the spin index,  $\epsilon_k \geq 0$  is the dispersion of the band electrons,  $V_d$  is the hybridization strength,  $L$  is the linear system size, and  $D$  is the dimensionality of the system. The prefactor  $1/\sqrt{L^D}$  in front of the coupling ensures that in real space the coupling to the impurity  $V_d$  is independent of the system size. The fermionic creation and annihilation operators obey the canonical commutation relations  $\{c_{ks}, c_{k's'}^\dagger\}_+ = \delta_{kk'} \delta_{ss'}$ , and  $\{d_s, d_{s'}^\dagger\}_+ = \delta_{ss'}$ . As usual,  $n_{ks} = c_{ks}^\dagger c_{ks}$  and  $n_{ds} = d_s^\dagger d_s$  are the number operators. We are interested in the situation where

$\Delta$  is the largest energy scale in the system:  $\Delta \gg V_d, \epsilon_k$ , and the coupling  $V_d$  between the conducting band and the impurity is small (compared to the Fermi energy). In this limit, the impurity can only be occupied by virtual processes, which effectively dress the low-energy conduction band electrons.

As Schrieffer and Wolff pointed out [102], standard perturbation theory fails to provide an accurate description of the weak-coupling limit,  $V_d \rightarrow 0$ , since higher order terms in  $V_d$  appear together with energy denominators  $\epsilon_k - \epsilon_{k'}$ . Near the Fermi surface, the latter can be arbitrarily small, and hence render perturbation theory inefficient. To solve this problem, they suggested to perform a unitary transformation, which later became known as the SW transformation [102]. This transformation eliminates the dependence of the Hamiltonian on  $V_d$  to linear order. As a result, the limiting procedure  $V_d \rightarrow 0$  becomes well-defined.

Here, we show that we can achieve a similar goal by first doing a transformation into a rotating frame with respect to the operator  $\Delta \sum_s n_{ds}$ , and subsequently applying the Magnus expansion to this new periodic Hamiltonian. This is a direct extension of the procedure we used for the two-site single-particle problem discussed above. By doing this transformation, we are eliminating the energy scale  $\Delta$  from the effective description at the expense of introducing a fast periodic time dependence in the hybridization term:

$$\begin{aligned} H^{\text{rot}}(t) &= H_{\text{band}} + e^{-i\Delta t} H^+ + e^{i\Delta t} H^-, \\ H_{\text{band}} &= \sum_{k,s} \epsilon_k n_{ks}, \quad H^+ = \frac{1}{\sqrt{L^D}} \sum_{ks} V_d c_{ks}^\dagger d_s, \quad H^- = (H^+)^\dagger. \end{aligned} \quad (50)$$

We can now apply the Magnus expansion, since we have a periodic Hamiltonian. Clearly, the time-averaged Hamiltonian,  $H_F^{(0)} = H_{\text{band}}$ , so the linear terms in  $V_d$  average to zero. Notice how the absence of linear terms, which can be considered as the main requirement for the choice of the generator of Schrieffer-Wolff transformations, arises naturally in this setup. The  $\Delta^{-1}$ -correction includes the following commutators (and their hermitian conjugates):

$$[H^+, H_{\text{band}}], \quad [H^+, H^-]. \quad (51)$$

The first commutator leads to  $V_d/(\sqrt{L^D}\Delta) \sum_{ks} \epsilon_k c_{ks}^\dagger d_s$ , i.e. it represents a new hybridization between the conduction electrons and the impurity, suppressed by a factor of  $1/\Delta$ . Because the occupation of the impurity atom remains unaffected by the transformation to the rotating frame, this hybridization will only contribute as a  $1/\Delta^2$ -correction to the scattering of the band electrons, and can be dropped to leading order in  $1/\Delta$ .

On the contrary, the commutator  $[H^+, H^-]$  leads to scattering between band electrons to order  $1/\Delta$ , and thus has to be taken into account. If we restrict the discussion to order  $1/\Delta$ , we find

$$H_F \approx H_{\text{band}} - \frac{|V_d|^2}{\Delta L^D} \sum_{kk'} \Psi_k^\dagger \Psi_{k'} + \frac{|V_d|^2}{\Delta} \Psi_d^\dagger \Psi_d, \quad (52)$$

where we introduced the compact spinor notation:

$$\Psi_k = \begin{pmatrix} c_{k\uparrow} \\ c_{k\downarrow} \end{pmatrix}, \quad \Psi_d = \begin{pmatrix} c_{d\uparrow} \\ c_{d\downarrow} \end{pmatrix}. \quad (53)$$

The second term in this effective Hamiltonian represents the static scattering from the impurity atom, while the third term is the new impurity potential. Within the Magnus expansion we can also recover the kick operator, which can be important for understanding non-stroboscopic dynamics and for defining the dressed density matrix and the dressed-operators. As in the two-level case from Sec. 4.1, the kick operator  $P(t)$  is given by the Hermitian conjugate of the rotating frame operator,  $P(t) = V^\dagger(t) = \exp[i\Delta t \sum_s n_{d,s}]$ . Usually, the associated subtleties are not discussed in the context of the SW transformation. Moreover, the SW transformation can become quite cumbersome if one needs to go to higher order.

*Schrieffer-Wolff transformation for periodically driven systems.* We now extend the SW transformation to periodically driven systems by adding an extra term

$$H_1 = -A \cos \Omega t \sum_s n_{d,s}$$

to the Hamiltonian (49). This system was realised from the point of view of Floquet theory in Refs. [90, 103, 104]. As in the example of the two-level system, we assume commensurate driving frequency and impurity energy:  $\Delta = n\Omega$ , where  $n \in \mathbb{N}$  (see the discussion in the two level case about the motivation for this assumption and how to relax it). Furthermore, as before we assume that  $\Omega$  and hence  $\Delta$  are the largest energy scales in the problem.

We eliminate the impurity level and the driving altogether, by going to the rotating frame defined by  $V(t) = \exp[i(\zeta \sin \Omega t - n\Omega) \sum_s n_{d,s}]$ ,  $\zeta = A/\Omega$ . This leads to

$$H^{\text{rot}}(t) = \sum_k \epsilon_k \Psi_k^\dagger \Psi_k + \frac{1}{\sqrt{L^D}} \sum_k V_d e^{i\zeta \sin \Omega t - in\Omega t} \Psi_k^\dagger \Psi_d + \text{h.c.} \quad (54)$$

We can now apply the Magnus expansion. The derivation of the Floquet Hamiltonian follows the same guidelines as that of the driven two-level system. The resulting time-averaged Hamiltonian and the leading correction are given by

$$\begin{aligned} H_F^{(0)} &= \sum_k \epsilon_k \Psi_k^\dagger \Psi_k + \frac{1}{\sqrt{L^D}} \sum_k V_d \mathcal{J}_n(\zeta) \Psi_k^\dagger \Psi_d + \text{h.c.}, \\ H_F^{(1)} &= -\frac{|V_d|^2}{\Delta L^D} g_n(\zeta) \sum_{k,k'} \Psi_k^\dagger \Psi_{k'} + \frac{|V_d|^2}{\Delta} g_n(\zeta) \Psi_d^\dagger \Psi_d, \end{aligned} \quad (55)$$

where the function  $g_n(\zeta)$  is defined in Eq. (48).

Contrary to the situation in the non-driven case, here in the high-frequency limit the hybridization terms which mix the band and the impurity levels do not vanish. This is very similar to the effect we already observed for the driven two-level system. But unlike the static case this linear coupling has direct physical implications, because the impurity level in the rotating frame is resonant with the bottom of the band. It then follows that the population of the impurity will be significant at any finite driving frequency as long as  $\mathcal{J}_n(\zeta)$  is not too small. Physically, this corresponds to multi-photon absorption processes.

Let us point out that one can similarly analyze the limits where  $\Delta = n\Omega + \delta\Delta$ , where  $|\delta\Delta| < \Omega/2$ . As we discussed earlier in the rotating frame there will be an extra static impurity potential  $\delta\Delta n_d$ . It is intuitively clear that the occupation of the impurity in the steady state will be sensitive to the position of this potential with respect to the Fermi level. A large impurity occupation is possible for  $0 \leq \delta\Delta \leq E_F$ . This mechanism of populating the higher level is expected to open up the way towards studying heating in

the high-frequency regime if e.g. we replace the impurity atom by an entire excited band. The issue of heating requires a separate careful analysis, which is beyond this review. We also refer the reader to recent works, where this issue was partially addressed for the Kondo model [85].

This example demonstrates the power of the Magnus expansion allowing us to treat driven and non-driven impurity models on the same footing. Moreover as we mentioned above within the Magnus expansion we also have access to the kick operator  $P(t) = V^\dagger(t)$  and hence can derive leading  $1/\Omega$  corrections to the dressed density matrix and operators important for the FNS time evolution.

*The Anderson Model.* Let us now go back to the static model and add an interaction term to the lab-frame Hamiltonian. The Hamiltonian describing repulsion between the electrons on the impurity is given by:

$$H_{\text{int}} = U n_{d\uparrow} n_{d\downarrow}. \quad (56)$$

For large interactions this term effectively penalizes the double occupancy of the impurity site. As is well known, this leads to the effective low-energy Kondo Hamiltonian [102].

To show the relation between the Magnus expansion and the SW transformation, we once again eliminate the high-energy impurity scale  $\Delta$  by going to the rotating frame:

$$V(t) = \exp \left( -i\Delta t \sum_s n_{ds} \right) \exp (-iU t n_{d\uparrow} n_{d\downarrow}). \quad (57)$$

Note that this transformation consists of the product of two commuting operators and it is a direct generalization of the transformation used in the non-interacting non-driven model above. The Hamiltonian in the rotating frame gets modified according to:

$$\begin{aligned} H^{\text{rot}}(t) &\longrightarrow H^{\text{rot}}(t) + e^{-i\Delta t} (e^{-iU t} - 1) W^+ + \text{h.c.}, \\ W^+ &= \frac{1}{\sqrt{L^D}} \sum_{ks} V_d c_{ks}^\dagger d_s n_{d,\bar{s}}, \end{aligned} \quad (58)$$

where  $H^{\text{rot}}(t)$  on the RHS above is the Hamiltonian (50), and  $\bar{s}$  denotes the opposite spin species to  $s$ . The additional term represents an interaction-dependent hopping from the conducting band to the impurity. In general, the interaction  $U$  and the impurity energy  $\Delta$  need not be commensurate, and thus the transformation to the rotating frame is not periodic. In the spirit of our previous discussion we assume commensurability,  $U = m\Delta$ , and moreover choose  $m = 1$ . One can check that the resulting Kondo Hamiltonian is correctly reproduced for any  $m$  and moreover by taking analytic continuation to non-integer  $m$  one obtains the correct result for any values of  $U$  and  $\Delta$ .

The interaction-dependent hopping  $W^\pm$  does not contribute to the time-averaged Hamiltonian  $H_F^{(0)}$ . Moreover, the contribution to the first-order correction due to  $[H_{\text{band}}, W^\pm]$  can be neglected for the same reasons as the correction due to  $[H_{\text{band}}, H^+]$  discussed above. Indeed, the commutator  $[H_{\text{band}}, W^\pm]$  leads to  $\sum_k \epsilon_k V_d / (\Delta \sqrt{L^D}) c_{ks}^\dagger d_s n_{d,\bar{s}}$  which contributes to the scattering of conduction band electrons starting from order  $1/\Delta^2$ , because to zeroth order the impurity state does not allow for double occupancy in the limit  $U \gg V_d$ . The interaction-dependent hopping gives an important contribution to the Hamiltonian coming from the commutators  $[W^+, W^-]$ ,  $[W^+, H^-]$ , and  $[W^-, H^+]$ .

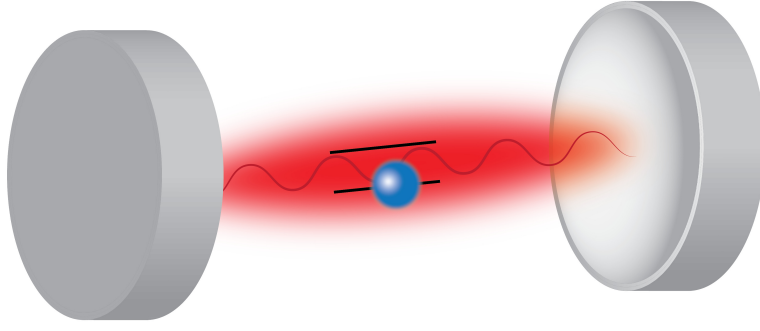


Figure 9. (Color online) The Rabi Model: a two-level system interacts with a quantized electromagnetic field.

Evaluating these explicitly, we find

$$\begin{aligned}
 H_F \approx H_{\text{band}} - \frac{g}{4LD} \sum_{kk'} \left( \Psi_k^\dagger \boldsymbol{\sigma} \Psi_{k'} \right) \cdot \left( \Psi_d^\dagger \boldsymbol{\sigma} \Psi_d \right) \\
 + \frac{g}{LD} \sum_{kk'} \left[ -1 + \frac{1}{4} \Psi_d^\dagger \Psi_d \right] \Psi_k^\dagger \Psi_{k'} + g \Psi_d^\dagger \Psi_d,
 \end{aligned} \tag{59}$$

where for our choice of parameters  $U = \Delta$  we have  $g = |V_d|^2/\Delta$ . This coupling  $g$  is precisely the Kondo coupling one derives from the original SW transformation [102].

In fact the Magnus expansion considered here is not identical to the SW transformation because the structure of the sub-leading terms is not the same. But clearly both expansions allow one to get the same low-energy Hamiltonian at least in the leading order in  $1/\Delta$ . As before, we note that the Magnus expansion, in addition to calculating the Floquet Hamiltonian, allows one to explicitly take into account both the slow dynamics of the system (due to the Floquet Hamiltonian), and the fast dynamics through the kick operator  $P(t) = V^\dagger(t)$ . Finally, we note in passing that including the driving in the interacting model is straightforward. The new term appearing in  $H_F^{(0)}$  will be identical to the one in Eq. (55) for the non-interacting model and the other terms will be modified by functions similar to  $g_n(\zeta)$ .

### 4.3. The Rabi Model

Another famous example in which a transformation to the rotating frame eliminates a highly excited state, is the Rabi model, which describes a two-level atom coupled to a quantized electromagnetic field. In the rotating frame the Rabi Hamiltonian is

$$H = H_0 + H^+(t) + H^-(t), \tag{60}$$

where

$$\begin{aligned} H_0 &= g \left( a^\dagger \sigma^- + a \sigma^+ \right), \\ H^+(t) &= g' e^{-i\Omega t} a \sigma^-, \quad H^-(t) = (H^+(t))^\dagger, \end{aligned} \quad (61)$$

and we have chosen the laser frequency  $\omega_L$  to match resonantly the difference of the energies of the two levels of the atom, in which case  $\Omega = 2\omega_L$ . We mention in passing that the Rabi model is integrable for  $g = g'$  in terms of the solution of a functional differential equation [105]. The couplings to the electromagnetic light are  $g, g' \sim \sqrt{\Omega}$ . Moreover by adding a magnetic field along the  $z$ -direction one can obtain a whole line of integrable points, where the generalized Rabi model is supersymmetric [106].

Applying the Magnus expansion to order  $\Omega^{-1}$  to the Rabi Hamiltonian gives:

$$H_F \approx g \left( a^\dagger \sigma^- + a \sigma^+ \right) + \frac{g'^2}{\Omega} \left( a^\dagger a \sigma_z - \sigma^+ \sigma^- \right) + \frac{gg'}{\Omega} \left( a^2 + (a^\dagger)^2 \right) \sigma^z. \quad (62)$$

In the large-frequency limit, the second and the third terms disappear and, as it is well known, the Rabi Hamiltonian reduces to the Jaynes-Cummings model. If we ignore the third term, e.g. assuming  $g' \gg g$ , then the Hamiltonian can be diagonalized analytically yielding the following spectrum:

$$E_n = -\frac{g'^2}{\Omega} \pm \sqrt{(1+n) \left( g^2 + \left( \frac{g'^2}{\Omega} \right)^2 (1+n) \right)}, \quad (63)$$

where  $n$  is the photon number. In the case of  $g' = 0$  the spectrum reduces to the Jaynes-Cummings one, as it should, and exhibits the hallmark feature of a quantized Rabi frequency  $\Omega_R = g\sqrt{n+1}$ . It is interesting to notice that the Magnus expansion captures the Bloch-Siegert shift  $g'^2/\Omega$ , which has been known to be the leading correction to the spectrum for a long time. The third term in Eq. (62) breaks the conservation of the total number of photons and spins, and significantly complicates the analysis of the Hamiltonian. Recently, it was shown that this type of term is important for the stabilization of finite-density quantum phases [107].

Using the Magnus expansion, it is straightforward to get the second order correction to the Floquet Hamiltonian:

$$\begin{aligned} H_F^{(2)} &= -\frac{2g^2g'}{\Omega^2} (a^2 a^\dagger \sigma^- - 2a \sigma^- - a^3 \sigma^+ + \text{h.c.}) \\ &\quad - 2\frac{g'^3}{\Omega^2} (na \sigma^- - 2a \sigma^- + \text{h.c.}) \\ &\quad + 2\frac{gg'^2}{\Omega^2} (2a^\dagger \sigma^- + a^\dagger n \sigma^- - \frac{1}{2} a^3 \sigma^- + \text{h.c.}). \end{aligned} \quad (64)$$

The Rabi model can be realised experimentally using highly controllable optical cavities, whose size determines the mode frequency  $\Omega$  through the quantisation/boundary conditions. In the same spirit as in the two-level system, and the Anderson model, one can imagine shaking the cavity boundaries out of phase periodically, which would induce a periodic modulation of the frequency  $\Omega$ . To study the physics of this model, one could go to a rotating frame and apply the Magnus expansion. Only this time, the counter-rotating (energy non-conserving) terms,  $g' a \sigma^- + \text{h.c.}$ , will not vanish to zeroth

order, in analogy with the emergent hybridisation terms at the level of the time-averaged Hamiltonian in the models discussed in Secs. 4.1 and 4.2.

Let us conclude this section by pointing out that, through the leading terms in the Magnus expansion, one can formally understand the generation of stationary optical lattice potentials used to trap neutral atoms [108]. It is then not difficult to find subleading terms including those responsible to various heating processes [109].

## 5. The Kapitza Class

We shall now move on to apply the formalism developed in Secs. 2 and 3 to specific examples. In the remainder of this paper, we review various models, in which the Floquet Hamiltonian exhibits a non-trivial high-frequency limit. By ‘non-trivial’ we mean not equal to the time-averaged lab-frame Hamiltonian. We shall also discuss leading corrections in the inverse driving frequency to the infinite-frequency limit, which are important for experimental realizations. As we discuss below different setups leading to non-trivial infinite-frequency Hamiltonians can be classified according to three generic classes of driving protocols. While this classification might not be exhaustive, it covers most of the examples known in the literature, and suggests possible routes for engineering new Floquet Hamiltonians in various types of systems.

Let us open the discussion by defining and studying the Kapitza class which is defined as a non-relativistic system with a quadratic in momentum kinetic energy and arbitrary (momentum-independent) interactions. The driving protocol couples only to operators which depend on coordinates. In other words, the Hamiltonian should be of the form:

$$H(p_j, \theta_j) = K(\{p_j\}) + H_{\text{int}}(\{\theta_j\}) + \Omega f(t) H_1(\{\theta_j\}), \quad (65)$$

where

$$K(\{p_j\}) = \sum_{j=1}^N \frac{p_j^2}{2m_j},$$

and  $f(t)$  is some periodic function of time with period  $T$  and zero mean. Note that the driving term  $H_1$  can include both a single particle external potential and interactions. When we say that the Hamiltonian should be of the form (65), we imply that it should be gauge-equivalent to this form. For instance, any time-dependent scalar potential can be absorbed into a vector potential by choosing a different EM-gauge, as it is well-known from classical electromagnetism. While we do not explicitly consider here systems in the presence of an orbital magnetic field, the Kapitza class can be extended to such situations as well. Such extension will simply result in few additional terms in the infinite frequency Hamiltonian and the leading inverse frequency corrections. We made the prefactor  $\Omega = 2\pi/T$  explicit in Eq. (65) to emphasize that, in order to get a non-trivial high-frequency limit, one needs to scale the driving amplitude linearly with the frequency. This scaling guarantees that, when the driving becomes infinitely fast, the system is strongly perturbed, and its evolution cannot be described by the time-averaged Hamiltonian at any frequency.

To derive the infinite-frequency Floquet Hamiltonian, we employ the Magnus expansion



(c.f. Eq. (28)) in the lab frame up to second order:

$$H^{(0)} = \frac{1}{2\pi} \int_0^{2\pi} d\tau H(\tau) = K + H_{\text{int}}, \quad (66)$$

$$H^{(1)} = \frac{1}{4\pi i} [K, H_1] \int_0^{2\pi} d\tau_1 \int_0^{\tau_1} d\tau_2 (f(\tau_1) - f(\tau_2)) = \frac{1}{4\pi i} [K, H_1] \int_0^{2\pi} d\tau_1 (2\tau_1 - 2\pi) f(\tau_1), \quad (67)$$

$$\begin{aligned} H^{(2)} = & -\frac{1}{12\pi\Omega} [[K, H_1], K] \int_0^{2\pi} d\tau_1 \int_0^{\tau_1} d\tau_2 \int_0^{\tau_2} d\tau_3 2f(\tau_2) - f(\tau_1) - f(\tau_3) \\ & -\frac{1}{12\pi} [[K, H_1], H_1] \int_0^{2\pi} d\tau_1 \int_0^{\tau_1} d\tau_2 \int_0^{\tau_2} d\tau_3 f(\tau_2)f(\tau_3) + f(\tau_2)f(\tau_1) - 2f(\tau_1)f(\tau_3), \end{aligned} \quad (68)$$

where  $\tau_i = \Omega t_i$ . In order to keep the notation consistent, here we choose a somewhat different expansion for the Floquet Hamiltonian:  $H_F = \sum_n H^{(n)}$ . This is to be contrasted with the proper inverse-frequency expansion  $H_F = \sum_n H_F^{(n)}$ , defined in Sec. 3 (note the difference in the notation: the subindex  $F$  in the expansion coefficients). The difference between the two expansions is due to the non-trivial scaling of the driving amplitude with frequency. In the former, the  $n$ -th order coefficient may contain terms containing mixed powers of  $1/\Omega$ , as we show below. On the other hand, the subindex  $F$  in the latter ensures that the  $n$ -th order operator-valued coefficient  $H_F^{(n)}$  scales strictly as  $\Omega^{-n}$ .

It becomes clear that, for  $\Omega \rightarrow \infty$ , the first term in  $H^{(2)}$  vanishes (it represents one of the subleading  $1/\Omega$  corrections) while the other term in  $H^{(2)}$  together with  $H^{(0)}$  and  $H^{(1)}$  give the correct Floquet Hamiltonian in the infinite-frequency limit. The term  $H^{(1)}$  in the Floquet expansion can always be set to zero by choosing an appropriate Floquet gauge, such that the time-integral appearing in Eq. (67) vanishes. For example, if the protocol is symmetric around the middle of the period:  $f(t) = f(T - t)$ , e.g.  $f(t) = \cos \Omega t$ , then this integral is identically zero. One has to be cautious, though, that this may not be the case in other gauges. For instance, if  $f(t) = \sin \Omega t$  then the integral in Eq. (67) is non-zero, and one either has to shift the stroboscopic point  $t_0$  to  $T/2$ , or deal with this term. Choosing the symmetric Floquet gauge, the time-ordered integral in the last term in Eq. (68) is finite, and has a well-defined non-zero infinite-frequency limit. Note that because the kinetic energy is quadratic in momentum this term depends only on the coordinates  $\{\theta_j\}$ , and hence represents an additional external potential or an interaction. Indeed,

$$[[K, H_1], H_1] = -\sum_{j=1}^N \frac{1}{m_j} \left( \frac{\partial H_1}{\partial \theta_j} \right)^2,$$

and thus, for symmetric driving protocols, the infinite-frequency limit of the Floquet Hamiltonian reads as:

$$H_F^{(0)} = K + H_{\text{int}} + A \sum_j \frac{1}{m_j} \left( \frac{\partial H_1}{\partial \theta_j} \right)^2, \quad (69)$$

where

$$A = \frac{1}{12\pi} \iiint_{0 < \tau_3 < \tau_2 < \tau_1 < 2\pi} d\tau_1 d\tau_2 d\tau_3 (f(\tau_2)f(\tau_3) + f(\tau_2)f(\tau_1) - 2f(\tau_1)f(\tau_3)). \quad (70)$$

The time integral here depends on the details of the periodic function  $f(\tau)$ . For instance, if  $f(\tau) = \lambda \cos(\tau)$  then  $A = \lambda^2/4$ . If the time average of  $f(\tau)$  is zero then one can show that

$$A = \frac{1}{4\pi} \int_0^{2\pi} \Delta^2(\tau) d\tau, \text{ where } \Delta(\tau) = \int_0^\tau f(\tau') d\tau'. \quad (71)$$

Let us argue that the asymptotic form of the Floquet Hamiltonian in the infinite-frequency limit given by Eq. (69) for the Kapitza class is exact. In other words, there are no other terms in the Magnus expansion which survive as  $\Omega \rightarrow \infty$ . From the structure of the expansion, it is clear that the only non-vanishing terms in the  $n$ -th order contribution are those which contain  $n$ -times the driving term  $H_1$ , and once the kinetic energy. Since the driving amplitude scales with frequency, each extra time integral (giving an extra factor  $1/\Omega$ ) will be precisely compensated for by the extra factor coming from the driving amplitude. So the only terms which survive have the structure of  $[[\dots [K, H_1], H_1], \dots H_1]$  multiplied by some dimensionless number. However, because the kinetic energy is quadratic in momentum, all such terms containing more than two commutators vanish identically. Hence, the only surviving terms beyond the second order must contain the kinetic energy at least twice, so they are at least of order  $\Omega^{-1}$ . Note that, in principle, one can evaluate the  $\Omega^{-1}$ -corrections to  $H_F^{(0)}$  in a similar way. But the general expressions become very involved so we shall rather show these corrections for a specific case of the Kapitza pendulum. As we shall show, it is much easier to derive these corrections going first to the rotating frame, where there is a systematic and convenient way to count the powers of frequency.

### 5.1. The Kapitza Pendulum

Let us now illustrate how the infinite-frequency limit, the leading corrections, the Floquet-gauge freedom, and the dressing of the observables and the density matrix emerge for a specific setup of a single Kapitza pendulum [3, 61]. At the end of the section, we shall briefly discuss many-particle generalizations of the Kapitza pendulum.

The Kapitza pendulum is a rigid pendulum of length  $l$  in which the point of suspension is being displaced periodically along the vertical direction according to the time-dependent protocol  $a \cos \Omega t$ . This driving results in a modulation of the velocity in the  $y$  direction:  $\dot{y} \rightarrow \dot{y} - a\Omega \sin \Omega t$ , which immediately translates to the modulation of the angular velocity

$$\dot{\theta} \rightarrow \dot{\theta} + \frac{a\Omega}{l} \sin \Omega t \sin \theta.$$

The Lagrangian for the Kapitza pendulum is given by

$$\mathcal{L} = \frac{ml^2}{2} \left( \dot{\theta} + \frac{a\Omega}{l} \sin \theta \sin \Omega t \right)^2 - \frac{ma^2\Omega^2}{2} \sin^2 \theta \sin^2 \Omega t + ml^2\omega_0^2 \cos \theta, \quad (72)$$

where  $\omega_0 = \sqrt{g/l}$ . Using the standard definitions for the canonical momentum  $p_\theta =$

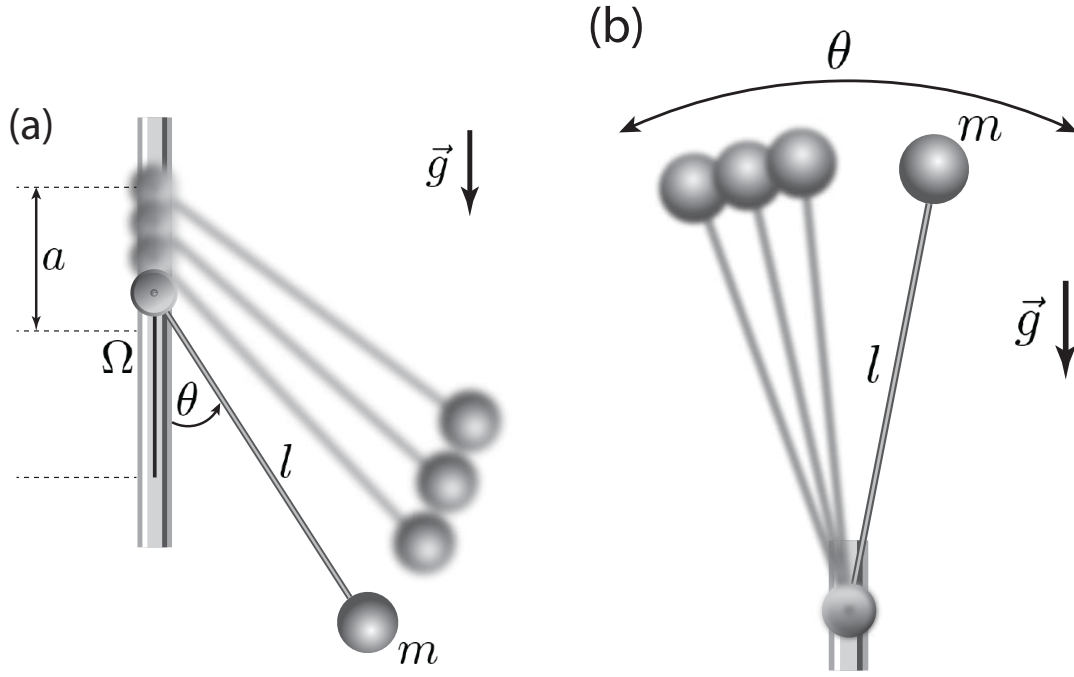


Figure 10. (Color online) The Kapitza pendulum. (a) The point of suspension of a rigid pendulum of mass  $m$  and natural frequency  $\omega_0 = \sqrt{g/l}$  is periodically modulated in the vertical direction with an amplitude  $a$  and frequency  $\Omega$ . (b) In the high-frequency limit, whenever  $\lambda = a\Omega/l > \sqrt{2}\omega_0$ , the upper equilibrium at  $\theta = \pi$  becomes dynamically stable and the system can oscillates around the inverted position.

$\partial\mathcal{L}/\partial\dot{\theta}$  and the Hamiltonian  $H = p_\theta\dot{\theta} - L$  we arrive at [3, 61]

$$H = \frac{1}{2ml^2} (p_\theta - mla\Omega \sin \theta \sin \Omega t)^2 - ml^2\omega_0^2 \cos \theta. \quad (73)$$

The shift in momentum can be removed by a standard gauge transformation on the Hamiltonian, resulting in the scalar potential, which effectively modulates the internal frequency  $\omega_0$ , so that the Hamiltonian becomes equivalent to

$$H = \frac{p_\theta^2}{2ml^2} - ml^2 \cos \theta \left( \omega_0^2 + \frac{a\Omega}{l} \cos \Omega t \right). \quad (74)$$

To simplify the notations we redefine  $ml^2 \rightarrow m$ ,  $a\Omega/l \rightarrow \lambda$  resulting in the celebrated Kapitza Hamiltonian

$$H = \frac{p_\theta^2}{2m} - m \cos \theta (\omega_0^2 + \lambda \cos \Omega t). \quad (75)$$

In this form the Kapitza Hamiltonian obviously belongs to the Kapitza class. As we discussed above, it has a well-defined infinite-frequency limit if we keep  $\lambda$  fixed, i.e. scale the driving amplitude linearly with frequency. Note that, formally one can obtain the Kapitza Hamiltonian by directly modulating the coupling constant in the cosine potential (gravitational constant  $g$  in this case). However, notice that the large frequency limit effectively corresponds to changing the sign of this coupling, which is not always easy to achieve.

The Floquet Hamiltonian in the infinite-frequency limit, Eq. (69), is

$$H_F^{(0)} = \frac{p_\theta^2}{2m} - m\omega_0^2 \cos \theta + m \frac{\lambda^2}{4} \sin^2 \theta \quad (76)$$

When  $\lambda > \sqrt{2}\omega_0$  the effective potential in Eq. (76) supports a stable local minimum at the inverted position  $\theta = \pi$ . In the absence of the driving, the equilibrium position  $\theta = \pi$  is clearly unstable. Therefore, by driving the pendulum it is possible to change the stability of the upper equilibrium. This phenomenon is known as dynamical stabilization and it is widely used in many areas of physics [110–113].

### 5.2. *The Kapitza Hamiltonian in the Rotating Frame. Floquet Gauge Freedom.*

In this section we demonstrate a simpler derivation of the infinite-frequency Floquet Hamiltonian by going to a rotating frame. In parallel, we explicitly discuss the Floquet-gauge transformation related to the phase of the driving protocol, which is equivalent to the shift of the stroboscopic time  $t_0$ , c.f. Sec. 2.

For this purpose, we consider a slightly more general form of the Kapitza Hamiltonian with an arbitrary phase shift  $\gamma$ :

$$H(t; \gamma) = \frac{p_\theta^2}{2m} - m\omega_0^2 \cos \theta - m\lambda\Omega \cos(\Omega t + \gamma) \cos \theta,$$

First, we transform the system to the rotating frame by

$$\begin{aligned} V(t; \gamma) &= \exp(-i\Delta_\gamma(t) \cos \theta) \\ \Delta_\gamma(t) &= -m\lambda [\sin(\Omega t + \gamma) - \sin \gamma]. \end{aligned} \quad (77)$$

As everywhere else in this paper,  $V(t)$  is the transformation which goes from the rotating to the lab frame.

It is often convenient to define the rotating frame such that  $V(0) = \mathbf{1}$ , so that the initial states in the lab and the rotating frame are the same. By construction, this transformation eliminates the divergence of the driving protocol with  $\Omega$  in the infinite-frequency limit. Hence, as  $\Omega \rightarrow \infty$  the Floquet Hamiltonian becomes effectively equivalent to the time-averaged Hamiltonian in the rotating frame, as discussed in Sec. 3. In the rotating frame, the transformed Hamiltonian is given by

$$\begin{aligned} H^{\text{rot}}(t; \gamma) &= V^\dagger(t; \gamma) \left[ \frac{p_\theta^2}{2m} - m\omega_0^2 \cos \theta \right] V(t; \gamma) \\ &= \frac{p_\theta^2}{2m} - m\omega_0^2 \cos \theta + \frac{\Delta_\gamma^2(t)}{2m} \sin^2 \theta + \frac{\Delta_\gamma(t)}{2m} \{\sin \theta, p_\theta\}_+, \end{aligned} \quad (78)$$

where  $\{\cdot, \cdot\}_+$  denotes the anti-commutator. Noting that  $\frac{1}{T} \int_0^T dt \Delta_\gamma(t) = m\lambda \sin(\gamma)$  and  $\frac{1}{T} \int_0^T dt \Delta_\gamma^2(t) = m^2 \lambda^2 (1/2 + \sin^2 \gamma)$ , we find for the infinite-frequency Floquet-

Hamiltonian  $H_F^{\text{rot},(0)}$ :

$$\begin{aligned} H_F^{\text{rot},(0)}[\gamma] &= \frac{p_\theta^2}{2m} - m\omega_0^2 \cos \theta + m \frac{\lambda^2}{4} \sin^2 \theta + \frac{m\lambda^2}{2} \sin^2 \gamma \sin^2 \theta + \frac{\lambda}{2} \sin \gamma \{\sin \theta, p_\theta\} + \\ &= \frac{(p_\theta + m\lambda \sin \gamma \sin \theta)^2}{2m} - m\omega_0^2 \cos \theta + m \frac{\lambda^2}{4} \sin^2 \theta. \end{aligned} \quad (79)$$

For  $\gamma = 0$ , we recover exactly the Hamiltonian from Eq. (76) showing the equivalence of the Floquet Hamiltonians in the lab and rotating frames. It is also clear that the Floquet Hamiltonians at different values of  $\gamma$  are related by a static gauge transformation, in agreement with the general theory of Sec. 3. Finally, we mention that this result is consistent with predictions based on classical mechanics, according to which the prefactor of the term  $\sin^2 \theta$  in Eq. (79) is proportional to the time integral of the squared driving protocol [15]. Let us make one remark, though, that according to Eq. (71), the average effective potential is proportional not to the average of the force squared but to the average of its time integral. This makes no difference for a simple  $\cos \Omega t$  driving but will be important for more complex periodic protocols, e.g.  $f(t) = \cos \Omega t + \cos 2\Omega t$ .

### 5.3. Finite-Frequency Corrections

The Magnus expansion allows one to identify leading finite frequency corrections to the effective Hamiltonian  $H_F^{(0)}$ . This can be done both in the lab frame and in the rotating frame. However, going to the rotating frame makes the calculations much simpler because, as we discussed, there the Magnus expansion coincides with the  $\Omega^{-1}$ -expansion while, in the lab frame, terms from different order in the Magnus expansion can have the same scaling with  $\Omega$ .

To see this explicitly, let us first identify all terms of order  $\Omega^{-1}$  appearing in the lab frame. To avoid lengthy expressions, we only state the relevant commutators, which have to be multiplied by the corresponding time integrals. Clearly, two-fold nested commutators appear in the second-order Magnus expansion in the lab frame,  $H^{(2)}$ , three-fold nested commutators appear in the third order, and so on. However, each additional commutator comes with an extra  $\Omega^{-1}$  suppression coming from the time integral. It is straightforward to see that all the terms which scale as  $\Omega^{-1}$  are those containing twice the static Hamiltonian  $H_0$

$$H_0 = \frac{p_\theta^2}{2m} - m\omega_0^2 \cos \theta,$$

and arbitrary many times the driving term

$$H_1 = -\lambda \cos \theta.$$

The relevant corrections are given by

$$\begin{aligned} &[H_0, [H_0, H_1]], \\ &[H_0, [H_1, [H_0, H_1]]], [H_1, [H_0, [H_0, H_1]]], \\ &[H_1, [H_0, [H_1, [H_0, H_1]]]], [H_1, [H_1, [H_0, [H_0, H_1]]]]. \end{aligned} \quad (80)$$

All higher order commutators containing only two  $H_0$  terms vanish because  $H_0$  is quadratic in momentum. If we work in the symmetric Floquet-gauge  $\gamma = 0$ , the driving

protocol becomes symmetric w.r.t. the origin of the time axis, i.e.  $\cos \Omega t$ . One can then show that all odd order terms in the Magnus expansion vanish identically [72] and, thus, only the second-order (first line in Eq. (80)) and the fourth-order (third line in Eq. (80)) terms contribute.

While the evaluation of all these terms and the corresponding time integrals is in principle possible, it is quite cumbersome and computationally heavy. Instead, it is much easier to get the same  $1/\Omega$  correction in the rotating frame by simply evaluating the first order Magnus expansion:

$$H_F^{(1)}[\gamma = 0] = \frac{1}{4\pi i \Omega} \int_0^{2\pi} d\tau_1 \int_0^{\tau_1} d\tau_2 [H^{\text{rot}}(\tau_1), H^{\text{rot}}(\tau_2)],$$

where  $H^{\text{rot}}(t)$  is the Hamiltonian of Eq. (78), with  $\gamma = 0$ , and  $\tau = \Omega t$ . Then the calculation of  $H_F^{(1)}$  becomes very simple and we find

$$H_F^{(1)}[0] = \frac{1}{\Omega} \left[ \frac{\lambda}{4m} (p_\theta^2 \cos \theta + 2p_\theta \cos \theta p_\theta + \cos \theta p_\theta^2) - m\omega_0^2 \lambda \sin^2 \theta - m \frac{\lambda^3}{2} \cos \theta \sin^2 \theta \right]. \quad (81)$$

Using this expression, one can examine the accuracy of the infinite-frequency Hamiltonian. In a similar fashion it is also straightforward to calculate higher-order corrections in the rotating frame.

#### 5.4. *Dressed observables and Dressed Density Matrix.*

Let us now derive the dressed operators and the dressed density matrix appearing in the definition of FNS expectations for a few simple observables (i.e. driving the system with a random initial phase and performing a measurement at a random time but within a fixed period, c.f. 2.3). All calculations can be done again both in the lab and in the rotating frames. But because they are simpler in the rotating frame, we show the derivations only in the latter case.

Since the dressed (or bar) operators and the dressed density matrix are Floquet-gauge independent, we can choose  $\gamma = 0$ . We consider the following natural observables:  $\theta$ ,  $\theta^2$ ,  $p_\theta$ , and  $p_\theta^2$ , and explicitly consider the initial state characterized by the Gaussian wave-function

$$\langle \theta | \psi_0 \rangle = \frac{1}{(2\pi)^{1/4} \sqrt{\sigma}} e^{-\frac{\theta^2}{4\sigma^2}} \quad (82)$$

with the corresponding density matrix

$$\rho_0(\theta_1, \theta_2) = \frac{1}{\sqrt{2\pi}\sigma} e^{-\frac{\theta_1^2 + \theta_2^2}{4\sigma^2}}. \quad (83)$$

Notice that in the rotating frame, the operators  $\theta$  and  $\theta^2$  remain the same as in the lab frame while the operators  $p_\theta$  and  $p_\theta^2$ , as well as the off-diagonal elements of the density

matrix acquire time dependence:

$$\begin{aligned} p_\theta^{\text{rot}}(t) &= V^\dagger(t) p_\theta V(t) = p_\theta + \Delta(t) \sin \theta, \\ p_\theta^{2,\text{rot}}(t) &= p_\theta^2 + \Delta(t)^2 \sin^2 \theta + \Delta(t) \{\sin \theta, p_\theta\}_+, \\ \rho^{\text{rot}}(\theta_1, \theta_2; t) &= e^{i\Delta(t)(\cos \theta_1 - \cos \theta_2)} \rho_0(\theta_1, \theta_2) \end{aligned} \quad (84)$$

where the operator  $V(t)$  and the function  $\Delta(t)$  are defined in Eq. (77) with  $\gamma = 0$ .

The Kick operator  $P(t)$  in the rotating frame is given by Eq. (7):

$$P(t) = T_t \exp \left[ -i \int_0^t H^{\text{rot}}(t') dt' \right] e^{iH_F t}, \quad (85)$$

and the dressed operators and density matrix are defined by Eqs. (22). As in the previous section, we focus on the leading and the first subleading terms in  $\Omega^{-1}$  for the dressed operators. Then we can rely on Eqs. (38) and (39). In the infinite-frequency limit, the dressed operators and density matrix are obtained from the corresponding time-averaged quantities in the rotating frame. This implies that all operators, which are functions of  $\theta$  are unaffected while the functions, which depend on momentum beyond linear order get dressed:

$$\overline{p_\theta} \approx p_\theta, \quad \overline{p_\theta^2} \approx p_\theta^2 + m^2 \frac{\lambda^2}{2} \sin^2 \theta. \quad (86)$$

The density matrix, being a function of both coordinates and momenta, also gets dressed. In particular

$$\begin{aligned} \overline{\rho}(\theta_1, \theta_2) &\approx \frac{1}{T} \int_0^T e^{i\Delta(t)(\cos \theta_1 - \cos \theta_2)} \rho_0(\theta_1, \theta_2) \\ &= \mathcal{J}_0(m\lambda(\cos \theta_1 - \cos \theta_2)) \rho_0(\theta_1, \theta_2). \end{aligned} \quad (87)$$

Note that the diagonal elements of  $\rho_0$ , defining the probabilities of a particular value of  $\theta$ , are not affected in the infinite frequency limit, while the off-diagonal elements, which determine the momentum distribution, get affected. To gain more intuition about this density matrix one can take a partial Fourier transform defining the Wigner function:

$$\overline{W}(\theta, p_\theta) = \frac{1}{2\pi} \int_{-\infty}^{\infty} d\xi \overline{\rho}(\theta + \xi/2, \theta - \xi/2) e^{ip_\theta \xi} \quad (88)$$

This can be readily done assuming that the uncertainty  $\sigma$  in the coordinates is small, and one can approximate  $\cos \theta$  by  $1 - \theta^2/2$ . Then

$$\begin{aligned} \overline{W}(\theta, p_\theta) &\approx \frac{e^{-\theta^2/(2\sigma^2)}}{(2\pi)^{3/2}\sigma} \int_{-\infty}^{\infty} d\xi e^{-\xi^2/(8\sigma^2)} J_0(m\lambda\theta\xi) e^{ip_\theta \xi} \\ &\approx \frac{e^{-\theta^2/(2\sigma^2)}}{(2\pi)^{3/2}\sigma} \int_{-\infty}^{\infty} d\xi e^{-\xi^2/(8\sigma^2)} e^{-m^2\lambda^2\theta^2\xi^2/4} e^{ip_\theta \xi} \\ &\approx \frac{1}{\pi\sqrt{1 + 2m^2\lambda^2\sigma^2\theta^2}} \exp \left[ -\frac{\theta^2}{2\sigma^2} - \frac{2p_\theta^2\sigma^2}{1 + 2m^2\lambda^2\sigma^2\theta^2} \right], \end{aligned} \quad (89)$$

where we used both  $\sigma \ll 1$  and  $\theta \ll 1$ . It follows that the off-diagonal elements of the

density matrix in the coordinate representation result, as expected, in a broadening of the momentum distribution. The new uncertainty in momentum is

$$\langle p_\theta^2 \rangle \approx \frac{1}{2\sigma^2} + m^2 \frac{\lambda^2}{2} \theta^2, \quad (90)$$

which is consistent with Eq. (86) given that we relied on  $|\theta| \ll 1$ . Not surprisingly, the momentum uncertainty of the dressed density matrix is precisely the uncertainty of the dressed  $\bar{p}_\theta^2$  operator calculated with the original density matrix (see Eq. (86)).

The first subleading terms to the dressed operators can be found using Eqs. (38) and (39). We emphasize again that to find the  $\Omega^{-1}$ -corrections, it is sufficient to know only the infinite-frequency Floquet Hamiltonian. Performing the integration over time, we find

$$\begin{aligned} \bar{\theta} &\approx \theta - \frac{\lambda}{\Omega} \sin \theta, \\ \bar{\theta}^2 &\approx \theta^2 - \frac{2\lambda}{\Omega} \theta \sin \theta \\ \bar{p}_\theta &\approx p_\theta + \frac{\lambda}{2\Omega} \{p_\theta, \cos \theta\}_+, \\ \bar{p}_\theta^2 &\approx p_\theta^2 + \frac{m^2 \lambda^2}{2} \sin^2 \theta + \frac{\lambda}{\Omega} \left( \frac{\{\cos \theta, p_\theta^2\}_+}{2} + p_\theta \cos \theta p_\theta - \cos \theta \sin^2 \theta \right). \end{aligned} \quad (91)$$

One can similarly find the first subleading correction to the density matrix.

$$\begin{aligned} \bar{\rho}(\theta_1, \theta_2) &\approx \bar{\rho}^{(0)}(\theta_1, \theta_2) - \frac{1}{\Omega} \bar{\rho}^{(1)}(\theta_1, \theta_2), \\ \bar{\rho}^{(0)}(\theta_1, \theta_2) &\approx \mathcal{J}_0(m\lambda(\cos \theta_1 - \cos \theta_2)) \rho_0(\theta_1, \theta_2) \\ \bar{\rho}^{(1)}(\theta_1, \theta_2) &\approx \left\{ \lambda \mathcal{J}_0(m\lambda(\cos \theta_1 - \cos \theta_2)) \left( \frac{1}{2}(\cos \theta_1 + \cos \theta_2) + \left( \frac{\theta_1}{2\sigma^2} \sin \theta_1 + \frac{\theta_2}{2\sigma^2} \sin \theta_2 \right) \right) \right. \\ &\quad \left. + m\lambda^2(\sin^2 \theta_1 + \sin^2 \theta_2) \mathcal{J}_1(m\lambda(\cos \theta_1 - \cos \theta_2)) \right\} \rho_0(\theta_1, \theta_2). \end{aligned} \quad (92)$$

The diagonal elements of the first correction can also be represented in the form  $\bar{\rho}^{(1)}(\theta, \theta) = -\lambda \partial_\theta (\sin \theta \rho_0(\theta, \theta))$ .

### 5.5. Multi-dimensional and Multi-particle Generalization of the Kapitza Pendulum

Last, let us discuss two generalizations of the Kapitza pendulum belonging to the Kapitza class, where one can realize other interesting Hamiltonians in the high-frequency limit. First, we consider a single particle multi-dimensional generalization. Namely, we analyze a particle of unit mass whose motion is constrained to a  $d$ -dimensional hyper-surface embedded in a  $D$ -dimensional coordinate space. For example, this can be a particle confined to a 2-dimensional sphere or other, more complicated surface. Let this surface be parameterized by the coordinates  $\mathbf{r} = (r_1(\theta_1, \dots, \theta_d), \dots, r_D(\theta_1, \dots, \theta_d))$  with  $\theta_1, \dots, \theta_d$  being local coordinates. Now, suppose we choose a preferred direction  $\mathbf{e}_i$  in  $\mathbb{R}^D$ , to shake the entire hyper-surface periodically:

$$\mathbf{r}(\theta_1, \dots, \theta_d) \rightarrow \mathbf{r}(\theta_1, \dots, \theta_d) + a \cos \Omega t \mathbf{e}_i = \mathbf{r}'(t). \quad (93)$$



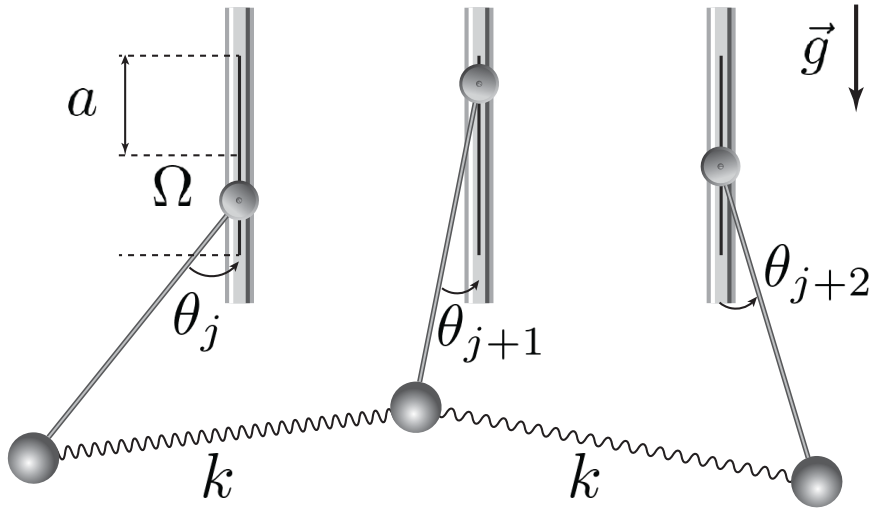


Figure 11. (Color online) A system of coupled Kapitza pendulums: a many-body representative of the Kapitza class.

The kinetic energy of the particle transforms according to

$$\begin{aligned} |\dot{\mathbf{r}}'(t)|^2 &= |\dot{\mathbf{r}}(t)|^2 - 2\Omega a \sin \Omega t \dot{r}_i + F(t) \\ &= |\dot{\mathbf{r}}(t)|^2 + 2\Omega^2 a \cos \Omega t r_i + F'(t), \end{aligned} \quad (94)$$

where we used integration by parts. The functions  $F(t)$  and  $F'(t)$  contain only full time derivatives and hence can be omitted. Hence, shaking the surface creates an additional time-dependent gravitational field along the shaking direction. As in the standard Kapitza case, the non-trivial infinite-frequency limit is achieved if we keep the product  $\lambda = a\Omega$  fixed. The resulting effective Hamiltonian can be found from Eqs. (69) – (71). All finite-frequency corrections as well as the dressed operators can be found by a simple extension of the corresponding results for the Kapitza pendulum. We emphasize again the crucial role of the embedding space: such a non-trivial scaling of the coupling strength cannot be naturally obtained by periodically driving any intrinsic model parameter (the bare gravity  $g$  in this case).

As a last example we generalize the Kapitza pendulum to a chain of coupled pendulums (see Fig. 11). Consider  $N$  coupled pendulums, shaken along the  $y$ -direction using some specific driving protocol. In a way this example can be thought of as a single particle confined to an  $N$ -dimensional hyper-surface embedded in a  $2N$ -dimensional space, where  $N$  is the number of pendulums. One can repeat the derivation of Sec. 5.1 to find that the Hamiltonian of this system reads as

$$H = \sum_{j=1}^N \frac{p_j^2}{2m} - J \cos(\theta_j - \theta_{j+1}) - m\omega_0^2 \cos \theta_j - m\lambda\Omega \cos \Omega t \cos \theta_j, \quad (95)$$

where  $J = kl^2$  is the coupling proportional to the spring constant. In the infinite-frequency and large-amplitude limit, this Hamiltonian leads to a discretized version of the Sine-Gordon model, which is also very close to the famous Frenkel-Kontorova model [114]:

$$H_F^{(0)} = \sum_{j=1}^N \frac{p_j^2}{2m} - J \cos(\theta_j - \theta_{j+1}) - m\omega_0^2 \cos \theta_j + m\frac{\lambda^2}{4} \sin^2 \theta_j. \quad (96)$$

This model can undergo a quantum phase transition, between the gapless and gapped phases, depending on the driving strength  $\lambda$  as well as the magnitude of the other couplings. It supports various interesting excitations, such as solitons and breathers, and their nature can change with varying  $\lambda$  [114]. This model is integrable in the limits  $\lambda \ll \omega_0$  and  $\lambda \gg \omega_0$  but non-integrable when these couplings are comparable to one another. This opens the possibility of studying interesting thermalization-type dynamics. Additionally, it becomes possible to create interesting infinite-frequency limits by driving different pendulums with different amplitudes and phases. Then, especially in two-dimensional coupled systems, the phases  $\gamma_j$  appearing in (79) can be used to generate artificial position-dependent gravitational fields, making the emergent physics even more interesting.

## 6. The Dirac Class

In this section, we consider periodically driven systems with a kinetic energy linear in momentum. According to relativistic quantum mechanics, this requires an additional spin structure in the Hamiltonian [115]. Such systems describe the low-energy physics of graphene [116], Weyl semi-metals [117], and other related systems [49, 118, 119].

### 6.1. Periodically Driven Magnetic Fields

We shall first focus on the *Dirac* class defined by the following Hamiltonian

$$\begin{aligned} H(t) &= H_0(\mathbf{r}, t) + H_{\text{int}}, \\ H_0(\mathbf{r}, t) &= K - \lambda \Omega \sin \Omega t \mathbf{B}(\mathbf{r}) \cdot \boldsymbol{\sigma}, \quad K = \mathbf{p} \cdot \boldsymbol{\sigma}, \end{aligned} \quad (97)$$

where the driving couples to the external magnetic field  $\mathbf{B}(\mathbf{r})$ . Here  $H_{\text{int}}(\mathbf{r})$  contains arbitrary spin-independent external potentials and (for many-particle systems) any spin-independent many-body interactions. Taking additional spin-dependent static external potentials into account is straightforward but will unnecessarily aggravate the discussion. Furthermore, to avoid technical complications, our analysis is restricted to situations where the magnetic field does not change its direction in time. To simplify the notations we shall keep the discussion at the single-particle level. We also assume that the momentum couples to the  $2 \times 2$  Pauli  $\sigma$ -matrices. We could similarly analyze a coupling to the  $4 \times 4$  Dirac  $\gamma$ -matrices without any need to define a new class.

Similarly to the Kapitza class, the analysis of the Magnus expansion for the Dirac class can be significantly simplified by performing a transformation to a rotating frame given by

$$\begin{aligned} V(t) &= \exp(-i\Delta(t)\mathbf{B}(\mathbf{r}) \cdot \boldsymbol{\sigma}), \\ \Delta(t) &= \lambda \cos \Omega t. \end{aligned} \quad (98)$$

Clearly,  $V(t)$  is a periodic function of time, but with our choice of  $\Delta(t)$ , it does not satisfy the condition  $V(0) = \mathbf{1}$ . Hence, the initial state in the rotating frame is related to the initial state in the lab frame via a unitary rotation by  $V(0)$ , i.e.  $|\psi^{\text{lab}}\rangle = V(0)|\psi^{\text{rot}}\rangle$ . One can of course change  $V(t)$  by redefining  $\Delta(t) \rightarrow \Delta(t) - \Delta(0)$ , but this leads to additional terms in the Floquet Hamiltonian which transforms according to  $H_F^{\text{lab}} = V(0)H_F^{\text{rot}}V^\dagger(0)$ . This is a manifestation of the Floquet-gauge, discussed in Sec. 2.

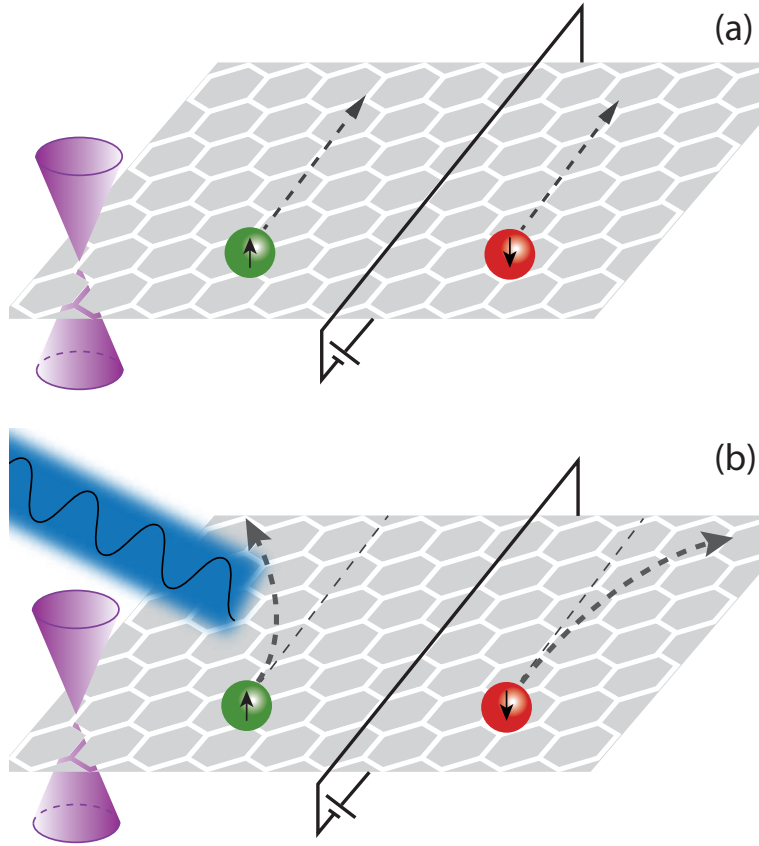


Figure 12. (Color online) Light induced spin-orbit coupling. Shining light on fermions with a relativistic dispersion, such as graphene close to the neutrality point, leads to spin-orbit coupling whose strength is controlled by the driving amplitude. (a) In absence of the driving, a potential bias generates a longitudinal current. (b) In presence of the driving, a potential bias generates a longitudinal and a *transverse* current whose direction depends on the value of the spin.

After the transformation the kinetic energy becomes

$$\begin{aligned}
 K^{\text{rot}}(t) &= V^\dagger(t) \mathbf{p} \cdot \boldsymbol{\sigma} V(t) \\
 &= \frac{1}{2} \{ \cos(2\Delta(t)B(\mathbf{r})), \mathbf{p} \cdot \boldsymbol{\sigma} - (\mathbf{n} \cdot \mathbf{p})(\mathbf{n} \cdot \boldsymbol{\sigma}) \}_+ - \frac{1}{2} \{ \sin(2\Delta(t)B(\mathbf{r})), (\mathbf{n} \times \mathbf{p}) \cdot \boldsymbol{\sigma} \}_+ \\
 &\quad - \Delta(t) \mathbf{n} \cdot \nabla B(\mathbf{r}) + (\mathbf{n} \cdot \mathbf{p})(\mathbf{n} \cdot \boldsymbol{\sigma}), \quad (99)
 \end{aligned}$$

where  $B(\mathbf{r})$  and  $\mathbf{n}$  are the magnitude and the direction of the magnetic field  $\mathbf{B}(\mathbf{r})$ .  $H_{\text{int}}$  is not affected by the transformation to the rotating frame. If the original Hamiltonian contains additional spin-dependent external fields or interactions, then the transformation to the rotating frame will lead to modification of  $H_{\text{int}}$ .

We can now readily obtain the effective high-frequency Floquet Hamiltonian by taking the time-average of Eq. (99) and including the spin-independent interaction term which remains unchanged in the rotating frame:

$$H_F^{\text{rot},(0)} = (\mathbf{n} \cdot \mathbf{p})(\mathbf{n} \cdot \boldsymbol{\sigma}) + \frac{1}{2} \{ \mathcal{J}_0(2\lambda B(\mathbf{r})), \mathbf{p} \cdot \boldsymbol{\sigma} - (\mathbf{n} \cdot \mathbf{p})(\mathbf{n} \cdot \boldsymbol{\sigma}) \}_+ + H_{\text{int}}, \quad (100)$$

where  $\mathcal{J}_0$  is the 0-th order Bessel function of the first kind. One can show that there are no  $\Omega^{-1}$ -corrections to this Floquet Hamiltonian for the chosen Floquet gauge. This follows from the observation that for a symmetric driving protocol, all terms in Eq. (99), as well

as in the time-independent interaction term, are even with respect to  $t \rightarrow T - t$  and, therefore, the odd terms in the contributions to the Floquet Hamiltonian vanish [72] (see Eq. (28)). Therefore the leading non-vanishing correction to this Floquet Hamiltonian is of order  $\Omega^{-2}$ . This allows one to control the Floquet Hamiltonian in this gauge to a better precision.

*Dresselhaus Spin-Orbit Coupling.* We now consider an example in which we drive a linearly polarized constant magnetic field along a fixed direction in the  $xy$ -plane. We find an effective Dresselhaus spin-orbit coupling (SOC) in the high-frequency limit. Proposals for Floquet realizations of SOC (see Fig. 12 for a schematic representation) have already been made for bosons using constant pulse sequences [120–123]. For fermions, the periodically driven spin-orbit coupling has been studied in graphene [124].

Let us consider the following Hamiltonian

$$H(t) = \mathbf{p} \cdot \boldsymbol{\sigma} - \Omega \lambda \sin \Omega t \mathbf{n} \cdot \boldsymbol{\sigma} + H_{\text{int}},$$

$$\mathbf{n} = \frac{1}{\sqrt{2}} (1, 1, 0). \quad (101)$$

Following the transformation in the rotating frame above, the resulting Floquet Hamiltonian is given by Eq. (100). For the particular choice of  $\mathbf{n}$  it is equivalent to

$$H_F^{\text{rot},(0)} = \left( \mathcal{J}_0(2\lambda) + \frac{1}{\sqrt{2}} (1 - \mathcal{J}_0(2\lambda)) \right) \mathbf{p} \cdot \boldsymbol{\sigma} + \frac{1}{\sqrt{2}} (1 - \mathcal{J}_0(2\lambda)) (p_x \sigma_y + p_y \sigma_x) + H_{\text{int}}, \quad (102)$$

Hence, besides the expected renormalization of the Fermi velocity, one finds an effective Dresselhaus spin-orbit coupling term without affecting the interactions.

## 6.2. Periodically Driven External Potentials

When one takes into consideration driving systems with a linear dispersion, there exists yet a second possibility in which the driving protocol couples to a scalar external potential. The general form of the lab-frame Hamiltonian is

$$H(t) = K + H_{\text{int}} + \lambda \Omega^2 \cos \Omega t H_1(\mathbf{r}), \quad K = \mathbf{p} \cdot \boldsymbol{\sigma}, \quad (103)$$

where  $H_1(\mathbf{r})$  is an arbitrary spin-independent scalar potential. We assume that both  $H_1$  and  $H_{\text{int}}$  are diagonal in spin space. Notice that this time the driving amplitude scales with  $\Omega^2$ . Below, we explain this rather peculiar scaling from two different perspectives: the lab-frame Magnus expansion, and a transformation to a rotating frame.

The requirement for the  $\Omega^2$ -scaling of the driving amplitude is intimately related to the existence of the additional spin structure in the Hamiltonian. To gain some insight into the complications induced by the latter, we can apply the Magnus expansion *in the lab frame*. The zeroth order term gives the time-averaged Hamiltonian  $K + H_{\text{int}}$ . The leading contribution to the Floquet Hamiltonian is derived from the terms

$$[K, [K, H_1]], [H_1, [K, H_1]].$$

In the non-relativistic Kapitza class, where the driving amplitude scales as  $\Omega$ , c.f. Sec. 5, the second of these terms is dominant in the high-frequency limit. However, for systems with a Dirac dispersion, the second term vanishes identically, because  $K$  is linear in

momentum and  $H_1$  is diagonal in spin space. As a result, only the term  $[K, [K, H_1]]$  contributes to the Floquet Hamiltonian. To keep this term well-behaved in the infinite-frequency limit, we need to scale the driving amplitude as  $\Omega^2$  in order to cancel the factor  $T^2$  coming from the double time integral (c.f. definition of the Magnus expansion in Sec. 3). Notice, however, that while in the Kapitza class the Magnus expansion in the limit  $\Omega \rightarrow \infty$  truncates in the lab frame after the second order, here this is not the case due to the additional spin structure in the kinetic energy term. For instance, consider the fourth-order commutator  $[K, [H_1, [K, [H_1, K]]]]$ , which scales as  $\Omega^4$ . Taking into account the factor  $\Omega^{-4}$  from the time-ordered integrals, we find that this term remains finite as  $\Omega \rightarrow \infty$ . Although the kinetic energy is linear in  $\mathbf{p}$ , this 4-nested commutator does not vanish due to the spin structure  $[\sigma_\alpha, \sigma_\beta] = 2i\varepsilon_{\alpha\beta\gamma}\sigma_\gamma$ . Similar expressions appear in any even higher-order terms in the expansion (all odd terms being zero due to the symmetry of the drive).

We now show that also for Hamiltonians with linear dispersion, in which the driving couples to an external potential, a transformation  $\tilde{V}(t)$  to a preliminary rotating frame proves very useful to organise the perturbative expansion. Let us rotate the Hamiltonian in Eq. (103) according to

$$\tilde{V}(t) = \exp(-i\lambda\Omega \sin \Omega t H_1(\mathbf{r})). \quad (104)$$

In this preliminary rotating frame the kinetic energy transforms as

$$\begin{aligned} \tilde{K}(\mathbf{r}, t) &= \tilde{V}^\dagger(t) \mathbf{p} \tilde{V}(t) \cdot \boldsymbol{\sigma} = \mathbf{p} \cdot \boldsymbol{\sigma} - \lambda\Omega \sin \Omega t \mathbf{B}(\mathbf{r}) \cdot \boldsymbol{\sigma}, \\ \tilde{H}(t) &= \tilde{K}(\mathbf{r}, t) + H_{\text{int}}. \end{aligned} \quad (105)$$

where  $\mathbf{B}(\mathbf{r}) = \nabla H_1(\mathbf{r})$  is the “magnetic field”, generated by the spatial gradient of the time-dependent scalar potential. This is only an analogy with real magnetic fields, which are always divergence-free, while the effective magnetic field is not. For example choosing a parabolic driving potential  $H_1(\mathbf{r}) = r^2$  induces an effective radial “magnetic field”  $\mathbf{B}(\mathbf{r}) = 2\mathbf{r}$  in the first rotating frame. The amplitude of this oscillatory “magnetic field” scales only linearly with the driving frequency, reflecting the re-summation of an infinite lab-frame Magnus subseries. The interaction term  $H_{\text{int}}$  is not affected by this transformation.

Notice that in this first rotating frame, the Hamiltonian in Eq. (105) assumes precisely the same form as the one, where the driving couples to the magnetic field, c.f. Eq. (97). Therefore, for the subsequent discussion we refer to Sec. 6.1. In fact, this is the reason why the Hamiltonian in Eq. (103) belongs also to the Dirac class. This also gives a different explanation for the  $\Omega^2$ -scaling assumed in Eq. (103). We stress that the Hamiltonian (105) can be used as a starting point instead of the Hamiltonian (97). Therefore, within the Dirac class of systems with a linear dispersion, one can either drive the system via a spatially dependent scalar potential with an amplitude scaling as  $\Omega^2$ , or with a spatially dependent “magnetic field” with an amplitude scaling linearly with  $\Omega$ . Using the scalar potential allows one to generate synthetic “magnetic fields”, which may not satisfy the ordinary Maxwell equations (in particular, this might allow one to introduce effective magnetic monopoles into the system).

*Periodically driven external potential.* As an illustration let us consider a graphene-type setup in which the momentum of the particle is confined to the  $x, y$ -plane. The external potential depends linearly on the out-of-plane coordinate  $z$  via  $H_1(z) = z$ . The Hamiltonian is

$$H(t) = K + H_{\text{int}} + \lambda \Omega^2 \cos \Omega t \, z. \quad (106)$$

Going to the first rotating frame we find a constant in space, time-dependent “magnetic field” along the  $z$ -axis:  $\mathbf{B} = \lambda \hat{\mathbf{z}}$  such that

$$\tilde{H}(t) = \mathbf{p} \cdot \boldsymbol{\sigma} + \Omega \sin \Omega t \, \mathbf{B} \cdot \boldsymbol{\sigma} + H_{\text{int}}.$$

We now do a transformation to a second rotating frame, as discussed in Sec. 6.1. For the model considered in this example, the general Floquet Hamiltonian in Eq. (100) reduces to

$$H_F^{\text{rot},(0)} = \mathcal{J}_0(2\lambda) (p_x \sigma_x + p_y \sigma_y) + H_{\text{int}}. \quad (107)$$

Note that there are no terms proportional to  $p_z$ , since the motion of the particles is confined to the two-dimensional  $xy$ -plane. This driving protocol essentially leads to a renormalised Fermi velocity, which can be tuned to zero by choosing  $2\lambda$  to coincide with the zero of the Bessel function  $\mathcal{J}_0$ . This can be used for enhancing interaction effects in weakly-interacting many-particle systems.

If in the same setup the effective potential linearly depends on  $x$  then the resulting Floquet Hamiltonian becomes anisotropic

$$H_F^{\text{rot},(0)} = H_{\text{int}}(\mathbf{r}) + p_x \sigma_x + \mathcal{J}_0(2\lambda) p_y \sigma_y \quad (108)$$

and tuning the strength of the field to the zero of the Bessel function makes the kinetic term one-dimensional.

## 7. The Dunlap-Kenkre (DK) Class

As a third class of Hamiltonians, where one can engineer interesting infinite-frequency limits, we consider a setup where the driving couples to a non-interacting term in an arbitrary interacting system. Examples include interacting particles with arbitrary dispersion relation in an external time-dependent electric field, or interacting spin systems in a periodic magnetic field, just to name a few. As we shall see in this section, this class of Hamiltonians is paradigmatic for ‘Floquet engineering’. Examples of such systems include Wannier-Stark ladders [53, 125–127], non-trivial tight-binding models with engineered dispersion relations [53, 128–130], including the Harper-Hofstadter Hamiltonian [47, 48, 71, 131] and other models exhibiting artificial gauge fields [42, 53, 132–134], effective spin Hamiltonians [135–137], quantum Hall states [38], topologically non-trivial Floquet Hamiltonians [40, 41, 44, 45, 49, 50, 138], and others.

To the best of our knowledge, the first theoretical proposal for the realization of a non-trivial high-frequency limit in a tight-binding model with an external periodic electric field was discussed by Dunlap and Kenkre in Refs. [139, 140]. They discussed the phenomenon of dynamical localization, where the hopping between sites can be completely suppressed in the high frequency limit by choosing an appropriate fixed ratio between the driving amplitude and the driving frequency. Motivated by their idea, we consider

the following general class of Hamiltonians

$$H(t) = H_0 + \Omega H_1(t), \quad (109)$$

where  $H_0$  represents some (interacting) lattice Hamiltonian, and

$$H_1 = \sum_m f_m(t) n_m \quad (110)$$

with  $n_m$  being the density operator on the  $m$ -th lattice site, and  $f_m(t)$  is an arbitrary site-dependent periodic function of time with period  $T$ . Notice that in Eq. (109), we have explicitly put the  $\Omega$ -dependence of the driving term  $H_1$  to highlight the non-trivial scaling of the driving amplitude with frequency.

Instead of the lattice system, we could consider a continuum model using  $\sum_m f_m(t) n_m \rightarrow \int d^d x f(t, \mathbf{x}) n(\mathbf{x})$  with the only condition that  $f(t + T, \mathbf{x}) = f(t, \mathbf{x})$ . Obviously, in the continuum limit there is an overlap between the DK class and the Kapitza class, if the kinetic energy in  $H_0$  is quadratic in momentum, and with the Dirac class if it is linear. In the DK class, we allow for arbitrary dispersion relations at the expense of restricting the driving to couple to single-particle terms. Later on, in Sec. 7.4, we shall show that the DK class extends to driven spin systems, where  $H_0$  describes some arbitrary interacting spin Hamiltonian, while the driving term couples to a spatially dependent, periodic in time magnetic field. The thermodynamics of the driven DK-class systems has been studied in Ref. [141].

After giving an overview of the general theory of the DK class, we will discuss the recent dynamical realization of the Harper Hamiltonian [47, 48], as a special case of the periodically driven Bose-Hubbard model. We will derive both the infinite-frequency limit, and the leading  $\Omega^{-1}$ -corrections to the Floquet Hamiltonian. We will also give examples for the dressed operators and density matrix. After that, we will continue with the fermionic case illustrated on the driven Fermi-Hubbard model, and discuss the infinite-frequency limit and the  $\Omega^{-1}$ -corrections, which are expected to be important for interacting Floquet topological insulators, as realized in Ref. [49]. Finally, we will discuss interacting driven spin chains.

To be specific, we assume that  $H_0$  is a sum of the kinetic energy term represented by the nearest neighbor hopping and additional density-density interactions which can also include a static external potential linearly coupled to the density:

$$H_0 = H_{\text{kin}} + H_{\text{int}}, \quad (111)$$

where

$$H_{\text{kin}} = -J_0 \sum_{\langle m, n \rangle} a_m^\dagger a_n + \text{h.c.}, \text{ and } [n_m, H_{\text{int}}] = 0.$$

The angular brackets here represent nearest neighbors.

The terms in the Magnus expansion, which do not vanish in the infinite-frequency limit are of the type

$$H_0, [H_1, H_0], [H_1, [H_1, H_0]], [H_1, [H_1, [H_1, H_0]]], \dots \quad (112)$$

Since each commutator brings an extra factor of  $1/\Omega$  from the time integral (see the discussion on the Magnus expansion in Sec. 3), and each  $H_1$  term brings an extra factor of  $\Omega$  due to the scaling of the driving amplitude, it is easy to see that all these terms are

of the same order in  $\Omega$ . Furthermore, it is easily seen that these are the only terms that survive in the infinite-frequency limit. However, unlike in the Kapitza class, this series does not terminate at any finite order and, thus, one has to re-sum an infinite lab-frame Magnus subseries to obtain the correct infinite-frequency limit.

From this structure of the Magnus expansion, it is also clear why the Hamiltonian  $H_1$  should couple linearly to the density. Only then do these nested commutators not grow both in space (meaning that the resulting effective operators remain local) and in the number of creation and annihilation operators (i.e. we avoid the generation of three- and higher-body interactions). One can also consider other situations where the commutators do not grow, for example, when the driving couples to the local in space density-density interaction between fermions [142] or even bosons [143–145] (though the bosonic case is more subtle), or when the protocol couples to local in space spin interactions for spin models with spin larger than one half.

While infinite re-summation of the Magnus (sub)series is possible and it yields the proper infinite-frequency limit, calculating subleading corrections directly becomes very involved. These complications can be overcome, as before, by going to the rotating frame, which is defined via the transformation

$$V(t) = \exp \left[ -i \sum_m \Delta_m(t) n_m \right], \quad \Delta_m(t) = \Omega \int^t dt' f_m(t'). \quad (113)$$

The lower limit of the integral defining  $\Delta_m(t)$  is a gauge choice, related to the Floquet-gauge. Applying this transformation eliminates the term linear in the density operator, which in the lab frame diverges linearly with the frequency. At the same time, in the rotating frame, a periodic drive is imprinted to the kinetic energy:

$$\begin{aligned} H^{\text{rot}}(t) &= W(t) + W^\dagger(t) + H_{\text{int}} \\ W(t) &= -J_0 \sum_{\langle mn \rangle} e^{i[\Delta_m(t) - \Delta_n(t)]} a_m^\dagger a_n. \end{aligned} \quad (114)$$

Notice that this transformation leaves the interaction term  $H_{\text{int}}$  invariant. As in the previous classes we discussed, going to the rotating frame generates an effective complex driving protocol, which is well-behaved in the infinite-frequency limit. The infinite-frequency limit of the Floquet Hamiltonian is then simply given by the time average of  $H^{\text{rot}}(t)$ . In the rotating frame, averaging over time is equivalent to a re-summation of an infinite lab-frame Magnus sub-series, in agreement with the general discussion in Sec. 3. Similarly to the Kapitza class, the Magnus expansion in the rotating frame coincides with the  $\Omega^{-1}$ -expansion of the Floquet Hamiltonian. Rather than discussing these corrections in the most general form, we will show and analyze them for specific examples.

### 7.1. *Noninteracting Particles in a Periodically Driven Potential: Floquet Theory and Experimental Realization*

As a first representative of the DK class, we consider a chain of noninteracting, periodically driven spinless particles, which can be either bosons or fermions (see Fig.13) with the following Hamiltonian

$$H(t) = -J_0 \sum_m \left( a_{m+1}^\dagger a_m + \text{h.c.} \right) + \sum_m \frac{V_0}{2} \sin(\Omega t - \Phi m + \Phi/2) n_m. \quad (115)$$



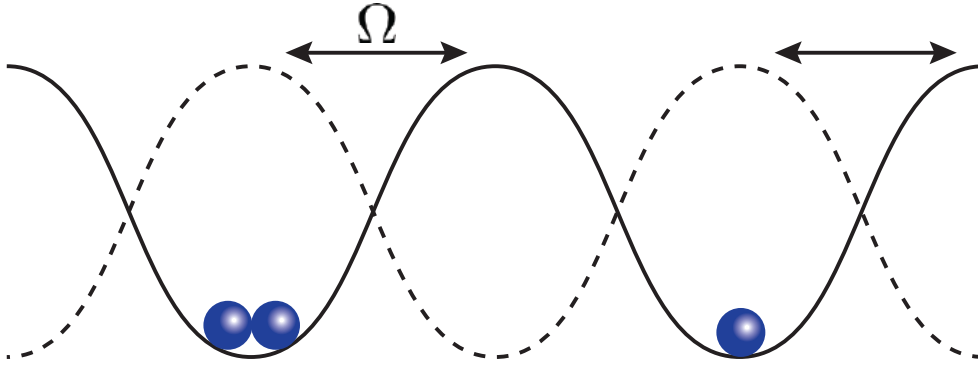


Figure 13. (Color online). A periodically driven (shaken) optical lattice in which the lattice is shifted periodically: the prototypical example of the DK class.

The operator  $a_m^\dagger$  creates a particle at site  $m$ , which can hop to its nearest neighbors gaining energy  $J_0$ . As anticipated, the driving protocol couples to the density breaking translational invariance through the site-dependent phase (which does not have to vary linearly in space). The driving amplitude  $V_0$  is constant in space and scales as  $\Omega$ . The above choice of the Floquet gauge (or the phase lag) ensures a simple form of the infinite-frequency Floquet Hamiltonian. In the next sections we shall generalize our analysis by adding interactions, a second spatial dimension, and finally by adding a spin degree of freedom.

The transformation to the rotating frame is done using Eq. (113) with  $\Delta_m(t) = -V_0/\Omega \cos(\Omega t - \Phi m + \Phi/2)$ . We pause to notice that, for this particular Floquet gauge choice,  $V(0) \neq 1$ . As a consequence, one needs to transform the initial state to the rotating frame as well.

Combining this with Eq. (114) we find:

$$H^{\text{rot}}(t) = -J_0 \sum_m g^{m,m+1}(t) a_{m+1}^\dagger a_m + \text{h.c.} \quad (116)$$

where

$$g^{m,m+1}(t) = e^{-i\zeta \sin(\Omega t - \Phi m)}, \quad \zeta = \frac{V_0}{\Omega} \sin(\Phi/2).$$

We label the function  $g^{m,m+1}(t)$  by two site indices to highlight that it is a link variable, i.e. defined on the bonds of the lattice. The infinite-frequency Floquet Hamiltonian and the leading correction are then found from the Magnus expansion:

$$\begin{aligned} H_F^{\text{rot},(0)} &= -J(\zeta) \sum_m \left( a_{m+1}^\dagger a_m + \text{h.c.} \right), \\ H_F^{\text{rot},(1)} &= -\frac{J_0^2}{\Omega} \sum_m \left( \mathcal{C}_{m,m+2}(\zeta) a_{m+2}^\dagger a_m + \text{h.c.} \right) \\ &\quad + \frac{J_0^2}{\Omega} \sum_m \mathcal{G}_{m,m+1}(\zeta) (n_m - n_{m+1}) \end{aligned} \quad (117)$$

with the renormalized hopping parameter  $J(\zeta) = J_0 \mathcal{J}_0(\zeta)$ , where  $\mathcal{J}_0$  is the 0-th order Bessel function of the first kind. The coupling constants  $\mathcal{C}_{m,m+2}(\zeta)$  and  $\mathcal{G}_{m,m+1}(\zeta)$  are given in Appendix B. The infinite-frequency Hamiltonian describes the original tight-

binding chain with a renormalized hopping amplitude. When the parameter  $\zeta$  is tuned to a zero of the Bessel function  $\mathcal{J}_0$ , the hopping is suppressed showing the phenomenon of dynamical localization as first discussed in Ref. [139], and experimentally verified in Ref. [146]. The leading correction represents an additional second-nearest-neighbor hopping term, and an extra static potential, which is periodic for any rational  $\Phi/\pi$ . Higher-order corrections in the inverse frequency appear as longer-range hopping terms, and modifications to the static potential.

Next we discuss the dressed operators emerging in the FNS evolution, i.e. the operators describing observables averaged over fast oscillations, c.f. Sec. 2.3. Two natural observables are given by the local density operator on site  $m$  and the local current operator flowing from site  $m$  to site  $m+1$ :

$$\begin{aligned} n_m &= a_m^\dagger a_m, \\ j_{m,m+1} &= -iJ_0(a_{m+1}^\dagger a_m - a_m^\dagger a_{m+1}). \end{aligned} \quad (118)$$

The transformation to the rotating frame leaves the density operator (commuting with the driving term) invariant, while the current operator (which does not commute with the driving) changes in the same way as the hopping term in the Hamiltonian. As we mentioned in Sec. 3.2, it is convenient to study the finite-frequency corrections to the Floquet dressed observables in the rotating frame. One then finds

$$\begin{aligned} n_m^{\text{rot}}(t) &= a_m^\dagger a_m = n_m^{\text{lab}}, \\ j_{m,m+1}^{\text{rot}}(t) &= J_0 \left( -ig^{m,m+1}(t) a_{m+1}^\dagger a_m + \text{h.c.} \right), \end{aligned} \quad (119)$$

Applying Eqs. (39) leads to the following infinite-frequency behavior of the dressed Floquet operators

$$\begin{aligned} \bar{n}_m &= n_m + \mathcal{O}(\Omega^{-1}), \\ \bar{j}_{m,m+1} &= J(\zeta)(-ia_{m+1}^\dagger a_m + \text{h.c.}) + \mathcal{O}(\Omega^{-1}). \end{aligned} \quad (120)$$

In the infinite-frequency limit, the observables  $\mathcal{A}$  which remain invariant under the transformation to the rotating frame  $V(t)$  do not get dressed, i.e.  $\bar{\mathcal{A}} = \mathcal{A}$ . On the other hand, observables which are not invariant w.r.t.  $V(t)$  get naturally dressed even in the infinite frequency-limit. In agreement with our general results (see Eq. (27)) the dressed current operator is precisely the current operator associated with the Floquet Hamiltonian. In other words, the dressed current describes the slow charge dynamics with respect to  $H_F$ . Such a dressed chiral current was successfully measured in a recent cold-atom experiment realizing the Harper-Hofstadter model in a ladder geometry [131].

Similarly to the Kapitza pendulum case  $\Omega^{-1}$ -corrections to the dressed operators are non-zero both for the density and for the current. They can be calculated with the help of the general expression (39). Since they are quite lengthy, we shall not show them explicitly. Physically the corrections are responsible for delocalization of the corresponding dressed operators, meaning that the operator support on the lattice grows as  $\Omega$  deviates from infinity. For example, the corrections to the dressed density involve terms which involve hopping between neighboring sites, etc.

Last, we show examples of the dressed density matrices. We consider two natural initial states for the system where the particle is either localized in position space or in

momentum space, corresponding to the density matrices:

$$\rho_m = |m\rangle\langle m|, \quad \rho_k = |k\rangle\langle k|. \quad (121)$$

We shall distinguish between the two density operators by the subindex  $m$  or  $k$ .

In the rotating frame, the two operators transform to

$$\begin{aligned} \rho_m^{\text{rot}}(t) &= |m\rangle\langle m|, \\ \rho_k^{\text{rot}}(t) &= \frac{1}{N_s} \sum_{mn} e^{ik(m-n)} e^{-i\frac{V_0}{\Omega} \sin \frac{\Phi(m-n)}{2} \sin(\Omega t - \Phi \frac{m+n-1}{2})} |m\rangle\langle n|. \end{aligned} \quad (122)$$

In the infinite-frequency limit, averaging over  $t$  leads to

$$\begin{aligned} \bar{\rho}_m &= |m\rangle\langle m|, \\ \bar{\rho}_k &= \frac{1}{N_s} \sum_{mn} e^{ik(m-n)} \mathcal{J}_0 \left( \frac{V_0}{\Omega} \sin \frac{\Phi(m-n)}{2} \right) |m\rangle\langle n|. \end{aligned} \quad (123)$$

As expected, the Fock-state density matrix, which commutes with the driving protocol, does not get any modifications (in the infinite-frequency limit). Hence, it still represents a pure state. On the contrary, the momentum-state density matrix gets dressed. In momentum space, this density matrix remains diagonal:

$$\bar{\rho}_k = \sum_q \sum_{l=-\infty}^{\infty} e^{i(k-q)l} \mathcal{J}_0 \left( \frac{V_0}{\Omega} \sin \frac{l\Phi}{2} \right) |q\rangle\langle q|. \quad (124)$$

This mixed density matrix represents a mixed state, which appears even in the infinite-frequency limit. Let us mention that finite-frequency corrections to the density matrices result in a mixed state even for the dressed Fock-state.

*Experimental Observation of Dynamical Localisation in Cold Atom Systems.* Let us briefly describe some recent experimental setups where the renormalisation of the hopping amplitude,  $J_0 \rightarrow J_0 \mathcal{J}_0(\zeta)$ , has been observed. Cold atom experiments in Floquet-engineered systems were initially motivated by the observation of dynamical localisation [146, 147] in a strongly driven chain of  $^{87}\text{Rb}$  atoms. First, the atoms are cooled down to form a BEC. With the help of acousto-optical modulators, the 1D optical lattice is moved back and forth, c.f. Fig. 13, creating a periodic net force on the atoms in the wells, of the form  $V_0 \sum_m m \cos \Omega t n_m$ . According to the predictions of Floquet's theory, the system is expected to exhibit dynamical localisation [39, 89] at the values where the effective hopping matrix element approaches the zeros of the Bessel function (the first zero occurring at  $\zeta \approx 2.4$ ), depending on the value of the driving amplitude, cf. Eq. (117). By turning down the confining potential along the lattice direction and letting the atom cloud expand, it is possible to determine the tunneling rate through the wells of the optical lattice [148] as it is shown in the left panel of Fig. 14 taken from Ref. [130]. The right panel in this figure shows an image of the cloud taken with a CCD camera from a similar experiment [149]. From this image one can extract the in situ width of the atom cloud after the expansion. It is clear that expansion is very slow near the zero of the Bessel function (plot c) indicating dynamical localization. The resulting data showed an excellent agreement with the theoretical predictions.

To investigate the coherence of the BEC in the driven system, both the confining potential and the lattice beams are switched off. The atom cloud undergoes a free fall,

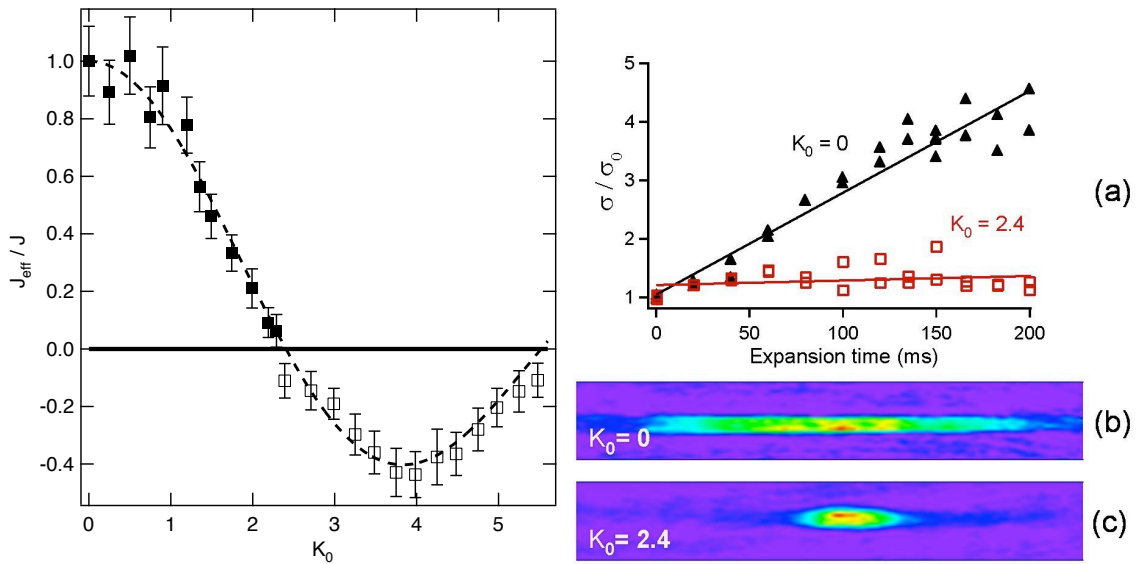


Figure 14. (Color online). Left panel (taken from Ref. [130]): Observation of dynamical localisation with cold atoms. The magnitude of the effective tunnelling coupling  $J_{\text{eff}}$  is extracted from an in situ image, while the relative sign is determined through the interference pattern using a TOF image. Right panel (taken from Ref. [149]): In situ images reveal the change in the condensate width  $\sigma$  during free expansion of a BEC condensate in an optical lattice. (a) Normalised expansion width  $\sigma/\sigma_0$  of the atomic cloud versus expansion time for  $K_0 = 0$  (black triangles) and  $K_0 = 2.4$  (red squares). (b) CCD in situ images of the condensate cloud for  $K_0 = 0$  and  $K_0 = 2.4$ . The parameters on the figure are related to those in the main text by  $J = J_0$ ,  $K_0 = \zeta = V_0/\Omega$  and  $J_{\text{eff}} = J_0 \mathcal{J}_0(\zeta)$ . For more details, see Refs. [39, 129, 130, 141, 146, 148, 149].

and the degree of phase coherence is determined from the visibility of the interference pattern after time-of-flight imaging. It was shown that the system starts losing its coherent behavior when dynamical localisation becomes more and more pronounced. The latter, however, is found to be restored soon after passing through the zero of the Bessel function. A recent theoretical work [150] investigated the coherence of *resonantly* driven condensates on the example of a bosonic Josephson junction model. It was found that, in the limit of high filling factors, the fluctuations destroy the coherence of the BEC and a mean-field description based on a macroscopically occupied Floquet state is expected to fail.

In the same experiments, the authors also investigated closely the regions of parameter space of the shaken Bose-Hubbard model which correspond to dynamical localisation [39, 129, 149]. There they found loss of coherence and attributed this to the Mott-insulator-to-superfluid transition. By performing time-of-flight measurements, the momentum distribution of the atom cloud was mapped out for different values of the driving amplitude. Far away from the zeros of the Bessel function, where the hopping is expected to be large compared to the atom-atom interactions, the experiments found a momentum distribution with well-defined peaks at quasimomentum  $q = 0$ , indicating that the system is in the phase-coherent superfluid state. However, when the value of the driving amplitude is tuned to the zero of the Bessel function where dynamical stabilisation is expected to occur, the visibility in the corresponding interference pattern is reduced drastically. The atoms lose phase coherence and the system is believed to enter the Mott insulating phase. Past the zero of the Bessel function, the hopping amplitude changes sign, since the Bessel function becomes negative, and the lowest Bloch band gets inverted. In agreement with theory, the position of the momentum peaks in the experiment reappears at quasimomentum  $q = \pi$  at the edge of the Brillouin zone. In particular, the phase coherence in the system is being restored.

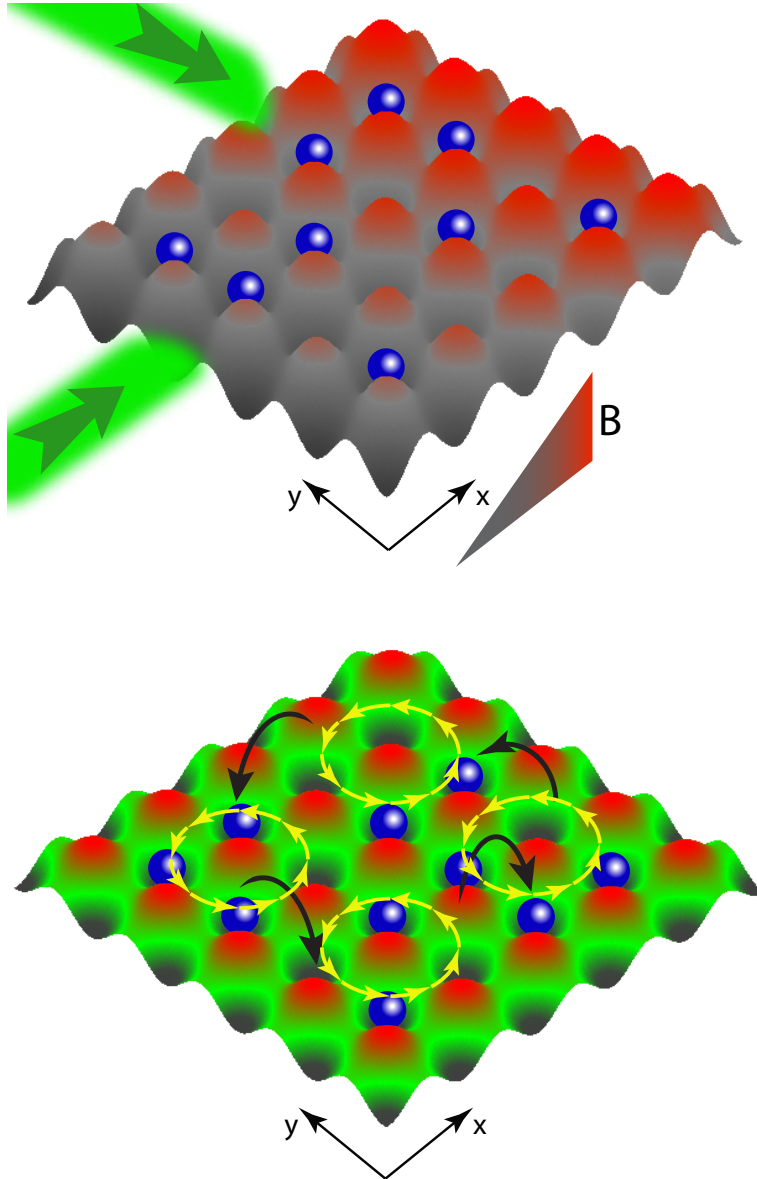


Figure 15. (Color online). The Floquet realization of the Harper-Hofstadter model. Electrically neutral bosons are loaded in an optical lattice and subject to a magnetic field gradient, which plays the role of the external potential, of value  $\Omega$ , along the  $x$ -direction. In addition, two Raman lasers of resonant frequency  $\Omega$ , with site-dependent phase lags, create a second running lattice. In the high-frequency limit, when the ratio of the amplitude of the Raman lasers and the driving frequency is held fixed, i.e.  $V_0/\Omega = \text{const.}$ , one generates an effective orbital magnetic field, realizing the bosonic Harper-Hofstadter Hamiltonian [153, 154]. Figure taken from Ref. [152].

## 7.2. Cold Atoms Realization of the Harper-Hofstadter Hamiltonian

We now extend the model from the previous section adding a second spatial dimension and a magnetic field gradient along this new direction. We discuss the setup, first proposed in Refs. [71, 151], for the simulation of the Harper-Hofstadter Hamiltonian with cold atoms. The model was recently realized in the experiments of Refs. [47, 48]. After giving an overview of the infinite-frequency limit, we discuss the leading  $\Omega^{-1}$ -corrections. These corrections, as well as the dressing of the operators, may be important for the existing experimental setups. The discussion of their effect on the dynamics goes beyond the scope of the present paper; they are discussed in a different work [152].

Consider a bosonic system on a square lattice subject to a periodically modulated

driving on top of a linear potential along the  $x$ -direction. In the case of recent cold atoms experiments [47, 48], the linear potential is achieved with the help of an external magnetic field gradient (or gravity), while the periodic driving - using a running (dynamical) optical lattice (c.f. Fig. 15). It is important to notice that an orbital magnetic field enters the Hamiltonian as a shift of the momentum by a vector potential  $p_j \rightarrow p_j - A_j$  (or equivalently a Peierls phase), and results in a Lorentz force leading to cyclotron orbits. This is to be contrasted with a static Zeeman magnetic field which acts as an external potential entering the Hamiltonian as  $-\boldsymbol{\mu}_B \cdot \mathbf{B}$ . It is the latter that was used in the experiment to apply the force gradient, while the periodic driving is responsible for the realisation of an effective orbital magnetic field.

The system is described by the following Hamiltonian:

$$H(t) = H_0 + H_1(t), \quad (125)$$

where

$$\begin{aligned} H_0 = & - \sum_{m,n} \left[ J_x \left( a_{m+1,n}^\dagger a_{mn} + \text{h.c.} \right) + J_y \left( a_{m,n+1}^\dagger a_{mn} + \text{h.c.} \right) \right] \\ & + \frac{U}{2} \sum_{m,n} n_{mn} (n_{mn} - 1), \\ H_1(t) = & \sum_{m,n} \left[ \frac{V_0}{2} \sin \left( \Omega t - \phi_{mn} + \frac{\Phi_\square}{2} \right) + \Omega m \right] n_{mn}. \end{aligned} \quad (126)$$

Here  $J_x$  and  $J_y$  denote the hopping amplitude,  $V_0$  is the strength of the oscillating electric field, which as in the previous example should scale linearly with the driving frequency  $\Omega$ , and we choose the field gradient to be resonant with  $\Omega$ . The non-resonant part, which does not scale with  $\Omega$ , can be always added to  $H_0$ . We choose the phase  $\phi_{mn} = \Phi_\square(n + m)$ . Notice that time reversal symmetry within the period, i.e.  $t \rightarrow T - t$  is broken by the inhomogeneous phase  $\phi_{mn}$ , ultimately allowing for a synthetic static magnetic field to appear in the infinite-frequency Hamiltonian. Upon applying a transformation to the rotating frame[48], the Hamiltonian takes the form

$$H^{\text{rot}}(t) = W(t) + W^\dagger(t) + H_{\text{int}}, \quad (127)$$

where

$$W(t) = - \sum_{m,n} \left[ J_x e^{-i\zeta \sin(\Omega t - \phi_{nm}) + i\Omega t} a_{m+1,n}^\dagger a_{mn} + J_y e^{-i\zeta \sin(\Omega t - \phi_{nm})} a_{m,n+1}^\dagger a_{mn} \right], \quad (128)$$

and  $\zeta = V_0/\Omega \sin(\Phi_\square/2)$ .

To zeroth order, the Magnus Hamiltonian is equivalent to the time-averaged one:

$$\begin{aligned} H_F^{(0)} = & -K \sum_{m,n} \left( e^{i\phi_{mn}} a_{m+1,n}^\dagger a_{mn} + \text{h.c.} \right) - J \sum_{m,n} \left( a_{m,n+1}^\dagger a_{mn} + \text{h.c.} \right) \\ & + \frac{U}{2} \sum_{m,n} n_{mn} (n_{mn} - 1), \end{aligned} \quad (129)$$

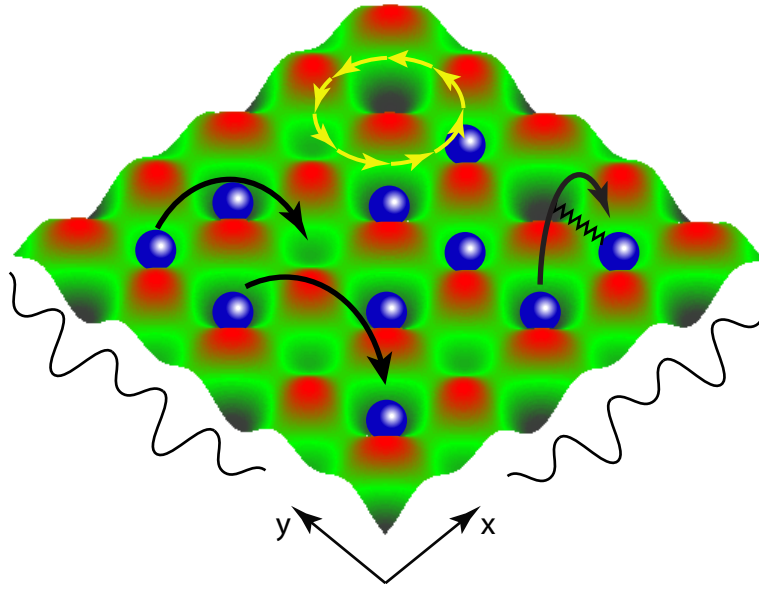


Figure 16. (Color online) The leading corrections in  $\Omega^{-1}$  to the Harper-Hofstadter Hamiltonian include: second-neighbor hopping including along the diagonal (solid black lines), interaction-dependent hopping (solid black lines connected to zig-zag lines) and a site-dependent chemical potential (indicated by the thin black lines on the side and the green color gradient).

where the effective hoppings are given by  $K = J_x \mathcal{J}_1(\zeta)$ ,  $J = J_y \mathcal{J}_0(\zeta)$ , and  $\mathcal{J}_\nu$  is the  $\nu$ -th Bessel function.

Going to the next order in the Magnus expansion allows one to identify the leading finite-frequency corrections to the Floquet Hamiltonian:

$$\begin{aligned}
 H_F^{\text{rot},(1)} = & - \sum_{m,n} \left( \frac{J_x^2}{\Omega} \rightarrow C_{m,m+2}^n(\zeta) a_{m+2,n}^\dagger a_{mn} + \frac{J_y^2}{\Omega} \uparrow C_m^{n,n+2}(\zeta) a_{m,n+2}^\dagger a_{mn} + \text{h.c.} \right) \\
 & - \sum_{m,n} \left( \frac{J_x J_y}{\Omega} \nearrow D_{m,m+1}^{n,n+1}(\zeta) a_{m+1,n+1}^\dagger a_{mn} + \frac{J_x J_y}{\Omega} \nwarrow D_{m,m-1}^{n,n+1}(\zeta) a_{m-1,n+1}^\dagger a_{mn} + \text{h.c.} \right) \\
 & + \sum_{m,n} \left( \frac{J_x^2}{\Omega} \rightarrow E_{m,m+1}^n(\zeta) (n_{m,n} - n_{m+1,n}) + \frac{J_y^2}{\Omega} \uparrow E_m^{n,n+1}(\zeta) (n_{mn} - n_{m,n+1}) \right) \\
 & - \sum_{m,n} \left( \frac{J_x U}{\Omega} \rightarrow B_{m,m+1}^n(\zeta) a_{m+1,n}^\dagger a_{mn} (n_{mn} - n_{m+1,n} + 1) \right. \\
 & \quad \left. + \frac{J_y U}{\Omega} \uparrow B_m^{n,n+1}(\zeta) a_{m,n+1}^\dagger a_{mn} (n_{mn} - n_{m,n+1} + 1) + \text{h.c.} \right). \tag{130}
 \end{aligned}$$

The arrows on the corresponding hopping coefficient indicates the direction of the hopping. The complex-valued functions  $B(\zeta)$ ,  $C(\zeta)$ ,  $D(\zeta)$  and  $E(\zeta)$  are defined on the bonds of the lattice. They are obtained from the time-ordered integrals in the Magnus expansion, and are given in Appendix C. We see that, when we include the  $\Omega^{-1}$ -corrections, the Floquet Hamiltonian becomes quite complex. These corrections introduce effective static potentials (periodic for rational  $\Phi_\square/\pi$ ) along both directions of the lattice, second-nearest-neighbor hopping both across the diagonals and along the lattice directions, and interaction-dependent hopping. The consequences of these corrections for the single-particle dynamics, as well as the dressing of the density matrix and observables, was

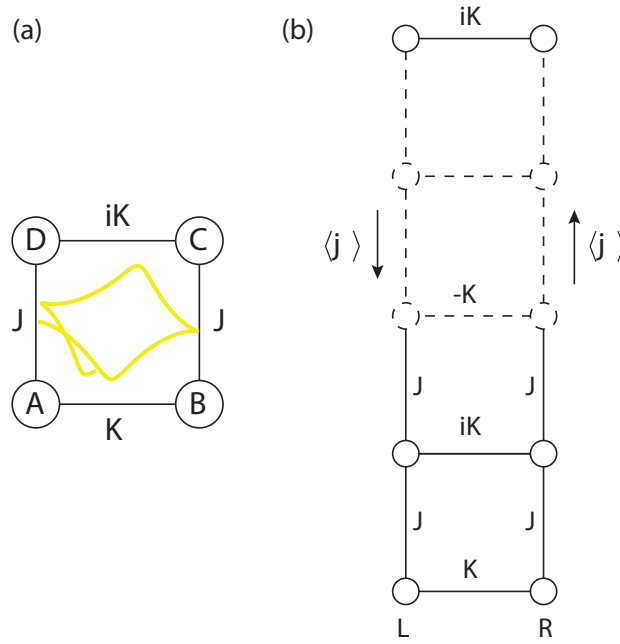


Figure 17. (Color online) (a) The plaquette geometry used to study the quantum cyclotron orbits (yellow) in the Harper-Hofstadter Hamiltonian. (b) The ladder geometry with the chiral currents used to study the transition between the vortex and the Meissner phases. Figure taken from Ref. [152].

discussed in a different work [152].

Before we close the discussion on the theoretical Floquet realisation of the Harper-Hofstadter model, we mention that a different method of engineering artificial gauge fields using a high-frequency periodic perturbation was proposed in Ref. [155] (but see also Ref. [156]), based on an oscillating field gradient, where  $H_1(t) = \sum_{mn} m(\Omega + V_0 \cos \Omega t) n_{mn}$ . Moreover, in Ref. [69] the flow-equation method, which is an alternative to the Magnus expansion, has been used to compute the finite-frequency corrections to the Floquet Hamiltonian. As expected, this method reproduces the same results as the Magnus expansion. Recently, the stability [157] of a related Bose-Hubbard model under a periodic driving, and scattering properties of periodically-driven lattice systems [158] have been studied too.

*Experimental realisation of the Harper-Hofstadter model.* The Harper-Hofstadter Model has been realised experimentally [47, 48, 50, 131] using cold atoms in optical lattices. First, Rb atoms are loaded in a 2D optical lattice and cooled down to form a BEC. Then a field gradient is applied along the  $x$ -direction, such that tunnelling along the  $x$ -direction is suppressed. The latter is then restored by a running lattice, which consists of two additional laser beams which interfere at an angle with respect to one another, c.f. Fig. 15. The resulting running lattice leads to a periodic on-site modulation with a site-dependent phase and the frequency of the running lattice is chosen to match with the magnetic field gradient effectively realizing the Hamiltonian (126) with  $\Phi_{\square} = \pi/2$ . This flux can be controlled by the angle between the running lattice beams. In the infinite frequency limit this flux is equivalent to a very strong static magnetic field (see Eq. (129)).

In the experiment of Ref. [47] the authors additionally introduced a static superlattice potential, which effectively divided the 2D lattice in  $2 \times 2$  plaquettes (see Fig. 17 (a)) suppressing tunnelling completely between them. Then the authors studied the analogue of the classical cyclotron orbit and found a good agreement with the predictions of the effective Hamiltonian (129). In another experiment [131], the segregating staggered superlattice was switched only along the  $x$ -direction, such that the 2D lattice was divided



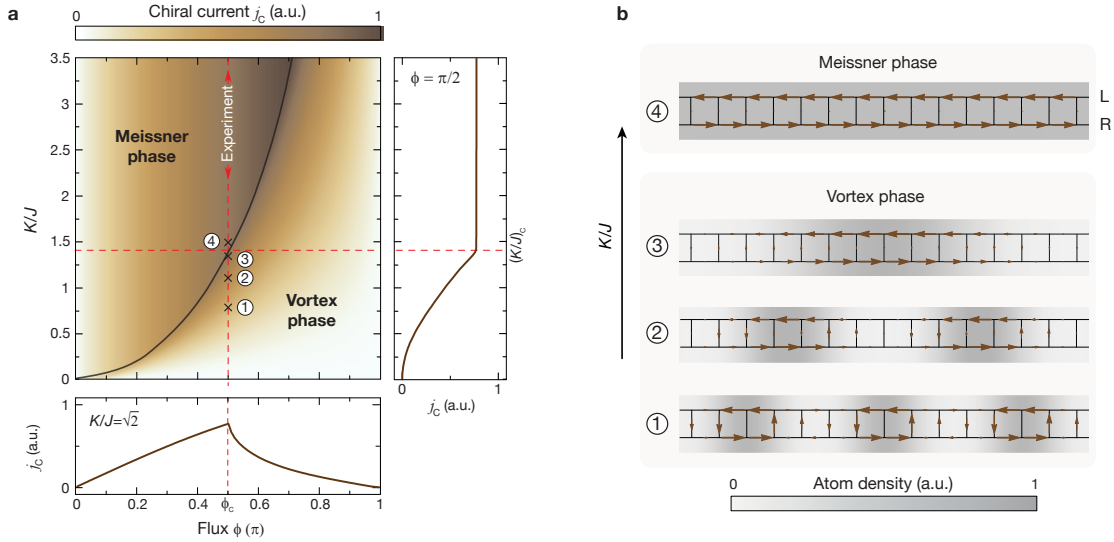


Figure 18. (Color online) (a) Phase diagram of the HH model on a ladder in  $(K/J, \phi)$ -space. The insets show the chiral current  $j_c$  as a function of the ratio hopping  $K/J$  and the flux per plaquette  $\phi$ . (b) Pictorial representation of the Meissner and vortex phases for several values of the ratio  $K/J$ . The parameters are related to those in the main text by  $\phi = \Phi_{\square}$ . Reprinted by permission from Macmillan Publishers Ltd: [Nature Physics] ([131]), copyright (2014).

into many ladders along the  $y$ -axis, c.f. Fig. 17 (b). The tunneling between different ladders was suppressed. The atoms occupying the ground state of the system move along the edges of the ladders in the form of chiral currents. Depending on the ratio between the effective hopping parameters in the  $x$ - and  $y$ -directions, a phase transition between a vortex phase and a Meissner phase was found at which the chiral current undergoes a cusp singularity. For the flux  $\Phi_{\square} = \pi/2$  this transition occurs at the ratio  $(K/J)_c = \sqrt{2}$ . At a smaller ratio (vortex phase) the current increases with  $K$  and the vortex density decreases with  $K$  until it hits zero (in the TD limit) at the critical ratio. For  $K/J > (K/J)_c$  (Meissner phase) the current at a fixed value of  $J$  is independent of  $K$ , see Fig. 18. Effectively the authors performed an FNS measurement of the current by projecting the system into an array of decoupled double wells along the horizontal direction. Then they fit the Josephson density oscillations in a double well to a simple formula with the chiral current entering through the initial conditions (see Ref. [131] for details).

In the follow up experiment, the realisation of the Harper-Hofstadter model has been optimised. The field gradient has been replaced by a superlattice, and the running lattice has been modified accordingly [50]. This experiment measured the Chern number of the lowest band by detecting the differential drift of the atom cloud in momentum space, which arises due to the Berry curvature of the band. The Chern number was measured to be quantised to unity with excellent precision. This most recent experiment also takes into account the relevant first order corrections to the time-averaged Hamiltonian.

### 7.3. The Periodically Driven Fermi-Hubbard Model. Floquet Topological Insulators

As a next example we analyze a spinful fermionic system on a bipartite lattice driven by a periodic external electric field. We focus on graphene, where two triangular lattices build up the hexagonal structure and consider the situation in which the driving frequency is higher than the band width. This scheme has been suggested theoretically to induce topological properties in graphene [41, 62, 159–164], and turn it into a Chern insulator.

Recent cold atom experiments managed to realize the Floquet Chern insulator in the laboratory [49, 50]. In Ref. [165] a similar scheme was proposed to realize a fractional Chern insulator, though in the interacting case that work missed some relevant terms in the Floquet Hamiltonian, namely the interaction dependent hopping, which may alter the phase diagram.

Let  $z$  be the lattice coordination number, and let  $A$  denote the set of all points in the sublattice  $A$ . We label the points on the sublattice  $A$  by a vector  $\mathbf{r}$ . Let us define the vectors  $\mathbf{s}_j$  ( $j = 1, \dots, z$ ) to connect a fixed point on the sublattice  $A$  to all its adjacent neighbors on the sublattice  $B$ . The vectors  $\mathbf{s}_j$  point from  $A$  to  $B$  (c.f. Fig 19, Panel (a)). To simplify the notation we skip the bold notation for vectors in the subscripts of operators.

The system is described by the Hamiltonian

$$\begin{aligned}
 H(t) &= H_0 + H_1(t) \\
 H_1(t) &= \frac{1}{z} \sum_{\mathbf{r} \in A} \sum_{j=1}^z \sum_{\sigma} \left( f_{\mathbf{r}}(t) n_{\mathbf{r},\sigma}^a + f_{\mathbf{r}+\mathbf{s}_j}(t) n_{\mathbf{r}+\mathbf{s}_j,\sigma}^b \right) \\
 H_0 &= H_{\text{kin}} + H_{\text{int}}, \\
 H_{\text{kin}} &= -J_0 \sum_{\mathbf{r} \in A} \sum_{j=1}^z \sum_{\sigma} \left( a_{\mathbf{r},\sigma}^{\dagger} b_{\mathbf{r}+\mathbf{s}_j,\sigma} + \text{h.c.} \right) \\
 H_{\text{int}} &= \frac{U}{2z} \sum_{\mathbf{r} \in A} \sum_{j=1}^z \sum_{\sigma} \left( n_{\mathbf{r},\sigma}^a n_{\mathbf{r},\bar{\sigma}}^a + n_{\mathbf{r}+\mathbf{s}_j,\sigma}^b n_{\mathbf{r}+\mathbf{s}_j,\bar{\sigma}}^b \right) \\
 &\quad + U' \sum_{\mathbf{r} \in A} \sum_{j=1}^z \sum_{\sigma, \sigma'} n_{\mathbf{r},\sigma}^a n_{\mathbf{r}+\mathbf{s}_j,\sigma'}^b.
 \end{aligned} \tag{131}$$

where the factors  $1/z$  are introduced to avoid overcounting,  $\sigma = \uparrow, \downarrow$  indicates the spin and we adopted the notation  $\bar{\uparrow} = \downarrow$ . The operators  $a_{\mathbf{r},\sigma}^{\dagger}$  and  $b_{\mathbf{r}+\mathbf{s}_j,\sigma}^{\dagger}$  create a fermion of spin  $\sigma$  on sublattices  $A$  and  $B$ , respectively. In the Hamiltonian,  $n_{\mathbf{r},\sigma}^a = a_{\mathbf{r},\sigma}^{\dagger} a_{\mathbf{r},\sigma}$  and  $n_{\mathbf{r}+\mathbf{s}_j,\sigma}^b = b_{\mathbf{r}+\mathbf{s}_j,\sigma}^{\dagger} b_{\mathbf{r}+\mathbf{s}_j,\sigma}$  denote the number operators on sublattices  $A$  and  $B$ . The tight-binding hopping matrix element is  $J_0$ , the on-site interaction strength which couples fermions of opposite spin is  $U$ , while the next-nearest neighbor interaction is  $U'$ . The driving protocol  $f_j(t) = f_j(t+T)$  is periodic and site-dependent.

In the rotating frame the Hamiltonian reads as:

$$\begin{aligned}
 H^{\text{rot}}(t) &= W(t) + W^{\dagger}(t) + H_{\text{int}}, \\
 W(t) &= -J_0 \sum_{\mathbf{r} \in A, \sigma} \sum_{j=1}^z \lambda_j(t) a_{\mathbf{r},\sigma}^{\dagger} b_{\mathbf{r}+\mathbf{s}_j,\sigma} \\
 \lambda_j(t) &= \exp \left( i \int^t dt' f_{\mathbf{r}+\mathbf{s}_j}(t') - f_{\mathbf{r}}(t') \right).
 \end{aligned} \tag{132}$$

To zeroth order of the Magnus expansion, the Floquet Hamiltonian is given by the time-average of the Hamiltonian above (similarly to the bosonic case described in Sec. 7.2):

$$H_F^{\text{rot},(0)} = \overline{W(t)} + \overline{W^{\dagger}(t)} + H_{\text{int}}. \tag{133}$$

It has the same form of Eq. (132) but with renormalized hopping parameters, i.e.  $J_0\lambda_j(t) \rightarrow J_j(\zeta)$ , where  $\zeta = V_0/\Omega$  is the ratio of the driving amplitude and the driving frequency.

The leading  $\Omega^{-1}$ -corrections to the Floquet Hamiltonian are given by

$$\begin{aligned}
H_F^{\text{rot},(1)} = & \frac{J_0^2}{\Omega} \sum_{r \in A} \sum_{j=1}^z \sum_{\sigma} \left[ F_{jj} \left( n_{r\sigma}^a - n_{r+s_j,\sigma}^b \right) \right] \\
& + \frac{J^2}{\Omega} \sum_{r \in A} \sum_{\sigma} \sum_{j>k=1}^z \left[ F_{jk} \left( a_{r\sigma}^\dagger a_{r+s_j-s_k,\sigma} - b_{r+s_k}^\dagger b_{r+s_j} \right) + \text{h.c.} \right] \\
& + \frac{J_0 U}{2\Omega} \sum_{r \in A} \sum_{j=1}^z \sum_{\sigma} \left[ G_j \left( n_{r\sigma}^a - n_{r+s_j,\sigma}^b \right) a_{r\bar{\sigma}}^\dagger b_{r+s_j,\bar{\sigma}} + \text{h.c.} \right] \\
& - \frac{J_0 U'}{\Omega} \sum_{r \in A} \sum_{j,k=1}^z \sum_{\sigma,\sigma'} \left[ G_j \left( n_{r+s_j-s_k,\sigma}^a a_{r\sigma'}^\dagger b_{r+s_j,\sigma'} - a_{r\sigma'}^\dagger b_{r+s_j,\sigma'} n_{r+s_k,\sigma}^b \right) + \text{h.c.} \right].
\end{aligned} \tag{134}$$

One readily sees that the first-order correction contains a static potential, next-nearest-neighbor hopping, and (in the presence of interactions) interaction-dependent hopping. Interaction-dependent hopping terms also appear in the Fermi-Hubbard model, when one drives the interaction term [142] It is intuitively clear that the on-site interactions lead to the interaction dependent-hopping between the two sublattices and nearest neighbor interactions induce the interaction-dependent hopping within the same sublattice. This is in agreement with our previous remark that the Magnus corrections effectively increase the spatial support of the operators, present in the non-driven Hamiltonian  $H_0$ . The Magnus coefficients can be obtained from the following integrals

$$\begin{aligned}
F_{jk} &= \frac{1}{4\pi i} \int_0^{2\pi} d\tau_1 \int_0^{\tau_1} d\tau_2 \lambda_j(\tau_1) \lambda_k^*(\tau_2) - (1 \leftrightarrow 2), \\
G_j &= \frac{1}{4\pi i} \int_0^{2\pi} d\tau_1 \int_0^{\tau_1} d\tau_2 [\lambda_j(\tau_1) - \lambda_j(\tau_2)],
\end{aligned} \tag{135}$$

where  $\tau_i = \Omega t_i$ . To analyze the relation between the coefficients  $F_{jk}$  and  $G_j$  we use that  $\lambda_j(\tau) = \lambda_j(\tau + 2\pi)$  is a periodic function and can be expanded into Fourier components:

$$\lambda_j(\tau) = \sum_{l \in \mathbb{Z}} c_l^j e^{il\tau}. \tag{136}$$

The coefficient  $c_l^j$  are related to the  $l$ -photon absorption processes and for a sinusoidal drive they are given by Bessel functions. In general one can show that

$$\begin{aligned}
F_{jk} &= \sum_{l \neq 0} \frac{1}{l} \left[ c_l^j \left( c_l^k \right)^* - c_0^j \left( c_l^k \right)^* - c_l^j \left( c_0^k \right)^* \right], \\
G_j &= - \sum_{l \neq 0} \frac{c_l^j}{l}.
\end{aligned} \tag{137}$$

The terms proportional to  $c_0^j$  in Eq. (137) are Floquet gauge dependent. However, they do not vanish for any fixed value of the Floquet gauge without special fine-tuning of the driving protocol (see also the discussion after Eq. (29)). As expected,  $F_{jk} = F_{kj}^*$  so that the Floquet Hamiltonian is hermitian. Note that the second-nearest-neighbor hopping is zero, i.e.  $F_{jk} = 0$ , if  $\lambda_j(\tau)$  and  $\lambda_k(\tau)$  are both symmetric under  $\tau \rightarrow 2\pi - \tau$ . For example, for a square lattice with  $z = 2$  in order to have nonzero diagonal hopping ( $F_{21} \neq 0$ ) one can use  $\lambda_1(\tau) = \cos(\tau)$  and  $\lambda_2(\tau) = \sin(\tau)$ . This also ensures that  $G_1 = 0$  while  $G_2 \neq 0$ . So there is an unwanted interaction-dependent hopping term along the 2-direction. However, if one uses a second harmonic

$$\lambda(\tau) = \sin(\tau) - 2\sin(2\tau)$$

then it is easy to see from Eq (135) or Eq. (137) that  $G_2$  also becomes zero while  $F_{21}$  remains non-zero. In general the periodic functions  $\lambda_j(\tau)$ , being related to the exponential of the integrated driving protocol, involve many harmonics and, in order to find the regime where the interaction-dependent hopping is zero, one clearly needs to fine-tune.

We would like to make a few remarks about a possible overlap of this model, as part of the DK class, with the Dirac class, defined in Sec. 6. The lattice models are allowed to have relativistic low energy dispersion, e.g. if we consider a graphene-type honeycomb lattice (see the next section). We analyze the limit, where the amplitude of the driving protocol scales with the driving frequency  $\Omega$  which is considered to be higher than the single-particle bandwidth. This makes the low energy relativistic description of the spectrum inadequate. In order to realize the Dirac class in e.g. graphene, one has to make sure that all involved energy scales, including the lattice potential, are small compared to the band width, so that only the linear part of the dispersion relation is important. The relation between lattice and continuum models is discussed in detail in App. A. In Sec. 6, we also used a symmetry argument to argue that there are no  $\Omega^{-1}$ -corrections to the infinite-frequency Floquet Hamiltonian in the Dirac class. That argument relied on the linear polarization of the driving protocol and does not apply to e.g. a circularly polarized protocol, where the phase of the driving depends on the direction. Such a protocol was suggested to realize a Floquet Chern Insulator [41] and we will briefly discuss it next.

*Circularly Polarized Drive and the Floquet Realization of Haldane's Model.* Let us briefly consider the prototypical example of driving a sample of spinful fermions on a honeycomb lattice with a circularly polarized electric field [41]. The driving protocol in this case reads as

$$f_r(t) = \mathbf{E}(t) \cdot \mathbf{r}, \quad \mathbf{E}(t) = V_0(\cos \Omega t, \sin \Omega t). \quad (138)$$

For a honeycomb lattice, the unit vectors  $\mathbf{s}_j$  point from the sublattice A to B (see Fig. 19, Panel (a)):

$$\mathbf{s}_1 = (0, -1), \quad \mathbf{s}_{2,3} = \frac{1}{2}(\pm\sqrt{3}, 1).$$

In the rotating frame, this leads to

$$\lambda_j(t) = \exp(i\mathbf{s}_j \cdot \mathbf{A}(t)), \quad \mathbf{A}(t) = \frac{V_0}{\Omega}(\sin \Omega t, -\cos \Omega t).$$

One can show that all three renormalized nn hopping amplitudes in  $H^{\text{rot},(0)}$  are real and equal in magnitude. As in the bosonic case, they are given by  $J_j = J_0 \mathcal{J}_0(\zeta)$ , where  $\zeta = V_0/\Omega$  is kept constant in the high-frequency limit and  $\mathcal{J}_0$  is the Bessel function of

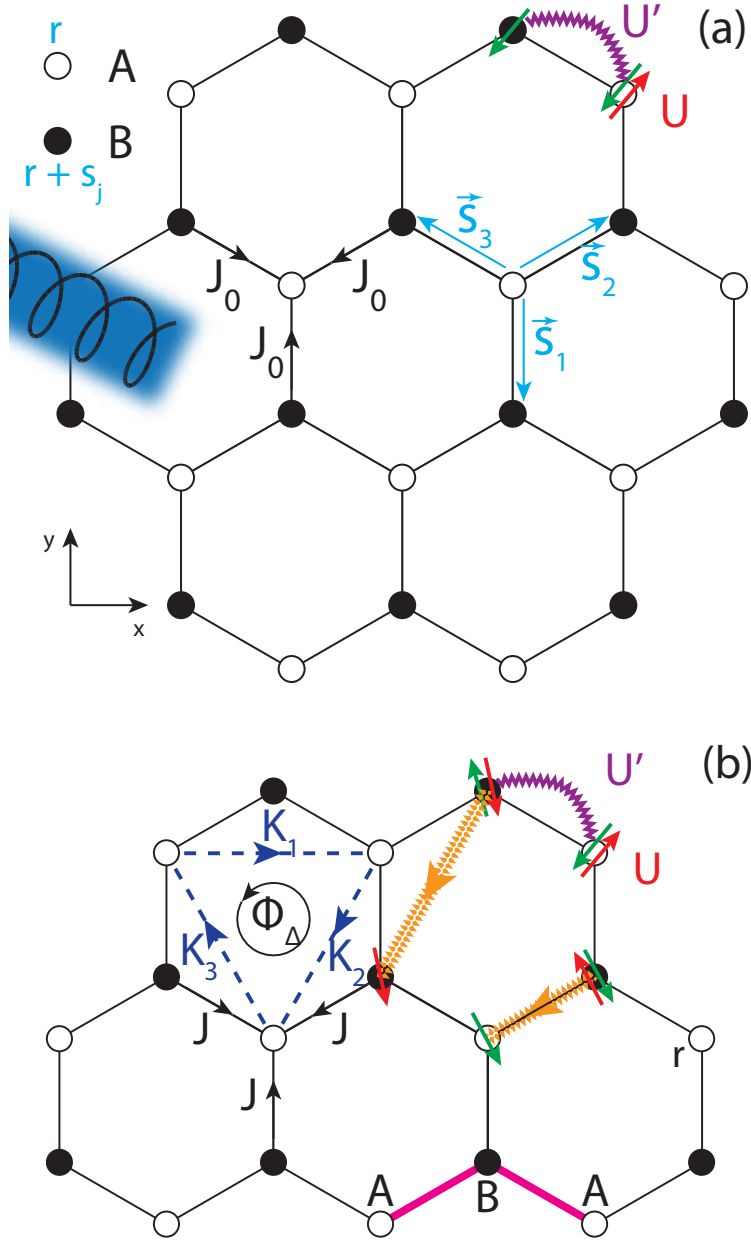


Figure 19. (Color online). Floquet realization of the Haldane-Fermi-Hubbard Model (see also Refs. [[41, 49]]). (a) A circularly polarized electric field is shone on a sheet of graphene. The non-driven model includes spinful fermions with hopping matrix elements  $J_0$ , on-site interactions  $U$  between spin-up (dark green arrows) and spin-down (dark red arrows) fermions, as well as nn interactions  $U'$  (purple full zigzag line) between either spin species. (b) To leading order the Floquet Hamiltonian has the same form as the non-driven Hamiltonian but with renormalized parameters. The leading  $\Omega^{-1}$ -corrections include complex next-nearest-neighbor hopping elements  $K_j$  (dashed blue lines), such that the flux through a sublattice is  $\Phi_\Delta = -\pi/2$ . If the system is interacting, to the same order in perturbation theory, an interaction-dependent hopping is induced (orange lines).

first kind. Furthermore, it follows that the site-dependent chemical potential vanishes identically for the circularly polarized drive owing to  $\sum_j F_{jj} = 0$ , while the next-nearest-neighbor terms are finite and complex. As proposed in Ref. [41] they can induce a topological transition. For the case of a circularly polarized drive, we further obtain that the next-nearest-neighbor hopping elements  $K_1 = J_0^2/\Omega F_{32}(\zeta)$ ,  $K_2 = J_0^2/\Omega F_{21}(\zeta)$ , and  $K_3 = J_0^2/\Omega F_{31}^*(\zeta)$ , where  $F_{jk}$  are defined in Eq. (135). Then the flux through a sublattice  $\Phi_\Delta = \arg(K_1^*) + \arg(K_2^*) + \arg(K_3^*) = -\pi/2$  (see Fig. 19, Panel (b)), and the model

realizes Haldane's Chern insulator [166].

If the non-driven system is interacting, i.e.  $U' \neq 0$ , the Floquet Hamiltonian includes interaction-dependent hopping. We find that the strength of the interaction-dependent hopping along the  $\mathbf{s}_1$ -direction,  $G_1 = 0$ , vanishes identically, but  $G_3 = -G_2 \neq 0$ . Therefore the interaction-dependent hopping is limited to the zig-zag paths along the  $x$  direction (see Fig. 19, Panel (b)). The phase, accumulated due to the interaction-dependent hopping for a spin- $\sigma$  fermion along the zig-zag path  $ABA$ , is obtained as  $\arg(G_3) + \arg(G_2^*) = \pi$ , provided that spin- $\bar{\sigma}$  fermions occupy the sites on the sublattice  $A$  of this path. We note that the interaction-dependent hopping appears at the same order in  $\Omega^{-1}$  as the next-nearest-neighbor hopping  $K_j$  which drives the topological transition. Therefore the interaction dependent hopping might affect the properties of the topological phase. This term was erroneously omitted in Ref. [165], which explored a similar setup in interacting Floquet topological insulators, see Ref. [167] for additional details.

*Experimental realisation of Haldane's model.* Haldane's model has been realised using ultracold fermionic  $^{40}\text{K}$  atoms in a brick-wall (almost hexagonal) optical lattice [49]. A superlattice induced an energy off-set between the two sublattices which resulted in a staggered potential  $\Delta_{AB}$ . By mechanically shaking the lattice position along the  $x$ - and  $y$ -direction using piezo-electric actuators, the lattice sites were moved on elliptical trajectories which mimic the application of elliptically polarised electric field in the plane of the lattice, and break time-reversal symmetry. As discussed in the previous paragraphs, this leads to complex-valued nnn hopping terms between sites of the same sublattice. As a result, the Dirac cones open up a topological band gap, which is reflected in the non-zero and opposite Chern numbers of the two lowest bands, see Fig. 20, left panel.

In a topologically non-trivial band, atoms moving in the Brillouin zone acquire a Berry phase. This, in turn, results in a force, perpendicular to the direction of movement, pretty much like the Lorentz force acts on a charged particle moving in a real-space region of nonzero *orbital* magnetic field<sup>3</sup>. By turning on a magnetic field gradient which acts as an external potential on the atoms, a constant force is applied on the atoms, leading to Bloch oscillations. Hence, the atoms are brought to explore the region of the Brillouin zone near the two Dirac cones, where the Berry curvature and, therefore, the force the atoms experience, is the strongest. The experiment measured the motion of the centre of mass of quasimomentum in the presence of the topological gap. Reversing the sign of the magnetic field gradient flips the sign of the force the atoms feel, and the drift is experienced in the orthogonal direction. Subtracting the two drifts from one another defines the differential drift, with the help of which one can measure the strength of the Berry curvature near the topological gaps, see Fig. 20, right panel.

A fraction of the atoms passing near the band gaps undergoes a Landau-Zener transition and transfers to the upper band. The precise band population can be extracted from the integrated column density in the absorption image following a band mapping technique. This provides a test for the existence of the Floquet-engineered dispersion relation of Haldane's model.

The experiment studied briefly the interacting model by switching on the interactions using a Feshbach resonance. In general, the topological phases of the interacting Fermi-Hubbard model are expected to be strongly susceptible to heating effects. In the experiment conducted in Ref. [49], the authors observed a 25% increase in entropy for the driven interacting system, when compared to the non-driven interacting case. We believe that the physical consequences of the interaction-dependent hopping deserve further careful investigation, since it is generic to all models in the DK class. Heating effects

---

<sup>3</sup>Note that an orbital magnetic field leads to cyclotron orbits, while a static a magnetic field gradient (a Zeeman field) acts as an external potential and is responsible for the hyperfine splitting of atoms.

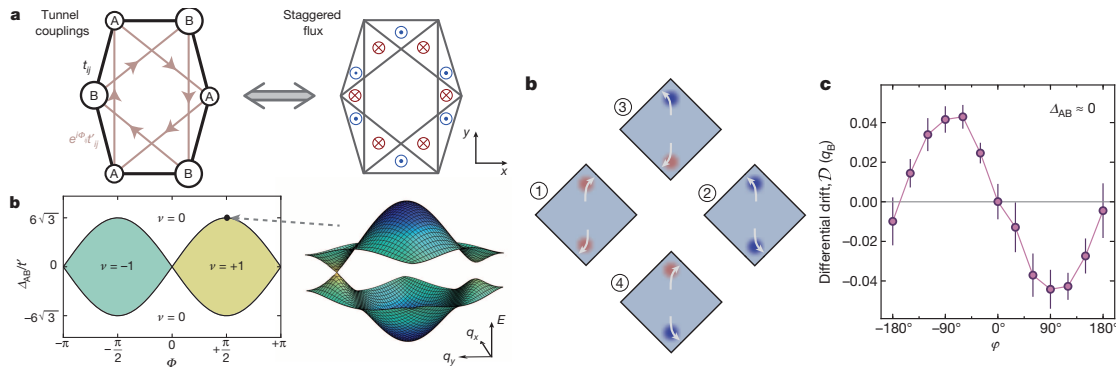


Figure 20. (Color online). Left panel: Cold atom realisation of Haldane's model. (a) The brick-wall lattice and the dynamically generated staggered flux pattern. (b) Topological phase diagram of Haldane's model and dispersion relation for the brick-wall lattice. Right panel: Differential drift of the fermions in the first Brillouin zone. (b) Pictorial representation of the differential drift near the Dirac cones for fixed parameters. (c) Differential drift vs. sublattice flux  $\phi$  for a near zero staggered potential  $\Delta_{AB} \approx 0$  Hz. The parameters are related to those in the main text by  $\varphi = \Phi_{\Delta}$ . Reprinted by permission from Macmillan Publishers Ltd: [Nature] ([49]), copyright (2014).

in the high-frequency limit are a subject of current research.

#### 7.4. Spin Systems

As a final in the DK class, we consider a spin-1/2 system on a lattice of arbitrary dimension, driven by a time-periodic, linearly-polarized external magnetic field. As we discussed in Sec. 3 the Magnus expansion works both for quantum and classical systems. So with minor modifications, such as the possibility of having local spin interactions, the results of this section apply equally to driven classical spins models. The effect of resonant driving on benchmark properties, such as the Rabi oscillations, was investigated [168]. Here, we assume that the magnetic field on each lattice site  $m$  points along a fixed axis in time, but its magnitude can vary from one lattice site to another. In agreement with the discussion in the introduction to the DK class, we assume that the amplitude of the magnetic field scales linearly with the frequency of the drive  $\Omega$ . The Hamiltonian in the lab frame reads as:

$$H(t) = H_0 + \Omega \sum_m f_m(t) \mathbf{n}_m \cdot \boldsymbol{\sigma}_m, \quad (139)$$

where  $H_0$  is time-independent and can include arbitrary spin-spin interactions,  $\boldsymbol{\sigma}_m = (\sigma_m^x, \sigma_m^y, \sigma_m^z)$  is the vector of the three Pauli matrices on the  $m$ -th site,  $\mathbf{n}_m$  is a time-independent unit vector, and  $f_m(t)$  is a periodic function with period  $T = 2\pi/\Omega$ .

The high frequency limit of the Floquet Hamiltonian is equal to the time-average of the Hamiltonian in the rotating frame:

$$H^{\text{rot}}(t) = V^\dagger(t) H_0 V(t), \quad (140)$$

where

$$V(t) = \exp \left[ -i \sum_m \Delta_m(t) \mathbf{n}_m \cdot \boldsymbol{\sigma}_m \right],$$

$$\Delta_m(t) = \Omega \int^t dt' f_m(t').$$

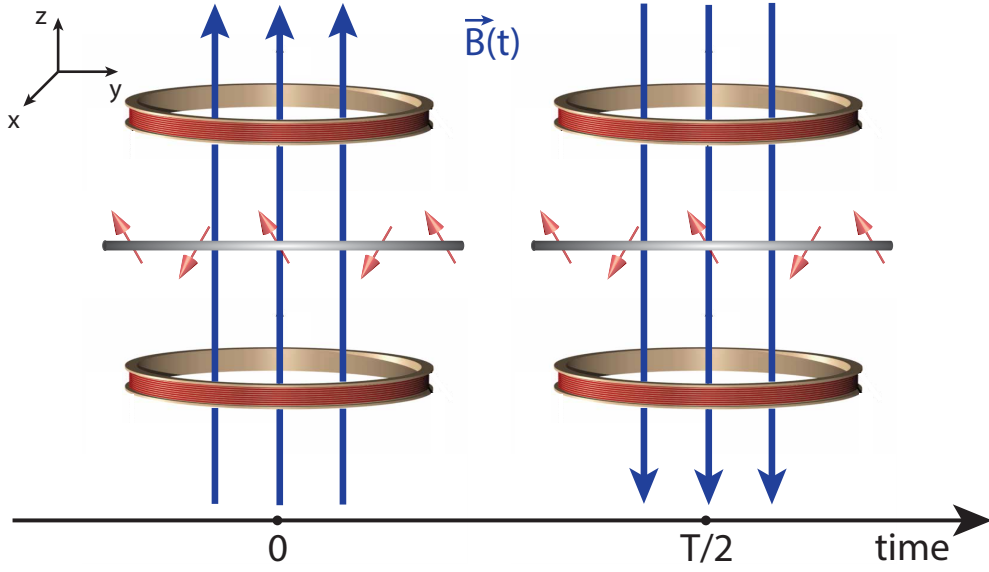


Figure 21. (Color online) The flip-flop model: a periodically modulated, spatially uniform magnetic field  $\mathbf{B}(t)$  is applied to a spin chain, c.f. Eq. (142).

Since spins at different sites commute, the operator  $V(t)$  factorizes, and can be written as

$$V(t) = \prod_m V_m(t), \quad V_m(t) = \exp[-i\Delta_m(t) \mathbf{n}_m \cdot \boldsymbol{\sigma}_m],$$

where  $V_m(t)$  is the operator rotating the spin at the site  $m$  by an angle  $\theta_m(t) = 2\Delta_m(t)$  around the direction  $\mathbf{n}_m$ . Using Eq.(140) it is easy to see that the Hamiltonian in the rotating frame is given by the Hamiltonian  $H_0$  with the substitution  $\boldsymbol{\sigma}_m \longrightarrow \boldsymbol{\sigma}_m^{\text{rot}}(t) = V_m^\dagger(t)\boldsymbol{\sigma}_m V_m(t)$  or explicitly:

$$\boldsymbol{\sigma}_m \longrightarrow \cos \theta_m \boldsymbol{\sigma}_m + \sin \theta_m \mathbf{n}_m \times \boldsymbol{\sigma}_m + (1 - \cos \theta_m) (\mathbf{n}_m \otimes \mathbf{n}_m) \boldsymbol{\sigma}_m, \quad (141)$$

where  $\times$  and  $\otimes$  indicate the vector and tensor product. The entries of the matrix  $M_m \equiv \mathbf{n}_m \otimes \mathbf{n}_m$  are defined by  $(M_m)_{\alpha,\beta} = n_m^\alpha n_m^\beta$ .

We now consider two specific examples. First let us assume that:

$$H(t) = H_0 + \alpha \Omega \cos \Omega t \sum_m \sigma_m^z$$

$$H_0 = J_0 \sum_{\langle m,n \rangle} (\sigma_m^x \sigma_n^x - \sigma_m^y \sigma_n^y) \quad (142)$$

Here the driving corresponds to a uniform magnetic field along the  $z$ -direction,  $\mathbf{n}_m = (0, 0, 1)$ , with oscillating intensity,  $f_m(t) = \alpha \cos \Omega t$ , c.f. Fig. 21. Using Eqs. (140) and (141) we find that the Hamiltonian in the rotating frame is obtained from  $H_0$  via the



substitutions:

$$\begin{aligned}\sigma_m^x &\longrightarrow \cos \theta(t) \sigma_m^x - \sin \theta(t) \sigma_m^y, \\ \sigma_m^y &\longrightarrow \cos \theta(t) \sigma_m^y + \sin \theta(t) \sigma_m^x, \\ \sigma_m^z &\longrightarrow \sigma_m^z,\end{aligned}\tag{143}$$

where  $\theta(t) = 2\Delta(t) = 2\alpha \sin \Omega t$ . After some algebra, we have:

$$H^{\text{rot}}(t) = J_0 \sum_{\langle m,n \rangle} \cos(2\theta(t)) (\sigma_m^x \sigma_n^x - \sigma_m^y \sigma_n^y) - \sin(2\theta(t)) (\sigma_m^x \sigma_n^y + \sigma_m^y \sigma_n^x) \tag{144}$$

In the infinite-frequency limit, the Floquet Hamiltonian can be calculated as:

$$H_F^{\text{rot},(0)} = \frac{1}{T} \int_0^T dt H^{\text{rot}}(t) = \mathcal{J}_0(4\alpha) H_0, \tag{145}$$

where  $\mathcal{J}_0$  is the Bessel function and we have used the mathematical identities:

$$\frac{1}{T} \int_0^T dt \cos(4\alpha \sin \Omega t) = \mathcal{J}_0(4\alpha), \quad \frac{1}{T} \int_0^T dt \sin(4\alpha \sin \Omega t) = 0.$$

By choosing  $\alpha$  to coincide with the zero of the Bessel function, periodically driven spin systems can exhibit dynamical freezing [169, 170].

We derive the leading  $\Omega^{-1}$ -corrections by computing the next term in the Magnus expansion. We choose to focus on a 1d chain for simplicity:

$$H_F^{\text{rot},(1)} = G \frac{J_0^2}{\Omega} \sum_m (\sigma_{m-1}^x \sigma_m^z \sigma_{m+1}^y + \sigma_{m-1}^y \sigma_m^z \sigma_{m+1}^x)$$

where  $G$  is a numerical factor of order one, given by the expression:

$$\begin{aligned}G = \frac{1}{\pi} \int_0^{2\pi} d\tau_1 \int_0^{\tau_1} d\tau_2 [\sin(4\alpha \sin(\tau_1)) \cos(4\alpha \sin(\tau_2)) \\ - \sin(4\alpha \sin(\tau_2)) \cos(4\alpha \sin(\tau_1))]\end{aligned}$$

We thus see that, in this example, the infinite-frequency limit results in a renormalization of the spin-spin interactions of the bare Hamiltonian, while the first subleading correction in  $\Omega^{-1}$  introduces 3-spin interaction terms. In the basis of  $\sigma_z$ , these terms play a role similar to the interaction-dependent hopping in Eqs. (130) and (134). They induce next-nearest-neighbor spin flip processes, whose amplitude depends on the direction of the spin at the middle-site.

Let now us analyze another, slightly more complicated example on a two-dimensional lattice. The system is driven by a linearly-polarized magnetic field along the  $z$ -direction

$$H(t) = H_0 + \alpha \Omega \cos \Omega t \sum_{m,n} m \sigma_{m,n}^z, \tag{146}$$

where  $H_0$  is a standard  $xy$  Hamiltonian:

$$H_0 = \sum_{m,n} J_y \left( \sigma_{m,n}^x \sigma_{m,n+1}^x + \sigma_{m,n}^y \sigma_{m,n+1}^y \right) + J_x \left( \sigma_{m,n}^x \sigma_{m+1,n}^x + \sigma_{m,n}^y \sigma_{m+1,n}^y \right) \quad (147)$$

and  $J_x$  and  $J_y$  are the bare coupling along the  $x$  and  $y$  directions. In analogy with the previous example, we find  $\theta_{m,n}(t) = 2\Delta_{m,n}(t) = 2m\alpha \sin \Omega t$ . Using the transformation in Eq. (143) we arrive at:

$$H^{\text{rot}}(t) = \sum_{m,n} J_y \left( \sigma_{m,n}^x \sigma_{m,n+1}^x + \sigma_{m,n}^y \sigma_{m,n+1}^y \right) + h(t) J_x \left( \sigma_{m,n}^x \sigma_{m+1,n}^x + \sigma_{m,n}^y \sigma_{m+1,n}^y \right), \quad (148)$$

where we defined

$$h(t) \equiv \cos(\theta_{m,n}(t) - \theta_{m+1,n}(t)) = \cos(2\alpha \sin \Omega t).$$

Observe that if the magnetic field were uniform, i.e. if there were no magnetic gradients, then  $h(t) \equiv 1$  and  $H^{\text{rot}}(t) = H_0$ . This is not surprising since, in this case, the driving would commute with  $H_0$ . In the infinite-frequency limit, the Floquet Hamiltonian reads as:

$$H_F^{\text{rot},(0)} = \sum_{m,n} J_y \left( \sigma_{m,n}^x \sigma_{m,n+1}^x + \sigma_{m,n}^y \sigma_{m,n+1}^y \right) + \mathcal{J}_0(2\alpha) J_x \left( \sigma_{m,n}^x \sigma_{m+1,n}^x + \sigma_{m,n}^y \sigma_{m+1,n}^y \right). \quad (149)$$

This expression shows that, for  $\Omega \rightarrow \infty$ , the coupling strength along the  $x$  direction is renormalized, while the one along the  $y$  direction is not. By changing the value of  $\alpha$  the Bessel function  $\mathcal{J}_0(2\alpha)$  can be tuned to zero or even take negative values, in the same spirit as the original work by Dunlap and Kenkre [139, 140]. This opens up possibilities for studying dimensional crossovers, effectively tuning the spin system between  $1d$  and  $2d$  regimes, and dynamically switching between ferromagnetic and anti-ferromagnetic couplings.

Finally, notice that a close analogue to the Harper-Hofstadter Hamiltonian can be realized for spins by choosing the static Hamiltonian on a two-dimensional lattice as in Eq. (147) and the periodic driving:

$$H_1(t) = \Omega \sum_{m,n} f_{m,n}(t) \sigma_{m,n}^z, \quad f_{m,n}(t) = m + \alpha \cos(\Omega t + \phi_{n,m}), \quad (150)$$

where  $\phi_{m,n} = \Phi_{\square}(n + m)$  (see Sec. 7.2 for details). The calculation of the dominant and subleading correction to the Floquet Hamiltonian follows closely the steps shown above and in Sec. 7.2. In the infinite-frequency limit, this leads to complex interaction amplitudes with a flux  $\Phi_{\square}$  per plaquette. Hence, one can expect to observe nontrivial spin-wave dynamics.

*Cold Atom Experiments with Spins Systems.* We now briefly mention some recent experimental realisations of classical spin systems using periodically driven cold atoms [52, 132, 135, 137, 159].

In Ref. [52] the authors employed a quantum system to simulate classical magnetism. A weakly-interacting  $^{87}\text{Rb}$  Bose gas was loaded in a two-dimensional triangular lattice. In the superfluid regime where phase fluctuations are suppressed and for high filling numbers, the system is effectively described by the classical  $XY$ -model

$$H_0 = -J \sum_{\langle ij \rangle} \cos(\varphi_i - \varphi_j) + \frac{U}{2} \sum_j (S_j^z)^2 = -J \sum_{\langle ij \rangle} \mathbf{S}_i \cdot \mathbf{S}_j + \frac{U}{2} \sum_j (S_j^z)^2,$$

where the effective spin interaction  $J$  is proportional to the boson hopping matrix element,  $U$  is the effective local interaction related to the Hubbard coupling in the Bose-Hubbard model, and  $\mathbf{S}_i$  is a unit vector confined to the  $XY$ -plane such that  $S_j^x = \cos \varphi_j$ ,  $S_j^y = \sin \varphi_j$ , which represents the classical spin or rotor variable. As we saw in Secs. 7.1, 7.2, 2.2, and 7.4, it is possible to modify the hopping matrix elements along the bonds by applying a periodic modulation. Mechanically moving the lattice along an elliptical orbit is equivalent to applying the force  $\mathbf{F}(t) = F_c \cos \Omega t \mathbf{e}_c + F_s \cos \Omega t \mathbf{e}_s$  where  $\mathbf{e}_{c/s}$  are two orthonormal vectors in the lattice plane and  $F_{c/s}$  are experimentally controlled amplitudes [137]. This driving protocol can be taken into account by the following effective spin Hamiltonian

$$H(t) = -J \sum_{\langle ij \rangle} \mathbf{S}_i \cdot \mathbf{S}_j + \sum_j \mathbf{F}(t) \cdot \mathbf{r}_j S_j^z + \frac{U}{2} \sum_j (S_j^z)^2. \quad (151)$$

The setup is very similar to the realisation of Haldane's model with circularly polarised electric field, c.f. Eq. (138). Using Eq. (143) together with the discussion after Eq. (146) and the identification  $\mathbf{S}_j \leftrightarrow \boldsymbol{\sigma}_j$ , we can transform to the rotating frame. This results in a modification of the hopping matrix elements  $J \rightarrow J\mathcal{J}_0(\zeta_{ij})$  with  $\zeta_{ij} = \Omega^{-1} \sqrt{(F_c \mathbf{e}_c \cdot \mathbf{r}_{ij})^2 + (F_s \mathbf{e}_s \cdot \mathbf{r}_{ij})^2}$ , where the vectors  $\mathbf{r}_{ij} = \mathbf{r}_i - \mathbf{r}_j$  connect nearest-neighbouring sites. Consequently, as a result of the periodic shaking, it is possible to establish control over the spin-interactions on the three bonds of the triangular plaquette. The infinite-frequency Floquet Hamiltonian is

$$H_F^{(0)} = - \sum_{\langle ij \rangle} J_{ij} \mathbf{S}_i \cdot \mathbf{S}_j + \frac{U}{2} \sum_j (S_j^z)^2, \quad (152)$$

where  $J_{23} = J_{31} = J'$  and  $J_{12} = J$ , c.f. Fig. 22. In the original paper [52] the last term did not appear in the Hamiltonian because the interactions were tuned to a small value and also because they do not affect the thermal phase diagram in the classical limit (large filling). By tuning the driving amplitudes  $F_c$  and  $F_s$ , it is possible to reach regimes in which the spin-interactions  $J, J'$  flip sign independently. This opens up the way towards studying a rich phase diagram where spin order competes with frustration due to the lattice geometry.

As a main tool to study the phase diagram, c.f. Fig. 23, the authors performed time-of-flight measurements which gives access to the momentum distribution of the superfluid Bose gas. By assigning a unique momentum distribution to the ground states of the candidate ordered phases, the phase diagram was mapped out with a very high precision. It was even possible to observe spontaneous symmetry breaking directly in the case where the two degenerate ground states lead to different time-of-flight images. For  $J, J' > 0$  the system was found in a rhombic state (R), while for  $J > 0, J' < 0$  it undergoes a first-order phase transition to a ferromagnet (F). On the transition boundary ( $J' = 0, J > 0$ ) FM-chains build up in the ground state. Frustration effects become relevant when  $J < -|J'|/2$ , where the system undergoes a second-order phase transition to two different spiral states, (SP2) and (SP1), depending on whether it is approached from the FM ( $J' < 0$ ) or the rhombic ( $J' > 0$ ) side, respectively. These spiral states are connected

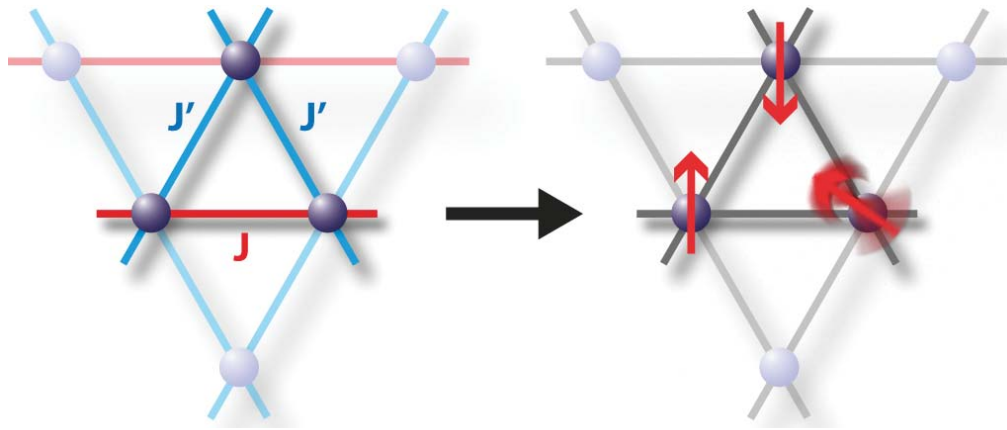


Figure 22. (Color online). Realisation of the classical XY-model on a frustrated triangular lattice using ultracold bosons. By applying a periodic driving, it is possible to establish independent control over the two spin interactions  $J, J'$ . From Ref. [52]. Reprinted with permission from AAAS.

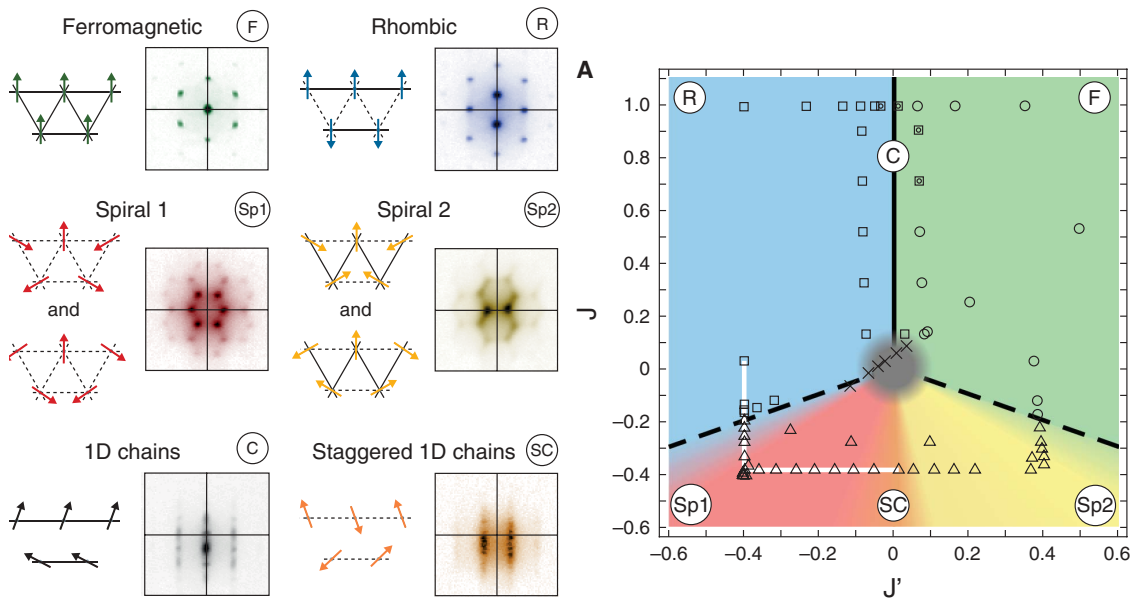


Figure 23. (Color online). Left panel: Ground states of the frustrated XY model on a triangular lattice for different values of the hopping parameters  $J$  and  $J'$  (see right panel). Right panel: Phase diagram of the frustrated XY model on a triangular lattice in the  $(J, J')$ -plane. The symbols refer to the states in the left panel. The solid line is a first-order, while the dashed lines represent a second-order phase transition. In the grey region where tunneling is suppressed the bosonic system is strongly interacting and the interference pattern is destroyed. From Ref. [52]. Reprinted with permission from AAAS.

by a continuous crossover at  $J' = 0$  and  $J < 0$ , where the ground state displays the order of staggered spin-chains (SC). For more details, see Ref. [52].

In a subsequent experiment [135], the interplay between the continuous  $U(1)$  symmetry of the XY-model in the presence of a  $\mathbb{Z}_2$  Ising-like artificial gauge field was studied. Once again,  $^{87}\text{Rb}$  was loaded in a 3D triangular lattice (weakly confined along the vertical direction) which realised the classical XY-model. In addition, an artificial magnetic field in the form of complex Peierls phases was imprinted in the hopping amplitudes  $J_{ij}$ , created by shaking the positions of the lattice wells according to an elliptically-polarised modulation. The model realises a nonzero net flux which penetrates the triangular plaquettes in an alternating fashion. This flux leads to mass currents along the plaquettes whose direction, clockwise or counter-clockwise, constitutes the classical Ising variable, which was indirectly measured through the occupation of the momentum modes. In addition from

such measurements the authors were able to identify thermal phase transitions between anti-ferromagnetic and paramagnetic phases.

## 8. Summary and Outlook

Periodically driven systems in the high-frequency limit can be used to engineer interesting effective Hamiltonians, which are very difficult or impossible to realize in equilibrium systems. They provide an important step towards the simulation of quantum condensed matter systems, and can be used to test predictions of physical theories in new regimes.

In this review, we have presented a systematic analysis of the high-frequency regimes in periodically driven (Floquet) systems. We have identified both the infinite frequency and first leading correction ( $\Omega^{-1}$ ) to the Floquet Hamiltonians. We have precisely defined the Floquet Stroboscopic (FS) and Floquet non-stroboscopic (FNS) dynamics and computed the dressed operators and the dressed density matrices required to correctly describe both these schemes. We discussed the Floquet gauge structure associated with the choice of the stroboscopic time and discussed how one can use the Floquet gauge freedom to find the Floquet Hamiltonian in its simplest form. We discussed that the Floquet non-stroboscopic dynamics (FNS), which suits very well the current experimental techniques, often opens the possibility of measuring Floquet gauge-invariant physical observables like the proper Floquet current.

As the main tool to study the high-frequency limit, we employed the Magnus expansion. We showed that it can be used to reliably calculate the leading corrections, to the infinite-frequency Floquet Hamiltonian. When applied to time-independent Hamiltonians in the rotating frame, one can use it to eliminate a high-energy scale from the problem and derive an effective dressed low-energy Hamiltonian with renormalized parameters similarly to the Schrieffer-Wolff transformation. Moreover we discussed how one can naturally extend this transformation to driven setups and identified new terms in the dressed Hamiltonian, which appear due to the driving and which lead to heating and other non-equilibrium effects. We briefly discussed the convergence of the Magnus expansion, which is not guaranteed for interacting many-body systems in the thermodynamic limit, and the relation between this mathematical question and (lack of) heating in periodically driven systems. These important questions are not yet settled. We hope that they will be resolved in future experiments and theoretical work.

A prerequisite for finding non-trivial high-frequency limits is a strong coupling of the driving protocol to the system, in the form of a driving amplitude which scales with a power of the driving frequency. Often times, a systematic way of studying the inverse-frequency expansion of the Floquet Hamiltonian is to first go to the rotating frame w.r.t. the driving Hamiltonian. We proved that this amounts to the resummation of an infinite lab-frame Magnus subseries and demonstrated it on several examples. Moreover, we identified three classes of universal high-frequency driving protocols leading to well defined local Floquet Hamiltonians (c.f. Fig. 24), but there may be more. For each class, we have calculated the form of the effective Floquet Hamiltonian which differs significantly from the time-averaged one.

The Kapitza class is characterized by a kinetic energy term which is quadratic in momentum, and a driving amplitude which scales linearly in  $\Omega$ . We gave examples of both a single- and many-body systems which realize this limit. The Dirac class is marked by a linear kinetic energy term which requires adding a spin structure via the Pauli matrices. One can periodically drive either an external magnetic field, in which case the amplitude should scale as  $\Omega$  or, alternatively, the drive can couple to an external potential and the driving amplitude is required to scale as  $\Omega^2$ . The Dunlap-Kenkre (DK) class applies to systems with arbitrary dispersion relation, where, one drives an external single-particle

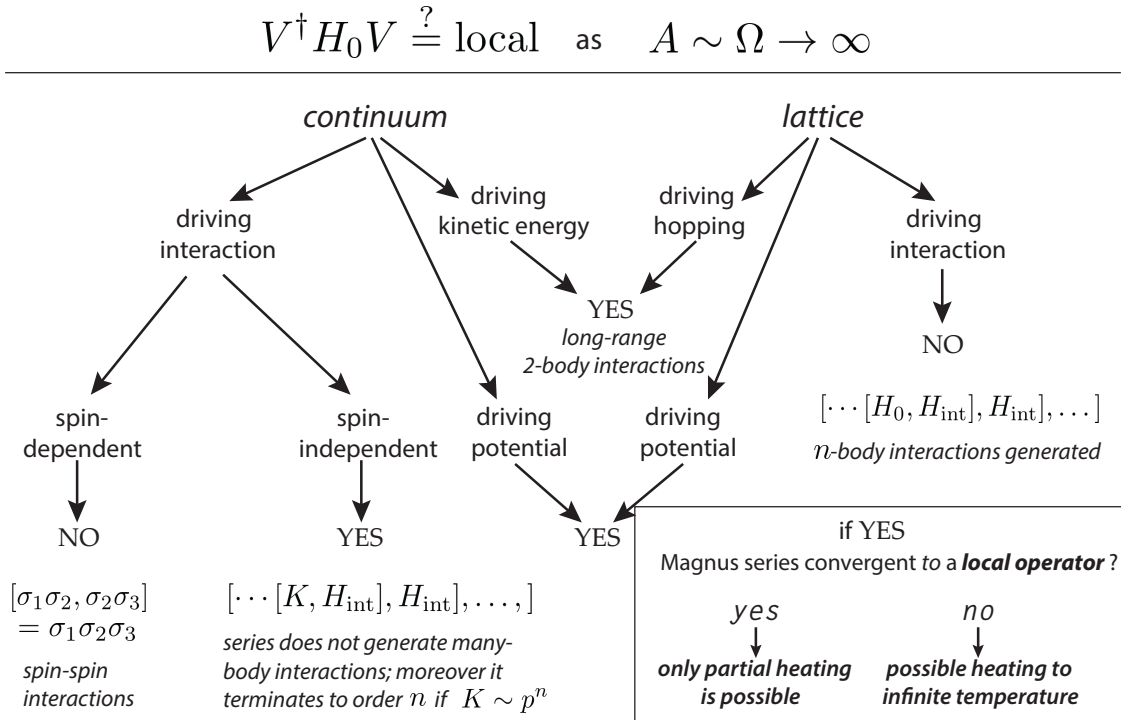


Figure 24. (Color online) The figure summarises the scenarios discussed in this review: globally periodically driven continuum and lattice models. Depending on whether one drives the interaction or the external potential the Magnus Hamiltonian can be local (YES) or a non-local one (NO). A local Magnus Hamiltonian is a sum of spatially local terms and can include only few-body interactions. Different scenarios might appear in locally driven systems. For example, driving any local in space term like the local hopping strength or the local interaction coupling does not produce any long-range terms in the infinite-frequency Floquet Hamiltonian.

scalar potential, whose amplitude scales linearly in  $\Omega$ . We illustrated all three classes with various examples and discussed recent experimental progress made with cold atoms.

While classical few body Floquet systems, such as the Kapitza pendulum and its variations, found a multitude of interesting and useful applications, the experimental realization and systematic theoretical analysis of many-particle periodically driven systems is very recent. We discussed several realizations of Floquet systems both in cold atoms and in solid state materials, where new, hard to achieve otherwise, regimes have been accessed using a periodic modulation. This lead to the emergence of a new research direction, dubbed “Floquet engineering”, which has the potential to develop systems with unique properties in the near future. Floquet systems constitute a playground for studying many different phenomena such as information and entanglement propagation in the absence of conservation laws, finding non-equilibrium optimum quantum annealing protocols, designing materials with tunable properties, and many more. There are also many open conceptual problems in Floquet systems, which we mentioned only briefly in this review but which are obviously important for our overall understanding of driven systems. In particular, the nature of steady states in open Floquet systems, i.e. Floquet systems coupled to a thermal bath, non-adiabatic response in Floquet systems with slowly changing external parameters, robustness and universality of topological Floquet phases, nature and classification of phase transitions in driven open and isolated systems and others. We hope that these and other questions will be understood in near future.

## Acknowledgements

The authors would like to thank A. George, P. Hauke, M. Heyl, D. Huse, T. Iadecola, S. Kehrein, M. Kolodrubetz, A. Rosch, P. Weinberg and P. Zoller for insightful and interesting discussions. We are very grateful to the experimental teams in the groups of E. Arimondo, I. Bloch, T. Esslinger and K. Sengstock for kindly allowing us to include some of the figures from their previous papers in this review. Last but not least, we would also like to thank J. G. Wright and B. S. Shastry for developing the software DiracQ[171] used to verify the commutator algebra calculations in this work. This work was supported by AFOSR FA9550-13-1-0039, ARO W911NF1410540, and NSF DMR-1206410.

## References

- [1] G. Casati, B. V. Chirikov, F. M. Izrailev, and J. Ford. *Lecture Notes in Physics*, Springer N. Y., 93:334–352, 1979.
- [2] B. V. Chirikov. *Research concerning the theory of nonlinear resonance and stochasticity*, Preprint N 267, Institute of Nuclear Physics, Novosibirsk, 1969.
- [3] P. L. Kapitza. *Soviet Phys. JETP*, 21:588, 1951.
- [4] B. V. Chirikov, F. M. Izrailev, and D. L. Shepelyansky. *Soviet Scientific Reviews. Section C*, 2:209, 1981.
- [5] S. Rahav, I. Gilary, and S. Fishman. *Phys. Rev. A*, 68:013820, 2003.
- [6] S. Rahav, I. Gilary, and S. Fishman. *Phys. Rev. Lett.*, 91:110404, 2003.
- [7] L. E. Reichl. *The transition to Chaos: Conservative Classical Systems and Quantum Manifestations*. Springer, New York, 2004.
- [8] F. Grossmann, T. Dittrich, P. Jung, and P. Hänggi. *Phys. Rev. Lett.*, 67:516519, 1991.
- [9] F. Grossmann and P. Hänggi. *Europhys. Lett.*, 18:571, 1992.
- [10] M. Gavrilă. *J. Phys. B: At. Mol. Opt. Phys.*, 35:R147R193, 2002.
- [11] M. Grifoni and P. Hänggi. *Physics Reports*, 304:229–354, 1998.
- [12] R. Bavlî and H. Metiu. *Phys. Rev. Lett.*, 69:13, 1992.
- [13] P. Neu and R. J. Silbey. *Phys. Rev. A*, 54:6, 1996.
- [14] H. W. Broer, I. Hoveijn, M. van Noort, C. Simó, and G. Vegter. *Journal of Dynamics and Differential Equations*, 16:897–947, 2004.
- [15] L. D. Landau and E. M. Lifshitz. *Mechanics*. Butterworth-Heinemann, 2007.
- [16] Q. Su and J. H. Eberly. *Phys. Rev. A*, 43:2474–2479, Mar 1991.
- [17] I. Bialynicki-Birula, M. Kalinski, and J. H. Eberly. *Phys. Rev. Lett.*, 73:13, 1994.
- [18] J. H. Eberly and K. C. Kulander. *Science*, 262:1229–1233, 1993.
- [19] B. Pirau and R. M. Potvliege. *Phys. Rev. A*, 57:6, 1998.
- [20] M. Pont and M. Gavrilă. *Phys. Rev. Lett.*, 65:19, 1990.
- [21] J. Zakrzewski and D. Delande. *J. Phys. B: At. Mol. Opt. Phys.*, 28:L667–L672, 1995.
- [22] M. Holthaus. *Chaos, Solitons & Fractals No 5*, 7:1143–1167, 1995.
- [23] A. Buchleitner, D. Delande, and J. Zakrzewski. *Physics Reports*, 368:409547, 2002.
- [24] V. M. Bastidas, C. Emary, B. Regler, and T. Brandes. *Phys. Rev. Lett.*, 108:043003, 2012.
- [25] V. M. Bastidas, C. Emary, G. Schaller, and T. Brandes. *Phys. Rev. A*, 86:063627, 2012.
- [26] G. Engelhardt, V. M. Bastidas, C. Emary, and T. Brandes. *Phys. Rev. E*, 87:052110, 2013.
- [27] V. M. Bastidas, P. Pérez-Fernández, M. Vogl, and T. Brandes. *Phys. Rev. Lett.*, 112:140408, 2014.
- [28] S. Denisov, L. Morales-Molina, S. Flach, and P. Hänggi. *Phys. Rev. A*, 75:063424, 2007.
- [29] A. Auerbach and G. Venketeswara Pai. *Phys. Rev. B*, 76:205318, 2007.
- [30] D. Poletti, G. Benenti, G. Casati, P. Hänggi, and B. Li. *Phys. Rev. Lett.*, 102:130604, 2009.
- [31] T. Salger, S. Kling, S. Denisov, A. V. Ponomarev, P. Hänggi, and M. Weitz. *Phys. Rev. Lett.*, 110:135302, 2013.
- [32] S. Denisov, S. Flach, and P. Hänggi. *Physics Reports*, 538:77120, 2014.
- [33] C. Grossert, M. Leder, S. Denisov, P. Hänggi, and M. Weitz. *arXiv:1407.0605*, 2014.
- [34] Z. Ovadyahu. *Phys. Rev. Lett.*, 108:156602, 2012.

- [35] S. Iwai, M. Ono, A. Maeda, H. Matsuzaki, H. Kishida, H. Okamoto, and Y. Tokura. *Phys. Rev. Lett.*, 91:057401, 2003.
- [36] S. Kaiser, D. Nicoletti, C. R. Hunt, W. Hu, I. Gierz, H. Y. Liu, M. Le Tacon, T. Loew, D. Haug, B. Keimer, and A. Cavalleri. *1205.4661v6*, 2014.
- [37] G. Goldstein, C. Aron, and C. Chamon. *arXiv:1406.7299*, 2014.
- [38] M. Hafezi, A. S. Sorensen, E. Demler, and M. D. Lukin. *Phys. Rev. A*, 75:023613, 2006.
- [39] A. Zenesini, H. Lignier, D. Ciampini, O. Morsch, and E. Arimondo. *Phys. Rev. Lett.*, 102:100403, 2009.
- [40] T. Oka and H. Aoki. *Phys. Rev. B*, 79:081406(R), 2011.
- [41] T. Kitagawa, T. Oka, A. Brataas, L. Fu, and E. Demler. *Phys. Rev. B*, 84:235108, 2011.
- [42] C. E. Creffield and F. Sols. *Phys. Rev. A*, 84:023630, 2011.
- [43] P. Hauke, O. Tieleman, A. Celi, C. Ölschläger, J. Simonet, J. Struck, M. Weinberg, P. Windpassinger, K. Sengstock, M. Lewenstein, , and A. Eckardt. *Phys. Rev. Lett.*, 109:145301, 2012.
- [44] T. Iadecola, D. Campbell, C. Chamon, C. Y. Hou, R. Jackiw, S. Y. Pi, and S. V. Kusminskiy. *Phys. Rev. Lett.*, 110:176603, 2013.
- [45] N. H. Lindner, G. Refael, and V. Galitski. *Nature Physics*, 7:490–495, 2011.
- [46] Y. H. Wang, H. Steinberg, P. Jarillo-Herrero, and N. Gedik. *Science*, 25:453–457, 2013.
- [47] M. Aidelsburger, M. Atala, M. Lohse, J. T. Barreiro, B. Paredes, and I. Bloch. *Phys. Rev. Lett.*, 111:185301, 2013.
- [48] H. Miyake, G. A. Siviloglou, C. J. Kennedy, W. C. Burton, and W. Ketterle. *Phys. Rev. Lett.*, 111:185302, 2013.
- [49] G. Jotzu, M. Messer, R. Desbuquois, M. Lebrat, T. Uehlinger, D. Greif, and T. Esslinger. *Nature*, 515:237240, 2014.
- [50] M. Aidelsburger, M. Lohse, C. Schweizer, M. Atala, J. T. Barreiro, S. Nascimbène, N. R. Cooper, I. Bloch, and N. Goldman. *arXiv:1407.4205*, 2014.
- [51] S. K. Baur, M. H. Schleier-Smith, and N. R. Cooper. *Phys. Rev. A*, 89:051605(R), 2014.
- [52] J. Struck, C. Ölschläger, R. Le Targatn, P. Soltan-Panahi, A. Eckardt, M. Lewenstein, P. Windpassinger, and K. Sengstock. *Science*, 333(6045):996–999, 2011.
- [53] N. Goldman, J. Dalibard, M. Aidelsburger, and N. R. Cooper. *arXiv:1410.8425*, 2014.
- [54] A. V. Ponomarev, S. Denisov, and P. Hänggi. *Phys. Rev. Lett.*, 102:230601, 2009.
- [55] A. V. Ponomarev, S. Denisov, and P. Hänggi. *Journal of Computational and Theoretical Nanoscience*, 7:2441–2447, 2010.
- [56] R. Blatt and C. F. Roos. *Nature Physics*, 8:277, 2012.
- [57] P. Zoller. private communication.
- [58] T. Prosen. *Phys. Rev. Lett.*, 80:1808, 1998.
- [59] T. Prosen. *Phys. Rev. E*, 60:3949, 1999.
- [60] M. Bukov and M. Heyl. *Phys. Rev. B*, 86:054304, 2012.
- [61] L. D’Alessio and A. Polkovnikov. *Annals of Physics*, 333:491, 2013.
- [62] L. D’Alessio and M. Rigol. *arXiv:1402.5141*, 2014.
- [63] P. Ponte, A. Chandran, Z. Papić, and D. A. Abanin. *arXiv:1403.6480*, 2014.
- [64] A. Lazarides, A. Das, and R. Moessner. *Phys. Rev. E*, 90:012110, 2014.
- [65] N. Goldman and J. Dalibard. *arXiv 1404.4373*, 2014.
- [66] M. M. Maricq. *Phys. Rev. B*, 25:6622, 1982.
- [67] M. M. Maricq. *Phys. Rev. B*, 37:7215–7229, 1988.
- [68] W. Magnus. *Commun. Pure Appl. Math.*, VII:649, 1954.
- [69] A. Verdeny, A. Mielke, and F. Mintert. *Phys. Rev. Lett.*, 111:175301, 2013.
- [70] H. P. Breuer and M. Holthaus. *Ann. Phys. (NY)*, 211:249, 1991.
- [71] D. Jaksch and P. Zoller. *Ann. Phys. (Amsterdam)*, 315:52, 2003.
- [72] S. Blanes, F. Casas, J. A. Oteo, and J. Rios. *Physics Reports*, 470:151–238, 2009.
- [73] T. P. Grozdanov and M. J. Raković. *Phys. Rev. A*, 38:1739, 1988.
- [74] C. Xu, A. Poudel, and M. G. Vavilov. *Phys. Rev. A*, 89:052102, 2014.
- [75] J. P. Dahlhaus, B. M. Fregoso, and J. E. Moore. *arXiv:1408.6811*, 2014.
- [76] M. Bandyopadhyay and S. Dattagupta. *Pramana – J. of Phys.*, 70, No 3:381398, 2008.
- [77] A. Alvermann and H. Fehske. *J. Comp. Phys.*, 230:59305956, 2011.
- [78] B. L. Altshuler, Y. Gefen, A. Kamenev, and L. S. Levitov. *Phys. Rev. Lett.*, 78:2803, 1997.



- [79] I. V. Gornyi, A. D. Mirlin, and D. G. Polyakov. *Phys. Rev. Lett.*, 95:206603, 2005.
- [80] D. M. Basko, I. L. Aleiner, and B. L. Altshuler. *Annals of Physics*, 321:1126, 2006.
- [81] V. Oganesyan and D. A. Huse. *Phys. Rev. B*, 75:155111, 2007.
- [82] A. Pal and D. A. Huse. *Phys. Rev. B*, 82:174411, 2010.
- [83] J. Z. Imbrie. *arXiv:1403.7837*, 2014.
- [84] T. Prosen. *J. Phys. A: Math. Gen.*, 31:L645, 1998.
- [85] M. Heyl and S. Kehrein. *Phys. Rev. B*, 81:144301, 2010.
- [86] M. Heyl. private communication.
- [87] A. Russomanno, A. Silva, and G. E. Santoro. *Phys. Rev. Lett.*, 109:257201, 2012.
- [88] A. Lazarides, A. Das, and R. Moessner. *Phys. Rev. Lett.*, 112:150401, 2014.
- [89] A. Eckardt and M. Holthaus. *Phys. Rev. Lett.*, 101:245302, Dec 2008.
- [90] T. Mori. *arXiv:1412.6738*, 2014.
- [91] H. P. Breuer, W. Huber, and F. Petruccione. *Phys. Rev. E*, 61:4883, 2000.
- [92] R. Ketzmerick and W. Wustmann. *Phys. Rev. E*, 82:021114, 2010.
- [93] D. Vorberg, W. Wustmann, R. Ketzmerick, and A. Eckardt. *Phys. Rev. Lett.*, 111:240405, Dec 2013.
- [94] T. Iadecola and C. Chamon. *arXiv:1412.5599*, 2014.
- [95] B. M. Fregoso, J. P. Dahlhaus, and J. E. Moore. *arXiv:1405.5973*, 2014.
- [96] M. Langemeyer and M. Holthaus. *Phys. Rev. E*, 89:012101, 2014.
- [97] H. Dehghani, T. Oka, and A. Mitra. *arXiv:1406.6626*, 2014.
- [98] W. Kohn. *J. of Stat. Phys.*, 103:417–423, 2001.
- [99] D. W. Hone, R. Ketzmerick, and W. Kohn. *Phys. Rev. E*, 79:051129, 2009.
- [100] C. A. Parra-Murillo, J. Madro nero, and S. Wimberger. *Phys. Rev. A*, 88:032119, 2013.
- [101] C. A. Parra-Murillo and S. Wimberger. *Acta Phys. Pol. A*, 124:1091, 2013.
- [102] J. R. Schrieffer and P. A. Wolff. *Phys. Rev.*, 149:491, 1966.
- [103] N. Yamada, K. Noba, S. Tanaka, and T. Petrosky. *Phys. Rev. B*, 86:014302, 2012.
- [104] K. Noba, N. Yamada, Y. Uesaka, S. Tanaka, and T. Petrosky. *J. Phys. A: Math. Theor.*, 47:385302, 2010.
- [105] D. Braak. *Phys. Rev. Lett.*, 107:100401, 2011.
- [106] M. Tomka, O. El Araby, M. Pletyukhov, and V. Gritsev. *arXiv:1307.7876*, 2013.
- [107] M. Schiró, M. Bordyuh, B. Öztop, and H. Türeci. *Phys. Rev. Lett.*, 109:053601, 2012.
- [108] I. Bloch. *Nature Physics*, 1:23, 2005.
- [109] H. Pichler, A. J. Daley, and P. Zoller. *Phys. Rev. A*, 82:063605, 2010.
- [110] G. Casati, I. Guarneri, and G. Mantica. *Phys. Rev. A*, 50:5018, 1994.
- [111] H. Wiedemann, J. Mostowski, and F. Haake. *Phys. Rev. A*, 49:1171, 1994.
- [112] M. Gavrila. *Atoms in Intense Laser Fields*. Academic Press, New York, 1992.
- [113] C. O. Reinhold, J. Burgdörfer, M. T. Frey, and F. B. Dunning. *Phys. Rev. Lett.*, 79:5226, 1997.
- [114] O.M. Braun and Yu. S. Kivshar. *Physics Reports*, 306:1, 1998.
- [115] J. J. Sakurai. *Modern Quantum Mechanics*. Addison–Wesley, 1993.
- [116] A. H. Castro Neto, F. Guinea, N. M. R. Peres, K. S. Novoselov, and A. K. Geim. *Rev. Mod. Phys.*, 81:109, 2009.
- [117] A. A. Burkov and L. Balents. *Phys. Rev. Lett.*, 107:127205, 2011.
- [118] T. Uehlinger, G. Jotzu, M. Messer, D. Greif, W. Hofstetter, U. Bissbort, and T. Esslinger. *Phys. Rev. Lett.*, 111:185307, 2013.
- [119] L. Tarruell, D. Greif, T. Uehlinger, G. Jotzu, and T. Esslinger. *Nature*, 483:302–305, 2013.
- [120] B. M. Anderson, I. B. Spielman, and G. Juzeliunas. *Phys. Rev. Lett.*, 111:125301, 2013.
- [121] Z.-F. Xu, L. You, and M. Ueda. *Phys. Rev. A*, 87:063634, 2013.
- [122] J. Struck, J. Simonet, and K. Sengstock. *arXiv:1407.1953*, 2014.
- [123] S. Zhang, W. S.Cole, A. Paramekanti, and N. Trivedi. *arXiv:1411.2297*, 2014.
- [124] A. López, Z. Z. Sun, and J. Schliemann. *Phys. Rev. B*, 85:205428, 2012.
- [125] P. Plötz, P. Schlagheck, and S. Wimberger. *Euro Phys. J D*, 63:47–53, 2011.
- [126] P. Plötz and S. Wimberger. *Euro Phys. J D*, 63:pp 199205, 2011.
- [127] R. Diener and Q. Niu. *J. Opt. B: Quantum Semiclass. Opt.*, 2:618627, 2000.
- [128] N. Gemelke, E. Sarajlic, Y. Bidel, S. Hong, and S. Chu. *Phys. Rev. Lett.*, 95:170404, 2005.
- [129] A. Eckardt, C. Weiss, and M. Holthaus. *Phys. Rev. Lett.*, 95:260404, 2005.

- [130] D. Ciampini, O. Morsch, and E. Arimondo. *Int. J. Quantum Inform.*, 09:139, 2011.
- [131] M. Atala, M. Aidelsburger, M. Lohse, J. T. Barreiro, B. Paredes, and I. Bloch. *Nature Physics*, 10:588593, 2014.
- [132] J. Struck, C. Ölschläger, M. Weinberg, P. Hauke, J. Simonet, A. Eckardt, M. Lewenstein, K. Sengstock, and P. Windpassinger. *Phys. Rev. Lett.*, 108:225304, 2012.
- [133] C. E. Creffield and F. Sols. *Phys. Rev. A*, 90:023636, 2014.
- [134] N. Goldman, G. Juzeliunas, P. Ohberg, and I. B. Spielman. *Rep. Prog. Phys.*, 77:126401, 2014.
- [135] J. Struck, M. Weinberg, C. Ölschläger, P. Windpassinger, J. Simonet, K. Sengstock, R. Höppner, P. Hauke, A. Eckardt, M. Lewenstein, and L. Mathey. *Nature Physics*, 9:738, 2013.
- [136] C. V. Parker, L-C. Ha, and C. Chin. *Nature Physics*, 9:769774, 2013.
- [137] A. Eckardt, P. Hauke, P. Soltan-Panahi, C. Becker, K. Sengstock, and M. Lewenstein. *EPL*, 89:10010, 2010.
- [138] V. M. Bastidas, C. Emary, G. Schaller, A. Gómez-León, G. Platero, and T. Brandes. *arXiv:1302.0781*, 2013.
- [139] D. H. Dunlap and V. M. Kenkre. *Phys. Rev. B*, 34:3625, 1986.
- [140] D. H. Dunlap and V. M. Kenkre. *Phys. Rev. B*, 37:6622, 1988.
- [141] E. Arimondo, D. Ciampini, A. Eckardt, M. Holthaus, and O. Morsch. *Adv. At. Mol. Opt. Phys.*, 61:515–547, 2012.
- [142] M. Di Liberto, C. E. Creffield, G. I. Japaridze, and C. Morais Smith. *Phys. Rev. A*, 89:013624, 2014.
- [143] S. Greschner, G. Sun, D. Poletti, and L. Santos. *Phys. Rev. Lett.*, 113:215303, 2014.
- [144] L. Morales-Molina J. Gong and P. Hänggi. *Phys. Rev. Lett.*, 103:133002, 2009.
- [145] T. Wang, X. Zhang, F. E. A. dos Santos, S. Eggert, and A. Pelster. *Phys. Rev. A*, 90:013633, 2014.
- [146] H. Lignier, C. Sias, D. Ciampini, Y. Singh, A. Zenesini, O. Morsch, and E. Arimondo. *Phys. Rev. Lett.*, 99:220403, 2007.
- [147] C. Sias, H. Lignier, Y. P. Singh, A. Zenesini, D. Ciampini, O. Morsch, and E. Arimondo. *Phys. Rev. Lett.*, 100:040404, 2008.
- [148] C. E. Creffield, F. Sols, D. Ciampini, O. Morsch, and E. Arimondo. *Phys. Rev. A*, 82:035601, 2010.
- [149] A. Zenesini, H. Lignier, O. Morsch, D. Ciampini, and E. Arimondo. *Laser Physics*, 20:1182–1189, 2010.
- [150] B. Gertjerenken and M. Holthaus. *Phys. Rev. A*, 90:053614, 2014.
- [151] E. J. Mueller. *Phys. Rev. A*, 70:041603, 2004.
- [152] M. Bukov and A. Polkovnikov. *Phys. Rev. A*, 90:043613, 2014.
- [153] P. Harper. *Proc. Phys. Soc. London Sect. A*, 68:874, 1955.
- [154] D. Hofstadter. *Phys. Rev. B*, 14:2239, 1976.
- [155] A. R. Kolovski. *EPL*, 93:20003, 2011.
- [156] C. E. Creffield and F. Sols. *EPL*, 101:40001, 2013.
- [157] S. Choudhury and E. J. Mueller. *arXiv:1410.4576*, 2014.
- [158] T. Bilitewski and N. R. Cooper. *arXiv:1410.5364*, 2014.
- [159] Z. Yan, B. Li, X. Yang, and S. Wan. *arXiv:1406.5087*, 2014.
- [160] P. M. Perez-Piskunow, G. Usaj, A. Balseiro, and L. E. F. F. Torres. *Phys. Rev. B*, 89:121401(R), 2014.
- [161] G. Usaj, P. M. Perez-Piskunow, L. E. F. F. Torres, and C. A. Balseiro. *arXiv:1406.1711*, 2014.
- [162] E. S. Morell and L. E. F. F. Torres. *Phys. Rev. B*, 86:125449, 2012.
- [163] H. L. Calvo, H. M. Pastawski, S. Roche, and L. E. F. F. Torres. *Applied Physics Letters*, 98:232103, 2011.
- [164] M. A. Sentef, M. Claassen, A. F. Kemper, B. Moritz, T. Oka, J. K. Freericks, and T. P. Devereaux. *arXiv:1401.5103*, 2014.
- [165] A. G. Grushin, A. Gómez-León, and T. Neupert. *Phys. Rev. Lett.*, 112:156801, 2014.
- [166] F. D. M. Haldane. *Phys. Rev. Lett.*, 61:2015, 1988.
- [167] L. D’Alessio. *arXiv:1412.3481*, 2014.

- [168] D. V. Khomitsky, L. V. Gulyaev, and E. Ya. Sherman. *Phys. Rev. B*, 85:125312, 2012.
- [169] A. Das. *Phys. Rev. B*, 82:172402, 2010.
- [170] S. S. Hegde, H. Katiyar, T. S. Mahesh, and A. Das. *Phys. Rev. B*, 90:174407, 2014.
- [171] J. G. Wright and B. S. Shastry. *arXiv:1301.4494*, 2013.

## Appendix A. Lattice vs. Continuum Models

In this appendix we discuss some subtle differences between the lattice and continuum models discussed in the Secs. 5, 6 and 7. In particular, we show how to combine the results of Sec. 6 and Sec. 7.3. We demonstrate the relation between the models for one-dimensional non-interacting systems, but the generalisation to higher dimensions including interactions is straightforward.

*Systems with linear dispersion.* Consider first the following static, non-interacting Hamiltonian with linear dispersion

$$H_{\text{cont}} = \int dx \frac{J_0}{2} \left( -i\psi^\dagger(x) \partial_x \psi(x) + \text{h.c.} \right). \quad (\text{A1})$$

To discretise the model, we put it on a lattice with lattice constant  $a$ . The corresponding lattice Hamiltonian is given by

$$H_{\text{latt}} = \sum_x \frac{J_0}{2a} (-i\psi^\dagger(x) \psi(x+a) + \text{h.c.}). \quad (\text{A2})$$

If one goes to momentum space, the dispersion relation is  $\varepsilon(k) = J_0/a \sin ak$ , and in the long-wavelength limit,  $ak \ll 1$ , we conveniently recover the continuum dispersion  $\varepsilon_k \approx J_0 k$ . In particular, it follows that in lattice theories with linear dispersion, the hopping matrix element should scale as  $1/a$ . If one, on the other hand, starts with a lattice theory, one can recover the Hamiltonian (A1) from Eq. (A2) in the limit  $a \rightarrow 0$  by using the identity  $\psi(x+a) = \psi(x) + a\partial_x \psi(x) + \mathcal{O}(a^2)$ , and collecting powers of  $a$ .

Let us now add to this Hamiltonian a time-dependent electric field with the amplitude  $V_0$  and frequency  $\Omega$ :

$$H(t) = \int dx \frac{J_0}{2} \left( -i\psi^\dagger(x) \partial_x \psi(x) + \text{h.c.} \right) + V_0 \cos \Omega t \, x \psi^\dagger(x) \psi(x). \quad (\text{A3})$$

In Sec. 6.2, we showed that the zeroth-order Floquet Hamiltonian for this relativistic continuum theory is not affected by the drive if we keep  $\zeta = V_0/\Omega$  independent of  $\Omega$ , i.e. scale the electric field amplitude  $V_0$  linearly with the frequency:

$$H_{F,\text{cont}}^{(0)} = \int dx \frac{J_0}{2} \left( -i\psi^\dagger(x) \partial_x \psi(x) + \text{h.c.} \right). \quad (\text{A4})$$

On the contrary, in Sec. 7.3 we considered the same Hamiltonian on the lattice, and found the following non-trivial zeroth-order Floquet Hamiltonian:

$$H_{F,\text{latt}}^{(0)} = \sum_x \frac{J_0}{2a} \mathcal{J}_0(\zeta a) \left( -i\psi^\dagger(x) \psi(x+a) + \text{h.c.} \right). \quad (\text{A5})$$

At first sight, the two results seem contradictory. To find the proper continuum theory, we expand Eq. (A5) in powers of the inverse lattice constant. Using the identity  $\mathcal{J}_0(\zeta a) = 1 + \mathcal{O}(a^2)$ , we see that the low-energy effective Hamiltonian is independent of  $\zeta$ . Consequently, all the non-trivial effects introduced by the driving vanish in the long-wavelength limit and, therefore, the lattice and continuum models are consistent and yield the same result. A similar derivation applies to higher order corrections in the Magnus expansion. From Eq. (A5) we also see the condition under which the continuum approximation holds:

$$\zeta a \ll 1 \Leftrightarrow V_0 a \ll \Omega. \quad (\text{A6})$$

The product  $V_0 a$  is the maximum energy difference generated by the driving potential between two lattice sites. So the continuum approximation holds only in the limit when this difference is small compared to the driving frequency. Once this condition is violated, the full lattice dispersion has to be taken into account and the continuum approximation breaks down.

*Systems with quadratic dispersion.* We now show the correspondence between the continuum and lattice theories for systems with quadratic dispersion. The non-driven continuum and lattice Hamiltonians read as

$$\begin{aligned} H_{\text{cont}} &= \int dx \phi^\dagger(x) (-\partial_x^2) \phi(x), \\ H_{\text{latt}} &= -\frac{J_0}{a^2} \sum_x \left( (\phi(x)^\dagger \phi(x+a) + \text{h.c.}) - 2\phi(x)^\dagger \phi(x) \right). \end{aligned} \quad (\text{A7})$$

Notice that in the case of a quadratic dispersion, the hopping matrix element scales as  $1/a^2$ .

Consider now the driven model

$$H(t) = \int dx \phi^\dagger(x) (-\partial_x^2) \phi(x) + V_0 \cos \Omega t f(x) \phi^\dagger(x) \phi(x). \quad (\text{A8})$$

Recall that the continuum model fits into the Kapitza class, c.f. Sec. 5, while the lattice model is part of the DK class, Sec. 7. A careful reader might be worried that in the former case, in the limit  $\Omega \rightarrow \infty$ , we found an emergent effective potential leading to dynamical stabilisation whereas, in the latter case, we obtained the following modification to the hopping matrix element:

$$H_{F,\text{latt}}^{(0)} = -\frac{J_0}{a^2} \sum_x \mathcal{J}_0(\zeta f(x+a) - \zeta f(x)) \left( \phi^\dagger(x+a) \phi(x) + \text{h.c.} \right) + \frac{2J_0}{a^2} \sum_x \phi(x)^\dagger \phi(x). \quad (\text{A9})$$

To reconcile the two approaches, again we take the limit  $a \rightarrow 0$ . In doing so, we write  $f(x+a) - f(x) = af'(x) + \mathcal{O}(a^2)$ , and use the expansion  $\mathcal{J}_0(z) = 1 - z^2/4 + \mathcal{O}(z^4)$ . The results is

$$H_{F,\text{cont}}^{(0)} = \int dx \phi^\dagger(x) \left( -\partial_x^2 + \frac{\zeta^2}{4} [f'(x)]^2 \right) \phi(x). \quad (\text{A10})$$

We therefore see that indeed the continuum theory features an emergent potential given by  $\zeta^2/4[f'(x)]^2$  which establishes the relation between the Kapitza and the DK classes (c.f. Eq. (69)).

## Appendix B. First-order Coefficients for the 1D Driven Boson Model

Here, we briefly list the expressions for the nnn hopping, and the staggered potential, found to first order in the Magnus expansion to the model discussed in Sec. 7.1.

We recall that

$$g^{m,m+1}(\tau; \zeta) = \exp[-i\zeta \sin(\tau - \phi_{nm})],$$

where  $\tau = \Omega t$ .

Then the coefficients to the Hamiltonian  $H_F^{(1)}$  given in Eq. 117 are given by the following time-ordered integrals

$$\begin{aligned} C^{m,m+2}(\zeta) &= \frac{1}{4\pi i} \int_0^{2\pi} d\tau_1 \int_0^{\tau_1} d\tau_2 [g^{m,m+1}(\tau_1) g^{m+1,m+2}(\tau_2) - (1 \leftrightarrow 2)], \\ \mathcal{G}^{m,m+1}(\zeta) &= \frac{1}{2\pi} \int_0^{2\pi} d\tau_1 \int_0^{\tau_1} d\tau_2 \operatorname{Im} \left\{ (g^{m,m+1}(\tau_1))^* g^{m,m+1}(\tau_2) \right\}. \end{aligned} \quad (\text{B1})$$

We mention that these expressions are the same as the corresponding one for nnn hopping along the  $y$ -direction  $\uparrow C_0^{m,m+2}(\zeta)$ , and a staggered potential along the  $y$ -direction and  $\uparrow E_0^{m,m+1}(\zeta)$  found in the 2D extension of the model from Sec. 7.2 (see below).

## Appendix C. First-order Coefficients for the Harper-Hofstadter Model

In this appendix we discuss the parameters of the leading correction, Eq. (130). Let us define two auxiliary functions  $f$  and  $g$  by

$$\begin{aligned} f_{m,m+1}^n(\tau; \zeta) &= \exp[-i\zeta \sin(\tau - \phi_{nm}) + i\tau] \\ g_m^{n,n+1}(\tau; \zeta) &= \exp[-i\zeta \sin(\tau - \phi_{nm})]. \end{aligned} \quad (\text{C1})$$

The coefficients  $B$ ,  $C$ ,  $D$ , and  $E$  in Eq. (130) are given by the following time-ordered integrals:

$$\begin{aligned} \rightarrow C_{m,m+2}^n(\zeta) &= \frac{1}{4\pi i} \int_0^{2\pi} d\tau_1 \int_0^{\tau_1} d\tau_2 [f_{m,m+1}^n(\tau_1) f_{m+1,m+2}^n(\tau_2) - (1 \leftrightarrow 2)], \\ \uparrow C_m^{n,n+2}(\zeta) &= \frac{1}{4\pi i} \int_0^{2\pi} d\tau_1 \int_0^{\tau_1} d\tau_2 [g_m^{n,n+1}(\tau_1) g_m^{n+1,n+2}(\tau_2) - (1 \leftrightarrow 2)], \\ \nearrow D_{m,m+1}^{n,n+1}(\zeta) &= \frac{1}{4\pi i} \int_0^{2\pi} d\tau_1 \int_0^{\tau_1} d\tau_2 \left[ f_{m,m+1}^n(\tau_1) g_{m+1}^{n,n+1}(\tau_2) \right. \\ &\quad \left. + f_{m,m+1}^{n+1}(\tau_2) g_m^{n,n+1}(\tau_1) - (1 \leftrightarrow 2) \right], \\ \nwarrow D_{m,m-1}^{n,n+1}(\zeta) &= \frac{1}{4\pi i} \int_0^{2\pi} d\tau_1 \int_0^{\tau_1} d\tau_2 \left[ (f_{m-1,m}^n(\tau_1))^* g_{m-1}^{n,n+1}(\tau_2) \right. \\ &\quad \left. + (f_{m-1,m}^{n+1}(\tau_2))^* g_m^{n,n+1}(\tau_1) - (1 \leftrightarrow 2) \right], \end{aligned}$$

$$\begin{aligned}
{}^{\rightarrow}E_{m,m+1}^n(\zeta) &= \frac{1}{2\pi} \int_0^{2\pi} d\tau_1 \int_0^{\tau_1} d\tau_2 \operatorname{Im} \left\{ (f_{m,m+1}^n(\tau_1))^* f_{m,m+1}^n(\tau_2) \right\}, \\
{}^{\uparrow}E_m^{n,n+1}(\zeta) &= \frac{1}{2\pi} \int_0^{2\pi} d\tau_1 \int_0^{\tau_1} d\tau_2 \operatorname{Im} \left\{ (g_m^{n,n+1}(\tau_1))^* g_m^{n,n+1}(\tau_2) \right\}, \\
{}^{\rightarrow}B_{m,m+1}^n(\zeta) &= \frac{1}{4\pi i} \int_0^{2\pi} d\tau_1 \int_0^{\tau_1} d\tau_2 [f_{m,m+1}^n(\tau_1) - f_{m,m+1}^n(\tau_2)], \\
{}^{\uparrow}B_m^{n,n+1}(\zeta) &= \frac{1}{4\pi i} \int_0^{2\pi} d\tau_1 \int_0^{\tau_1} d\tau_2 [g_m^{n,n+1}(\tau_1) - g_m^{n,n+1}(\tau_2)]. \tag{C2}
\end{aligned}$$

All the coefficients are defined on the bonds between sites, labelled by  $(m, n)$ . Apart from  $E$ , the coefficients  $B$ ,  $C$ , and  $D$  are complex numbers, and hence modify the properties of the artificial magnetic field. Furthermore, the diagonal hoppings  $\nearrow D$  and  $\nwarrow D$  are different, due to broken rotational symmetry.